1-1-2012

Targeted Proteomics and Biochemical Fractionation: New Tools for Deciphering the Synapse in Schizophrenia

Matthew Luke MacDonald
University of Pennsylvania, macdonl@mail.med.upenn.edu

Targeted Proteomics and Biochemical Fractionation: New Tools for Deciphering the Synapse in Schizophrenia

Abstract

Schizophrenia is a chronic and debilitating psychiatric illness affecting approximately 1% of the world's population for which there is no cure and treatment options are limited. Poor understanding of disease pathology and the difficulty in modeling psychiatric symptoms in animal models has hindered the search for a cure. Despite these difficulties great progress has been made on several fronts. Genetic studies have identified risk genes for disease, while fMRI and histology experiments have located brain regions with altered activity and cytoarchitecture. Pharmacology, molecular and immunology studies have identified receptor signaling pathways that are perturbed as well.

One of the biggest challenges currently facing the field is elucidating the mechanisms linking genetic and environmental risk to the altered processes observed in the brains of schizophrenic patients. One approach to this question may be to investigate the postmortem brain tissues of patients. The goal of this thesis is to use mass spectrometry based proteomics to investigate the expression and partitioning of postsynaptic density proteins in these tissues. The postsynaptic density is implicated in disease pathology by genetic, cytoarchitecture and molecular studies. Thus, there is a good possibility that its protein composition reflects the crossroads of genetic risk and dysregulated molecular and developmental processes.

A qualitative analysis of the human postsynaptic density was performed to catalog the proteins therein. Data from this experiment was harnessed to develop a mass spectrometry method for the targeted quantification of over 200 synaptic proteins. This method was then used to validate subcellular fractionation of human postmortem brain tissue to capture synaptic microdomains. Finally, this targeted mass spectrometry method was utilized to quantify synaptic protein expression and PSD partitioning in postmortem brain tissues of subjects and patients. The enrichment of PSD proteins was elevated in tissue from schizophrenic subjects compared to controls, while total protein expression was unaltered. This data suggests that partitioning, not expression, of postsynaptic proteins is altered in schizophrenia. The results of this study demonstrate the power of a targeted mass spectrometry approach and provide an important context in which to study the dysregulation of synaptic processes in schizophrenia.

Degree Type
Dissertation

Degree Name
Doctor of Philosophy (PhD)

Graduate Group
Pharmacology

First Advisor
Chang-Gyu Hahn

TARGETED PROTEOMICS AND BIOCHEMICAL FRACTIONATION: NEW TOOLS FOR DECIPHERING THE SYNAPSE IN SCHIZOPHRENIA

Matthew L. MacDonald

A Dissertation

In

Pharmacology

Presented to the Faculties of the University of Pennsylvania in Partial Fulfillment of the Requirements for the Degree of Doctor of Philosophy

2012

Supervisor of Dissertation:

Signature:_____
Chang-Gyu Hahn, MD, PhD, Associate Professor of Psychiatry

Co-supervisor of Dissertation:

Signature:_____
Ian A. Blair, PhD, A.N. Richards Professor of Pharmacology

Graduate Group Chairperson:

Signature:_____
Vladimir Muzykantov, MD, PhD, Professor of Pharmacology

Dissertation Committee:
David Manning, PhD, (Committee Chair) Professor of Pharmacology
Harry Ischiropoulos, PhD, Research Professor of Pediatrics
James Eberwine, PhD, Professor of Pharmacology
David Lynch, MD, Associate Professor of Neurology and Pediatrics
Steven E. Arnold, Professor of Psychiatry and Neurology

DEDICATION

To my parents,

For their inspiration and support

"Home.

Home was BAMA, the Sprawl, the Boston-Atlanta
Metropolitan Axis.

Program a map to display frequency of data exchange,
every thousand megabytes a single pixel on a very large screen.
Manhattan and Atlanta burn solid white. Then they start to pulse,
the rate of traffic threatening to overload your simulation. Your
map is about to go nova. Cool it down. Up your scale. Each pixel a
million megabytes. At a hundred million megabytes per second,
you begin to make out certain blocks in midtown Manhattan,
outlines of hundred-year-old industrial parks ringing the old core
of Atlanta..."

- William Gibson, *Neuromancer*

ACKNOWLEDGMENTS

iii

ABSTRACT

Targeted Proteomics and Biochemical Fractionation:

New Tools for Deciphering The Synapse in Schizophrenia

Matthew L. MacDonald

Advisors:

Chang-Gyu Hahn

Ian A. Blair

Schizophrenia is a chronic and debilitating psychiatric illness affecting approximately 1% of the world's population for which there is no cure and treatment options are limited. Poor understanding of disease pathology and the difficulty in modeling psychiatric symptoms in animal models has hindered the search for a cure. Despite these difficulties great progress has been made on several fronts. Genetic studies have identified risk genes for disease, while fMRI and histology experiments have located brain regions with altered activity and cytoarchitecture. Pharmacology, molecular and immunology studies have identified receptor signaling pathways that are perturbed as well.

One of the biggest challenges currently facing the field is elucidating the mechanisms linking genetic and environmental risk to the altered processes observed in the brains of schizophrenic patients. One approach to this question may be to investigate the postmortem brain tissues of patients. The goal of this thesis is to use mass spectrometry based proteomics to investigate the expression and partitioning of postsynaptic density proteins in these tissues. The postsynaptic density is implicated in disease pathology by genetic, cytoarchitecture and molecular studies. Thus, there is a good possibility that its protein composition reflects the crossroads of genetic risk and dysregulated molecular and developmental processes.

A qualitative analysis of the human postsynaptic density was performed to catalog the proteins therein. Data from this experiment was harnessed to develop a mass spectrometry method for the targeted quantification of over 200 synaptic proteins. This method was then used to validate subcellular fractionation of human postmortem brain tissue to capture synaptic microdomains. Finally, this targeted mass spectrometry method was utilized to quantify synaptic protein expression and PSD partitioning in postmortem brain tissues of subjects and patients. The enrichment of PSD proteins was elevated in tissue from schizophrenic subjects compared to controls, while total protein expression was unaltered. This data suggests that partitioning, not expression, of postsynaptic proteins is altered in schizophrenia. The results of this study demonstrate the power of a targeted mass spectrometry approach and provide an important context in which to study the dysregulation of synaptic processes in schizophrenia.

TABLE OF CONTENTS

LIST OF TABLES

LIST OF FIGURES

CHAPTER ONE
GENERAL INTRODUCTION

1. Schizophrenia

Schizophrenia (SCZ) is a chronic and debilitating psychiatric illness affecting approximately 1% of the world's population[1,2]. Disease etiology is not currently understood, and while some symptoms can be controlled with therapeutics, no cure exists.

SCZ has broad diagnostic criteria and is defined by cognitive, sensory and emotional disturbances of mind. Schizophrenia-diagnosed mathematician Dr. John Nash described his experience with the disease thus:

> "…I started to think I was a man of great religious importance, and to hear voices all the time. I began to hear something like telephone calls in my head, from people opposed to my ideas. ...The delirium was like a dream from which I seemed never to awake."[3]

SCZ symptoms are multilayered, and can be divided into three groups for research purposes: 1) positive symptoms, 2) negative symptoms and 3) cognitive symptoms. Positive symptoms are disturbances of perception and thought content, making it difficult for patients to interpret or accurately compare their own beliefs to reality. Typical manifestations include hallucinations (often auditory), along with delusions and chaotic thinking (inability to organize thoughts and associations), which often results in bizarre behavior and speech. Negative symptoms include alogia, apathy and anhedonia, which can compromise the ability to perform normal social behaviors[4,5]. Patients can withdraw socially, lack the ability to feel or express emotion and have difficulty communicating. Cognitive symptoms encompass impairments in working memory and executive function. This final class is usually the most consistent over time, persisting even when positive and negative symptoms are controlled or absent.

Disease onset typically occurs in the age range of the late teens to early twenties, with women having a later average onset age as compared to men[1,2]. A "prodromal" period, categorized by cognitive decline, along with mild positive and negative symptoms, typically precedes full emergence of disease symptoms[6]. However, many prodromal symptoms overlap with other psychiatric diseases, as well as with normal adolescent affects. Thus, they are not predictive and often only diagnostically helpful in

retrospect[7]. Additionally, the full array of disease symptoms do not usually present simultaneously. Positive and negative symptoms can fluctuate in intensity, while cognitive symptoms tend to be more consistent. After the first interaction with a psychiatrist, months or even years can be required to establish the pattern and persistence required for an accurate diagnosis. For those who have been diagnosed with SCZ, the long-term outlook points toward an arduous track. Only 30% of those diagnosed with SCZ are able live without assistance, 6% are homeless, 6% are incarcerated and 15% will commit suicide[89].

While therapeutic agents can control some of the symptoms, there is no cure for the disease. Positive symptoms are the most likely to respond to pharmacologic intervention, while negative symptoms are less responsive and cognitive symptoms are largely resistant to intervention. Complicating pharmacologic interventions are the severe side effects that can accompany therapeutics, which patients often find intolerable. Examples of such side effects include tardive dyskinesia, which can arise as a side effect of high potency typical neuroleptics, and weight gain, which can be a side effect of some atypical neuroleptics.   The presence of severe side effects is notable in that they can contribute to medication non-compliance and recurrent hospitalization [10, 11].

SCZ has been demonstrated to have a strong genetic component[12, 13], with 50% of monozygotic twins and 6-17% of first-degree relatives sharing the disease[14]. Additionally, a variety of environmental factors, including exposure to infectious, autoimmune, toxic, nutritional, or traumatic insults during pre- and/or postnatal development, have been proposed as contributing factors accounting for a portion of what cannot be explained by genetics alone[15]. Current theories of disease etiology postulate that genetic vulnerabilities and environmental insults converge to impair multiple brain circuits during development, manifesting full disease symptoms almost two decades into life.

2. Schizophrenia is a disease of mind

SCZ is a disease of mind. In his autobiography In Search of Memory, Nobel laureate Dr. Eric Kandel described mind as:

"… a set of operations carried out by the brain, much as walking is a set of operations carried out by the legs, except dramatically more complex."[16]

In the brain, neural circuits connecting different regions carry out the operations. To
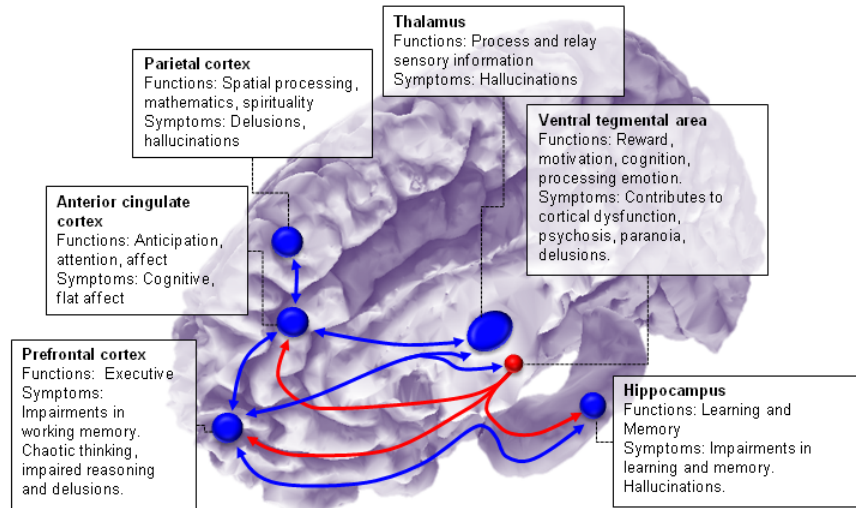
Figure 1-1. Relevant brain areas in schizophrenia. The diverse symptoms of schizophrenia implicate multiple brain areas and circuits. The prefrontal cortex receives and sends to/from many of these brain areas. These areas, their connections, functions and associated symptoms are depicted.

investigate a disease of mind is to study the biology of the underlying brain regions and circuits that perform disturbed operations. The multiple dimensions of mental operations perturbed in SCZ suggest that several brain regions and circuits are involved, likely in a complex manner. Advances in neuroimaging technologies, most notably functional magnetic resonance imaging (fMRI), have allowed researchers to look into the active brain, while histological techniques have made it possible to investigate neuronal cytoarchitecture in the postmortem brain tissues of patients. Using these techniques, skilled and dedicated researchers have linked specific brain areas to certain disease features, and cataloged neuroanatomical irregularities. Figure 1-1 depicts several brain areas that have been implicated in SCZ, their suggested relationships to particular symptoms and anatomical findings in diseased tissue.

2.1 Cognitive symptoms are a core feature of disease

Although positive symptoms tend to be more prominent, cognitive symptoms are more persistent and difficult to treat. Cognitive symptoms are observed in a majority of patients, present independently from psychotic symptoms[17], and are endure throughout

the lifespan[18-21]. Additionally, milder cognitive deficits can be observed in non-SCZ relatives[22], suggesting a genetic link, which is expanded on further below. Finally, cognitive symptom severity is a strong predictor of poor functional recovery[17, 23]. Thus, cognitive symptoms are now considered to be a core feature of the disease.

Working memory, the ability to transiently maintain and process information, and executive function, the coordination of different brain areas and neural processes to guide thoughts and actions, are the most intensely studied of the cognitive symptoms. More than any other brain region, the prefrontal cortex (PFC) is thought to be the primary orchestrator of these functions[24].

2.2   The prefrontal cortex is the seat of executive function.

The PFC is the anterior section of the frontal lobes, and is responsible for heterogeneous mental functions. It can also be defined as the area of the cerebral cortex that receives inputs from the thalamic mediodorsal nucleus. In primates, the PFC is differentiated from the rest of the frontal cortex by the presence of a well-developed granular layer 4. PFC size distinguishes humans within the primate family, representing 29% of the total human cortex, while comprising only 17% in chimps and 11.5% in macaques[25 24]. The general cytoarchitecture of the PFC is similar to that of other cortical regions, consisting of stratified layers of cells with regular and systematic connections (Figure 1-2). Within this basic template, the PFC is architecturally diverse. Broadmann used classical histological techniques to identify 10 distinct regions, and modern techniques have identified further anatomical diversity within these areas. The PFC receives inputs from a wide variety of brain areas, most notably the thalamus, brain stem tegmentum, amygdala, hippocampus, cingulate cortex, cerebellum, locus coeruleus, ventral tegmental area and the raphe. In turn, the PFC extends projects to multiple structures, including the thalamus, hippocampus and other cortical regions. The PFC is also extensively connected to the motor and sensory cortices[24]. The PFC is therefore, a demonstrably vital hub for motor, spatial, memory, internal state and emotional information
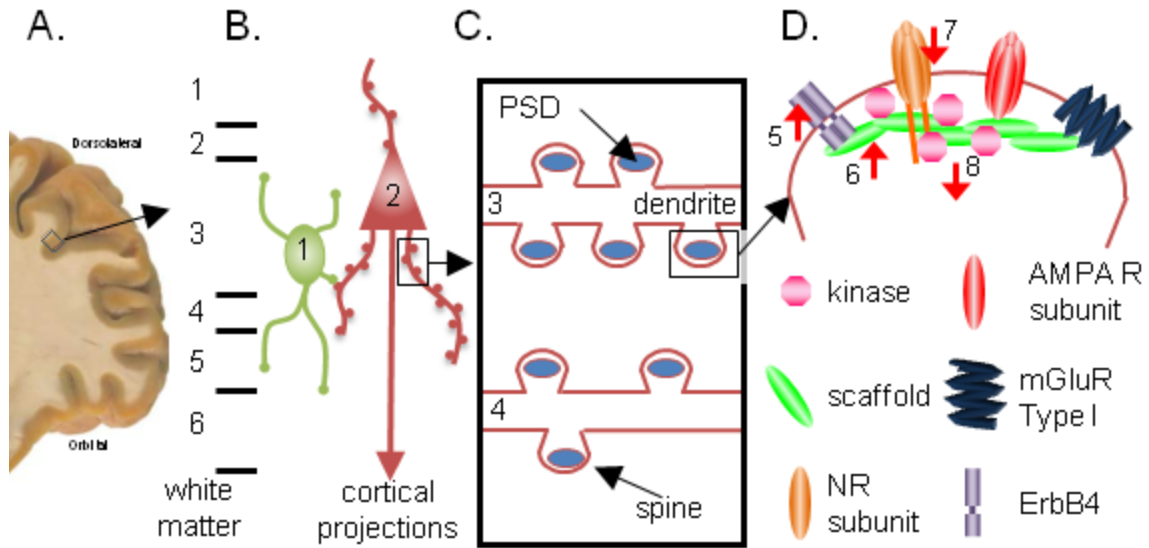
Figure 1-2. Dorsolateral prefrontal cortex cytoarchitecture and NMDA receptor signaling is perturbed in schizophrenia. A. "an unstained coronal block cut immediately anterior to the corpus callosum through the left hemisphere of a postmortem human brain." – Lewis et al. 2008[43]. **B,** Cortical layers and two basic neuron types. **1.** GABAergic inhibitory neurons synapse locally within the cortex to regulated and coordinate pyramidal neuron activity. **2.** Excitatory glutamatergic pyramidal neurons represent 75% of the neuronal population of the DLPFC. Pyramidal neuron dendrites receive information locally and project axons to other cortical areas, the striatum or thalamus, depending on the layer. The majority of layer 2 and 3 pyramidal neurons project to other cortical areas. **C.** Dendritic spine density is decreased in layers 2 and 3 of the DLPFC in schizophrenia[35, 43]. **3,** depicts a dendrite in a normal subject and **4,** a dendrite in a schizophrenia subject. **D,** depicts some of the major PSD proteins[58] and recent findings from the Hahn lab[84] of altered protein-protein interactions and signaling. **5.** NRG1 induced activation of ErbB4 is increased as is ErbB4 – PSD95 – NR association in schizophrenia (**6.**). **7.** NMDA/glycine induced NR activation is decreased in schizophrenia, while ErbB4 attenuation of NR activation is increased. As PSD95 complexes ErbB4 to NR and PSD95 – ErbB4 association is required for ErbB4 activation; these results suggest that altered protein composition or interactions at the PSD could contribute to NR hypofunction in schizophrenia. **8.** src kinase activity is decreased in schizophrenia as well, also likely contributing to NR hypofunction.

PFC cytoarchitecture is highly organized and complex. Like all cortical areas it is composed of stratified orders of cells with regular connective patterns (Figure 1-2). Pyramidal cells, excitatory glutamatergic neurons, constitute 75% of these layers[24]. Generally speaking, neurons in different layers project to different brain regions. Those in layers 2 and 3 project to other cortical regions, 5 to the striatum and brain-stem, 6 to the thalamus. Likewise, projections from other brain areas tend to target discreet layers. Most of the other 25% of PFC neurons are inhibitory GABAergic interneurons that both

receive and project within the same PFC area[24]. Interneurons serve to coordinate interneuron function, participating in important inhibitory feedback loops[26].

Joaquin Fuster has proposed that the PFC orchestrates three executive function processes: **1)** Complex action (planning), **2)** Goal-oriented behavior and **3)** Executive attention. In this theory, the PFC is thought to process information and conduct activity from numerous other brain areas, culminating in the ability to perform executive function. This view fits well with the findings of PFC cytoarchitecture and connections discussed above. Thus, the PFC is a compelling target in which to study the biology of SCZ, as a plethora of functions to which it is connected are perturbed, and the complexity of the PFC structure mirrors the complexity of the disease. fMRI and cytoarchitectural studies have consistently implicated three brain areas in connection with the cognitive symptoms of SCZ: the dorsolateral prefrontal cortex (DLPFC), anterior cingulate cortex (ACC) and hippocampus[42 43]. The remainder of this introduction will focus on the DLPFC, as the studies described in the following chapters were performed using tissue from this area of the PFC.

2.3   Altered DLPFC activation is associated with impaired working memory in schizophrenia

Neuroimaging studies have implicated dysregulated DLPFC functioning in connection with cognitive symptoms of SCZ. Specifically, alterations in both blood flow and glucose utilization in the DLPFC have been observed in SCZ patients performing working memory and executive function tasks. During low difficulty tasks, increased DLPFC blood flow and glucose utilization have been observed, with no performance deficits. During more difficult tasks, however, a decrease in DLPFC blood flow and glucose utilization was observed, and performance deficits were exhibited[27 28]. These performance deficits are not reliably observed during resting, and appear to be unique to SCZ among neuropsychiatric diseases[29 30].

In addition to task-dependent alteration in DLPFC activity, deficits in brain tissue have been observed in SCZ patients. Meta-analyses of reports on grey matter volume in SCZ indicate moderate loss in the PFC and hippocampus[31 32]. The combination of task-

related and grey matter deficits implicates the DLPFC in cognitive symptoms, although the exact mechanisms underlying the connections between symptoms and anatomy are not yet clear. However, PFC histological and molecular investigations have begun to provide some insight into this question.

2.4   Synaptic connectivity of pyramidal neurons is decreased in schizophrenia

Three observations, repeated by several groups across different cohorts, point to decreased synaptic connectivity, without neuronal loss, in the DLPFC, proving a compelling explanation for decreased grey matter volume. **1)** Neuropil, the connective processes between neurons, are decreased in SCZ while the total number of neurons appears to be unaltered[33][34]. **2)** The dendritic spine density of pyramidal neurons, per dendrite length, in DLPFC layers II and III is decreased in SCZ[35][36]. It is important to note that decreases in dendritic spine density and neuropil are not limited to the DLPFC and extend to other brain regions with impaired function in SCZ including the visual, auditory and temporal cortices and the hippocampus [37-39]. **3)** Pyramidal neuron cell volume and dendrite length is also decreased in SCZ in the DLPFC and other affected brain areas. These observations are not as large or consistent as the decreases in neuropil and spine density. Additionally, efforts to link decreased spine density to decreases in pyramidal neuron cell volume in several brain areas in SCZ have returned modest or insignificant correlations[37][35][40][41].

To summarize the findings outlined above, pyramidal neuron dendritic spine density is decreased in layers 2 and 3 of the DLPFC in SCZ, while the total number of pyramidal neurons is unaltered. This decrease in spine density is per spine length and thus is independent of decreased length or branching. Pyramidal cell volume is also decreased to a lesser extent in these layers, but does not correlate strongly with decreased spine density. Importantly, the few studies that have directly counted axon terminals in cortical regions of SCZ tissues have observed a loss similar to spines[37].

The fact that dendritic spine loss is observed across several cortical areas suggests that it could represent the end point of a common pathology. The loss of synaptic

connectivity likely explains the decrease in cortical grey mater and is widely believed to underlie the function deficits observed in the DLPFC, and other cortical areas, of SCZ.

The number of synaptic connections, and spines, increases steadily through development, reaching its zenith in late childhood/early adolescence and decreases gradually through adulthood into old age[6, 42]. This decrease is referred to as "pruning". Increased pruning is one of several hypotheses put forward to explain the decreased spine density observed in the tissues of elderly SCZ patients investigated[6, 42]. An alternate hypothesis posits that synaptic numbers in SCZ patients simply never reach the amounts present in normal individuals[42]. These hypotheses are difficult to test, as brain tissues from normal children are extremely rare and SCZ diagnosed children are, for all practical purposes, nonexistent. Never the less, both of these hypotheses hinge upon aberrant neuroplasticity, the term that describes the broad mechanisms by which neurons form, strengthen and prune synaptic connections. The involvement of neuroplasticity in SCZ pathology is well supported by evidence from genetic, pharmacological, behavioral and immunological studies. A brief primer on neuroplasticity, postsynaptic glutamate signaling and the synaptic microdomain in which it occurs, the postsynaptic density (PSD), is required to put this evidence in context.

3. Glutamate signaling at the postsynaptic density is an essential component of neuroplasticity

The constant forming, strengthening and pruning of synapses in the brain are crucial aspects of brain functioning, and are essential for learning and memory[43]. Neuroplasticity describes the progression from short-term processes, such as the ligand receptor interactions and membrane depolarization, through long term consequences, the changes in gene expression that ultimately result in neuron and synapse structure remodeling. Glutamate signaling is central in initiating and maintaining this process.

3.1 Glutamate receptors

Glutamate signaling is critical for the formation and maintenance of synaptic connections in both the developing and mature brain[44]. Glutamate acts through ionotropic and metabotropic receptors to mediate Ca^{2+} influx, which activates signal

transduction cascades. Cascades include kinases and phosphatases that can alter the phosphorylation state of receptors, ion channels, transcription factors and other signaling proteins with diverse and far-reaching effects. Three families of glutamate receptors play a role in regulating neuroplasticity.

The N-methyl-D-aspartate receptor (NR) is a slow-acting ionotropic glutamate receptor, named for the ligand to which it selectively responds[45, 46]. The NR is a heterotetramer comprised of subunits from three families: two obligate NR1 subunits, of which there are eight splice variants, and two NR2 subunits, of which there are 4 types (A,B,C and D)[45, 47-49]. The expression of alternate NR1 splice variants regulates trafficking to the synapse[50], while NR2 subunits differ in their affinity for ligand binding, channel conductance, and downstream signaling[51, 52]. A third family of NR subunits (NR3) suppresses glutamate-induced currents[53].

2-amino-3-(5-methyl-3-oxo-1,2- oxazol-4-yl propanoic acid (AMPA) and kainite receptors are also ionotropic receptors, composed of four subunits. AMPA receptors are primarily postsynaptic while kainite receptors have both pre- and post-synaptic functions (Ref). Conductance of these tetramers is determined by subunit compositions[48].

Activated ionotropic glutamate receptors are permeable to Na^+ and K^+ and Ca^{2+}. NR activation requires the presence of both glutamate and glycine, as well as the absence of Mg^{2+} in the channel pore. Mg^{2+} removal is voltage dependent, mediated by AMPA receptor-dependent membrane depolarization. Thus, the NMDA and AMPA receptor function together as a coincidence detector, which is believed to be central for tightly regulating neuroplasticity[54].

A third family of glutamate receptors, metabotropic glutamate receptors (mGluRs), also have an important role in regulating glutamate release and NR activity. mGluRs are seven transmembrane G-protein coupled receptors. Eight subtypes and three family groupings have been identified. Group I mGluRs (mGluR1 and mGluR5) activate the production of cyclic AMP and arachidonic acid via phospholipase C (PLC)[55], while group II (mGLuR2 and 3) and group III (mGluRs 4,6,7 and 8) inhibit adenylate cyclase activity. Postsynaptic mGluRs can impact neuroplastic signaling cascades by regulating

the release of intracellular calcium stores. Additionally, group I mGluRs are complexed to the NR, with the ability to regulate its activity and permeability[56, 57].

In summary, diverse receptor families with robust interactions mediate glutamate activation of neuroplasticity. Signaling molecules and scaffolding proteins facilitate receptor interactions in the postsynaptic density (PSD)[58].

3.2   The postsynaptic Density

The postsynaptic density (PSD) is a thickening of the dendritic membrane, sometimes considered to be an "open organelle"[58]. The PSD is rich in glutamate receptors, as well as scaffolding proteins and kinases (Figure 1-2)[58]. Here, interactions and signaling events proceed in a complicated, non-linear fashion to integrate the pre-, post- and extra-synaptic signaling events described above that regulate the neuroplasticity-defining transcription, translation and protein trafficking events as well as cytoskeletal changes[44, 58-60]. The PSD is a fluid, but highly organized structure. This organization is mediated by several families of scaffolding proteins[58, 59] that tether glutamate receptors to the membrane, linking them with other receptors, channels and signaling molecules. Several of these scaffolding proteins also have important roles in receptor trafficking[58].

4.   Aberrant neuroplasticity and NMDA receptor function in schizophrenia

Several lines of evidence, from pharmacological, immunological and genetic studies reviewed below, have convincingly linked NR hypofunction to various symptom domains of SCZ.

4.1   Pharmacologic evidence for NMDA receptor hypofunction in schizophrenia

Pharmacological studies provided the first evidence for NR hypofunction in SCZ. The noncompetitive NR antagonists phencyclidine (PCP) and ketamine produce positive, negative and cognitive symptoms in normal human subjects, and exacerbate these symptoms in SCZ subjects for prolonged periods following NMDA antagonist administration[61, 62]. PCP and ketamine also induce behavioral correlates of positive and negative symptoms in non-human primates and rodents, such as cognitive and

sensorimotor gating impairments, hyperlocomotion and social impairments[63].Importantly, treatment with antipsychotic drugs has been demonstrated to ameliorate these behaviors[64].

Concordant with the evidence that antagonizing NR function produces the behavioral and cytoarchitectural abnormalities observed in SCZ, agents that boost NR functions, such as D-serine, sarcosine and N-acetyl-cysteine, have demonstrated value as adjunct therapies[65-68]. Additionally, one meta-analysis of clinical trials reports that NR function-boosting agents have exhibited efficacy in improving negative symptom treatment outcomes when administered alongside typical antipsychotics[69].

4.2   NMDA receptor encephalopathies produce schizophrenia-like symptoms

Recent characterizations of NR encephalopathies also provide compelling evidence for NR dysfunction in SCZ. NR autoantibodies producing a SCZ-like syndrome in patients that is completely resolved following dialysis, provides further supporting evidence for NR involvement in SCZ[70]. Furthermore, studies in rats have demonstrated that NMDA antibodies obtained from encephalopathy patients internalize NRs, decrease NR-mediated currents and impair learning and memory[71].

4.3   Schizophrenia risk genes impact NMDA receptor and PSD signaling

Many of the most reproducibly identified SCZ risk genes are directly connected to NR signaling at the PSD[72-76][77]. Four well studied examples of NMDA-associated proteins that are also risk genes include disrupted in SCZ 1 (DISC1), regulator of G-protein signaling 4 (RGS4), neuregulin 1 (NRG1) and v-erb-a erythroblastic leukemia viral oncogene homolog 4 (ErbB4)[72, 74, 78-80 81, 82]. NRG1-ErbB4 signaling attenuates NR activity through an Src-dependent pathway[83, 84]. DISC1 has been shown to regulate trafficking of NRs[85] , and RGS4 attenuates mGluR5 activation, which complexes to the NR via PSD scaffolding proteins[81, 82].

From a broader standpoint, recent bioinformatics analyses of proteins identified in human PSD enrichments and mouse immune-precipitated (IP) PSD95 complexes revealed the presence of a significant number of risk genes for multiple neuropsychiatric diseases relative to the total genome[76, 86]. Of these diseases, risk genes for SCZ were

12

found to be the most significantly represented among all known risk genes for neuropsychiatric illnesses[75, 86, 87].

4.4   NMDA receptor activity and PSD signaling are perturbed in PFC tissue of patients

The pharmacological and immunological evidence presented above strongly suggest the involvement of NR hypofunction in SCZ symptoms. Genetic studies have identified a number of risk genes that indirectly mediate PSD and NR activity, trafficking and downstream signaling[72, 74, 77]. Many of the genetic investigations share the goal of identifying risk genes that could explain disease symptoms and neuronal cytoarchitecture, mediated through neuroplasticity and developmental processes. The PSD has been repeatedly implicated in SCZ, as seen in the vast array of risk genes participating in PSD processes, the prominent role of the PSD in NR activity regulation and the complexity of PSD signaling processes[75, 76, 86]. Based on the multiplicity of PSD-related findings, several researchers have suggested that the PSD could act as a point of convergence for the genetic and environmental risk factors, which thereby manifest themselves impaired neuroplasticity and resulting in the anatomic abnormalities believed to underlie disease symptoms[75, 78, 88 89]. However, the NR hypofunction and PSD hub hypotheses have been difficult to test directly in human patient tissues. Utilizing a novel *ex-vivo* stimulation paradigm, our lab has investigated NR activity, downstream signaling and protein interactions in human patient tissues.

NMDA/glycine-induced NR activation was found to be attenuated in post-mortem PFCs of SCZ patients as assessed by three independent metrics: NR2A tyrosine phosphorylation and recruitment of PLCγ and nNOS4[90]. Surprisingly, MK-801 binding capacity of synaptic membranes and NR1/PSD-95 complexes was enhanced, as was the amount of NR1 in PSD enrichments as measured by Western Blot. NR association with its signaling partners, phospholipase C gamma (PLCγ) and protein kinase C gamma (PKCγ) were significantly decreased in patient PSDs. Additionally, NR mediated activation of PKCγ, protein tyrosine kinase 2 (Pyk-2), and the tyrosine kinase Src was also reduced in patient tissues (Banerjee et al. in review). To test if such changes in

kinase association and activation could account in part for dysregulation of NR function in SCZ, Src activity was assessed independent of its upstream kinases. Indeed, src activity was significantly decreased in response to src-SH2 domain binding peptides in the synaptic membranes of the SCZ patient group (Banerjee et al. in review).

Activity of the risk gene ErbB4 was also altered in SCZ patients. NRG1 activation of ErbB4 signaling was dramatically increased in SCZ subjects, as was NRG1-ErbB4 attenuation of the NR. Interestingly, these changes were accompanied by a significant enhancement in the association of ErbB4 with PSD-95 in SCZ subjects[90]. Since coupling between ErbB4 and PSD-95 is crucial for its activation[91, 92] this study suggests that altered protein-protein interactions could contribute to altered ErbB4 signaling.

4.5   Attenuation of NMDA receptor activity reduced cortical spine density

Numerous studies have demonstrated that attenuating NR function, either directly or through proximal proteins or pathways, can result in decreased dendritic spine density. The complete knockdown of NR1 from pyramidal neurons in the cortex results in a 40% decrease in spine density in layers 2 and 3[93]. In a more subtle manipulation of NR activity *in vivo*, Balu et al. demonstrated that decreased amounts of the NR co-agonist serine (induced by serine racemase knockout) decreased cortical spine density. Decreased amounts of the endogenous NR antagonist glycine (induced by knocking out one copy of glycine transporter GlyT1) increased cortical spine density[94].

4.6   The link between genetic risk for disease and PSD/NMDA receptor hypofunction is implied, but has not been observed

Pharmacological, behavioral and immunological studies have demonstrated that attenuation of NR function produces a variety of SCZ-like symptoms in humans and their behavior corollaries in animals. Transgenic studies in mice have demonstrated that both extreme complete loss and subtle attenuation of NR function can mimic the decreased spine density observed in SCZ. The *ex-vivo* stimulation experiments performed in the Hahn lab directly observed NR hypofunction the tissues of SCZ patients. Together these

studies powerful evidence that NR hypofunction can acutely induce SCZ like symptoms and impact neuronal development resulting in dendritic spine loss.

Genetic studies have identified a SCZ risk genes, many of which are directly involved in NR and PSD signaling. The elucidation of these genes provides a roadmap in which genetic insults would converge on PSD signaling, impairing synaptic plasticity, resulting in the decreased spine density that is linked to SCZ symptoms. Unfortunately, this body of work does not provide information as to how genetic risk genes converge to dysregulate NR function. For example, increased NRG1-ErbB4 attenuation of NR in SCZ tissue provides a concrete link between the *activity* of a risk gene products and NR hypofunction at the postsynaptic density. But, genetic variation in ErbB4 can realistically account for only a small fraction of SCZ cases. Indeed, genetic variation in ErbB4 cannot even explain ErbB4 hyperactivity in SCZ.

While the studies described above have made great strides in uncovering the genetic risk factors and perturbed neuronal systems that ultimately result in SCZ symptoms, the mechanism by which genetic risk factors set in motion these perturbations is currently unknown. Thus, recent studies into SCZ pathology have focused on this question, searching for molecular correlates that can link risk genes, NR hypofunction and decreased spine density. All three of these lines of evidence predict that such correlates should exist, but concrete observations have proven elusive. The next section discusses this conundrum in more detail.

5. Molecular correlates of genetic risk and reduced spine density are elusive

The loss of neuropil in the DLPFC of SCZ, specifically decreased dendritic spine density, may predict alterations in pre- and post-synaptic microdomains and a paralleled decrease in PSD proteins. Likewise, a likely point of convergence for genetic risk factors to exert their effect on NR function and synaptic plasticity is through altered PSD protein composition and/or interactions[72, 75, 78, 88]. Thus, based on this evidence, one might predict that synaptic protein levels would be decreased in the DLPFC of SCZ subjects, while the protein composition, interactions and/or posttranslational modifications of PSD proteins would be altered.

Several research groups, including ours, have investigated the transcription and/or translation of synaptic genes in the prefrontal cortex using a variety of techniques, including real time PCR, *in situ* and Western blot, and micro array. Despite this intense scrutiny, no consensus has emerged as to the existence or direction of changes in synaptic protein expressions levels between disease and control tissues (Note, the term *expression* is used here, and throughout the text, interchangeably with *level* and *amount* and is not meant to imply that transcription is the sole determiner of mRNA or protein amounts in a cell). Presynaptic mRNAs were once widely believed to be decreased in the DLPFC of SCZ subjects[95], although a recent review of studies from the last decade shows that altered expression of presynaptic mRNAs and proteins has not been consistently observed [96]. As for PSD protein and mRNA expression, Table 1-1 reviews the findings of some of the most recent studies investigating PSD95, NR1, NR2A and NR2B mRNA and protein levels in the PFC of SCZ patients[97-105]. This table highlights the lack of consistency in mRNA findings, as measured by *in-situ* hybridization and real-time PCR (qPCR), with most studies finding either a decrease or no change in transcriptions. Western blot (WB) investigations report more consistent results, with all but one study finding no difference in protein levels for PSD95 and NR subunits. Decreased spine density however, suggests that total amounts of both pre- and postsynaptic-proteins should be decreased in the DLPFC of SCZ subjects.

Author/Year	Tech.	Area	PSD95	NR1	NR2A	NR2B
Fung 2012, in review	qPRC	DL-PFC		↓	■	■
Martucci 2006	qPCR	DL-PFC				■
Dracheva 2001	qPCR	DLPFC		↑	↑	
Sokolov 1998	qPCR	FC		↓		
Beneyto 2008	IS	DL-PFC	■	↓	↓	■
Kristiansen 2006	IS	DL-PFC		■	■	■
Ohnuma 2000	IS	BA 9	↓			
Akbarian 1996	IS	PFC		■	■	■
Banerjee 2012, in review	WB	DL-PFC	■	■	■	■
Funk 2011	WB	DL-PFC	■			
Funk 2009	WB	DL-PFC	■			
Hahn 2006	WB	DL-PFC	■	■		
Kristiansen 2006	WB	DL-PFC		■	■	■

Table 1-1. Translation and transcription of PSD95 and NMDA receptor subunits have been repeatedly measured in the PFC of schizophrenia by several methods. This table summarizes some of the more prominent studies from the last 15 years. Technique: *Tech.: Technique used, WB: Western Blot, IS: in situ hybridization, RT-PCR: Real Time PCR.* Area: the brain area used as reported in the manuscript: *FC: Frontal cortex, PFC: Prefrontal cortex, DL-PFC: Dorsolateral prefrontal cortex, BA 9: Brodmann Area 9.* ■: *No change* ↓: *Increase* ↑: *Decrease.* [97-105]

There are two main reasons that likely contribute to these conflicting and inconsistent results: **1) mRNA and protein levels could be differentially regulated.** The largest discrepancy in the literature is the difference between mRNA and proteins levels. Differences in the regulation of transcription and translation as well as degradation of mRNA and proteins are prime candidates to explain these differences. Currently, technologies for quantifying mRNA are superior to those for protein in terms of multiplexing, accuracy and throughput. However, mRNA amounts may not reflect protein amounts. **2) Lack of spatial resolution.** One advantage histological studies have over expression technologies such as real-time PCR and Western blot, is the ability to resolve the unit being quantified, e.g. spines, in space. The ability to differentiate between cortical layers, neuronal subtypes and synaptic compartments (e.g. pyramidal neuron vs inter neuron and spine vs axon terminal) was essential to the successful investigation of total neuron number, pyramidal cell volume, dendritic branching and spine density. Thus, the signals of differences in mRNA or protein amount between SCZ and control tissues that are localized to a specific layer, neuronal type or synaptic compartment could be lost in the noise of a homogenized tissue sample. The introduction of laser-capture and linear amplification strategies have mitigated this issue somewhat, allowing for quantification of mRNAs in discreet cortical layers and specific neuronal populations[106-108]. Laser-capture – mRNA quantification strategies, however, are still unable to asses protein amount, partitioning or post-translational modifications.

Considering that the observation of decreased dendritic spines was made in specific cortical layers and on/about a discreet part of the neuron, the synapse, it is not surprising that investigations with current strategies have observed either no difference between SCZ or control or small inconsistent findings. Thus, there is a need to overcome the technical challenges described above, as identifying the molecular correlates of decreased spine density is likely essential for linking genetic risk to NR hypofunction. The observation of these correlates requires an approach with advancements over traditional strategies that allows for multiplex quantification of synaptic proteins, with high precision and accuracy and spatial resolution for synaptic microdomains, cortical layers and neuronal subtypes.

Several groups have turned to some combination of subcellular fractionation, immunoprecipitation and/or mass spectrometry (MS) based proteomics to qualify and quantify synaptic microdomain and receptor complex proteomes in animal tissues[109-111]. Unfortunately, MS proteomic strategies as currently configured are ill suited for addressing this specific question in human tissues. In the next section I provide a brief review of the more popular quantitative MS proteomics strategies and propose a more targeted approach to overcome some of the technical hurdles described above.

6. Proteomics strategies in neuroscience

Mass spectrometry (MS) based proteomics has been used extensively to catalog protein expression in neuronal systems[109-115, 160], but application to the study of human disease has been limited[116, 117]. Technical hurdles have precluded quantitative proteomics investigations of synaptic microdomains, fine brain areas and discrete cell types in patient populations as sensitive and high-throughput proteomics methods have lagged behind technologies for assaying DNA and RNA. The last two decades have witnessed an explosion of sequencing, expression array and RT-PCR technologies, allowing for the routine and timely analysis of thousands of transcripts. The addition of linear amplification strategies[118, 119] has allowed these techniques to be applied to selected neuronal or even sub-neuronal populations. Thus, expression analyses in brain tissues, discrete layers, and even selected populations are now routinely performed on tens to hundreds of clinical samples. Proteomics methodologies, while useful for identifying thousands of proteins in an abundant sample, have been ill suited for the types of analyses now routinely performed on genetic materials.

6.1   Multi-dimensional protein identification technologies

MS approaches to protein analysis vary, but most workflows share four concepts features. 1) Enzymatic cleavage of proteins into predictable peptide components. 2) Separation of proteins and/or peptides to overcome dynamic range differences in expression. 3) MS assessment of abundant peptide ions followed by isolation, fragmentation and assessment of peptide fragment ions. 4) Informatics analysis of these data matching MS spectra to predicted peptide products in a database, culminating with

the identification of proteins present in the sample. This strategy is often referred to as Multi-Dimensional Protein Identification Technology (MudPIT)[120]. Used in this way, MS based proteomics represents an unparalleled tool for the identification of proteins and posttranslational modifications (PTMs).

Quantification of these peptide fragments can serve as a quantitative measure of protein amount. Two popular strategies of quantification in MudPIT are Stable Isotope Labeling In Cell Culture (SILAC)[121][122] and isobaric labeling techniques such as isobaric Tags for Relative and Absolute Quantitation (iTRAQ)[109, 123, 124]. SILAC has been widely employed for *in vitro* studies. The cell type to be studied is grown in media in which the only source of the amino acids (AA) lysine (K) and leucine (L) are labeled with stable ^{13}C and/or ^{15}N. After several passages, the cells will have fully incorporated the labeled AA and the resulting "heavy" proteome serves as an internal standard[122].

In iTRAQ the digested peptide products are chemically labeled with isobaric agents. The different isobaric tags will produce fragment ions with different mass to charge m/z ratios that can be used as a quantitative measure of the tagged peptide. Proteomes prepared from different samples can be tagged, pooled and analyzed together. This method has the advantage of allowing for multiplexed samples analysis. Currently up to eight proteomes can be multiplexed. This strategy also allows for protein quantification in which a SILAC standard cannot be generated. However, isobaric labeling strategies are predicated on the assumption that chemical labeling is both complete and consistent, which may not always be the case. Additionally, concerns have recently been raised that multiple tagged peptide sequences may contribute to the quantitative signal assigned to a single peptide identification, confounding fidelity of protein quantification [125]. An additional round of fragmentation may be required to address this issue, which could decrease the number of proteins quantified and further complicate an already involved bioinformatics process.

6.2   Limitations of current strategies

The main drawback to both these strategies is the heroic separations efforts necessary to overcome the large dynamic range of protein expression. Abundant proteins can confound the observation and quantification of less abundant species in several ways. Ion trap instrumentation widely used for these types of experiments is limited in both the number of ions it can hold and sequence (and thus, quantify) in a given time. More abundant peptides will be sequenced first at the expense of less abundant species. Thus deep analysis of a proteome requires fractionating the sample as much as possible. In practice

Figure 1-3. Selected reaction monitoring (SRM). A, depicts triple quadrupole MS selecting for "light" version of the peptide LIEDNEYTAR. In the first quadrupole (Q1) the mass-to-charge ratio (m/z) of the peptide (612.3) is selected for, conveying it the second quadrupole (Q2) while discarding other ions (filtered out by m/z). In the Q2 the peptide ion collides with an inert gas, often argon, and fragments into smaller polypeptides, which are conveyed to the third and final quadrupole (Q3). Here an m/z, corresponding with a known fragment ion (997.4), is selected to move onto the detector, while all other m/z's are discarded. **B.** Depicts the same operation performed on "heavy" (stable isotope labeled) LIEDNEYTAR. **C.** Chromatograms resulting from the selected monitoring of the "light" and "heavy" species of LIEDNEYTAR when the SRM is coupled with liquid chromatography. Calculating the area under the curve for each peak, and utilizing the "heavy" peptide as a standard facilitates relative or absolute quantification of the selected peptide in a complex biological matrix.

this results in two dimension of separation. The first dimension is often strong cation exchange or hydrophilic interaction chromatography to separate peptides or 1D gel electrophoresis to separate proteins, both resulting in tens of fractions. These fractions are then separated in a second dimension, often reverse phase chromatography, over gradients of one to two hours. Thus, in the absence of multiplexing, the time requirement

for analysis of a single sample can approach twenty-four hours. Additionally, MudPIT has relatively high protein requirements, which is problematic if the goal is to assay protein composition of microdomain enrichments, neuronal layers or discreet neuronal populations. In the limited number of quantitative proteomics studies performed on human brain tissue to date, the time and protein requirements have often necessitated subject pooling, severely limiting statistical power and eliminating the ability to observed protein patterns of individuals. Clearly, if quantitative proteomics is to meet the challenges described at the end of section 5, a new strategy is required.

6.3   Selected reaction monitoring, a more selective approach

Selected reaction monitoring (SRM) is a MS methodology routinely used for the quantification for specific ions in a complex sample matrix[126-128]. As opposed to the quantitative MudPIT strategies described above, SRM is usually performed on a triple stage quadrupole (QqQ) MS instrument. When configured for peptide quantification, the first quadrupole selects for the m/z of the peptide conveying it the second quadrupole while discarding other m/z's. In the second quadrupole the peptide ion collides with an inert gas, often argon, and fragments into smaller polypeptides ions, which are conveyed to the third and final quadrupole. Here an m/z, corresponding with a known fragment ion, is selected to move onto a detector, while all other m/z's are discarded (Figure 1-3). Coupled with high performance liquid chromatography (HPLC), the filtering for two m/z's specific to a target peptide SRMs on QqQ instruments can monitor the intensity of a that peptide in a highly complex biological matrix. The addition of a stable isotope labeled internal standard facilities accurate quantification[128]. State of the art QqQ instruments can perform this operation up to 200 times in a second while maintaining sensitivity in the attomole range. Additionally, SRMs can be timed to correspond with peptide elution in HPLC. Thus with a priori knowledge SRM strategies can facilitate the quantification of hundreds of target peptides in a complex matrix. The development and application of this type of approach is described in detail in Chapter 3.

7. Summary and Research Scope

Multiple lines of evidence implicate decreased spine density, perturbed neuroplasticity and NR hypofunction in the pathology of SCZ. NRs are localized to PSDs, where extra- and intra-synaptic factors converge non-linearly to regulate NR activity and neuroplasticity, while PSDs are located at dendritic spines. Many SCZ risk genes code for PSD proteins, implicating the PSD as a site of convergence at which genetic risk factors converge to impair plasticity over development.

Decreased spine density in the DLPFC of SCZ subject suggest that levels of PSD proteins could be decreased as well, while some combination of altered PSD protein amount, partitioning, interactions and posttranslational modifications likely underlie NR hypofunction. These same molecular correlates of decreased spine density and NR function are believed to fingerprints of genetic risk factors. Thus, the elucidation of these molecular differences between SCZ and control is currently an important goal of SCZ research.

Investigation of molecular alterations in postmortem brain tissue of patients has been hindered by the lack an approach capable of assaying large numbers of proteins, with high sensitivity, accuracy, precision, throughput and spatial resolution. The goal of this thesis work is to develop and validate an MS based method to meet some of these needs and utilize it to investigate PSD protein expression and partitioning in the DLPFC of SCZ subjects.

The following aims were developed to address these goals and represent the scope of this thesis research:

Research Aim I

Catalog the proteins present in PSD enrichments prepared from human postmortem brain tissue to generate the database necessary for development of an MS method.

Research Aim II

Develop and validate an LC-SRM/MS method for the selective quantification of hundreds of targeted mammalian synaptic proteins, and utilize this method to further validate biochemical fractionation of human postmortem brain tissue.

Research Aim III

Characterize protein expression and PSD protein composition in the lateral PFC of SCZ and matched control subjects.

CHAPTER TWO
CHARACTERIZATION OF HUMAN POSTSYNAPTIC DENSITY PROTEOMES

1. Abstract

Recent molecular genetics studies have suggested various trans-synaptic processes for pathophysiologic mechanisms of neuropsychiatric illnesses. Examination of pre- and post-synaptic scaffolds in the brains of patients would greatly aid further investigation. Biochemical fractionation in human postmortem tissue has yet to be tested and current proteomics methods used to analyze these preparations in animal models are not well suited for clinical applications. I performed a two-dimensional liquid chromatography-tandem mass spectrometry (2D LC-MS/MS) analysis of human PSD fractions, prepared with a protocol validated by Western blot (WB) and electron microscopy (EM). This study represents the first analysis of PSD enrichments from human tissue. Over 1800 proteins were observed and were striking similar to data sets generated by similar analyses of rodent tissues. These results demonstrate that PSD fractions isolated from human postmortem brain tissues are assayable by MS proteomics, and lay the foundation for development of a targeted quantitative method.

2. Introduction

Recent studies in neuropsychiatric illnesses have implicated various trans-synaptic mechanisms[72, 74, 75], for which protein compositions in sub-cellular microdomains are crucial[44, 59, 129, 130] [8-12]. The postsytnaptic density (PSD) is a particularly interesting microdomain since multiple candidate genes for psychoses and mood disorders converge on their signaling mechanisms[72, 74, 7577]. Thus, the ability to isolate these domains and quantify the proteins there in will greatly aid our understanding of neuropsychiatric illnesses. We, and others, have recently applied similar approaches to human postmortem brains [131, 132], but the feasibility and validity have not been fully elucidated. Additionally, while the MS proteomics strategies described in Chapter 1 have been extensively utilized for microdomains derived from rodent brains[109, 133, 134] [14-17], they are ill suited for clinical studies as throughput is limited. A targeted approach with greater throughput and sensitivity is required[111]. The design of this type of method first requires a qualitative analysis of the target proteome, which has not been performed in microdomains prepared from human postmortem brain tissue. In this study, the protein composition of biochemical fractions enriched in the PSD of human postmortem brains is

evaluated by two-dimensional liquid chromatography-tandem mass spectrometry (2DLC-MS/MS).

The PSD is a highly organized biochemical apparatus attached to the postsynaptic membrane[129], which can be visualized as an electron dense thickening under electron microscopy. The PSD contains glutamatergic receptors, N-methyl-D-aspartic acid (NMDA), alpha-amino-3-hydroxy-5-methyl-4-isoxazolepropionic acid receptor (AMPA), the group I metabotropic glutamate receptors (mGluRs) and numerous signaling molecules[129]. As a molecular scaffold, the PSD brings together various sets of signaling molecules and modulates their interactions and their activities.

The PSD is relatively insoluble in non-ionic detergents and can be purified by differential centrifugation [135]. Various protocols have been used to isolate the PSD from rodent brains based on a fundamental principle of: a) purification of synaptic membranes, b) extraction of the membranes with non-ionic detergents and c) separation of the resultant disk-shaped protein structures. Protocols have often differed in the degree of detergent extraction, thereby determining the inclusiveness of proteins in the final fractions. These include Triton X-100 or N-lauryl sarcosinate and the use of harsher detergents retrieves a more stripped down version of proteins[135]. Indeed, variations of these methods allowed separation of fractions containing synaptic vesicles and synaptic membranes from the PSD[136, 137].

Protein composition of protein complexes can be profiled using proteomic analysis. Several groups have analyzed the rodent PSD using 2D fluorescence difference gel electrophoresis (2D DIGE) or LC-MS/MS and identified sets of proteins, including known PSD proteins previously characterized by the immunoblot method[111, 115]. However, depending on the methods of fractionation and proteomics analysis, these studies have reported variable numbers of proteins in PSD enrichments, ranging from a few hundred to more than a thousand. Posttranslational modifications (PTM) appear to be maintained through the rigorous biochemical fractionation procedure, and groups have identified phosphorylation sites on PSD proteins[109, 134, 138, 139]. Biochemical fractionation of postmortem brain tissues faces special challenges due to various confounding factors inherent to these tissues[140, 140]. They include prolonged agonal state, complicating

26

medical conditions, the post-mortem interval (PMI), inconsistent pH, and duration of storage and temperature of the tissues. These conditions are thought to disrupt the integrity of proteins, ultrastructures or microdomains[141-143]. Therefore, few attempts have been made to isolate the PSD or other sub-cellular fractions from human postmortem brains [37]. In the present study, we have isolated PSD fractions from human postmortem brain tissues, verified the enrichment, protein composition, and integrity of ultrastructures using Western blot, electron microscopy and performed qualitative proteomic analysis.

3. Materials and Methods

3.1 Human tissues:

Tissue samples were dissected from the prefrontal cortex (Brodmann area 9) of two healthy control human brain samples in order to provide sufficient confidence in protein identifications. Consent for tissue collection was granted prospectively by patients and autopsy consent granted by the next-of-kin at time of death. The postmortem enrollment was conducted under Conte Core A, IRB number 703835 and postmortem protocol was conducted under IRB number 188200.

3.2 Biochemical fractionation:

300-350 mg of frozen postmortem brain tissue was dissected and homogenized in 1.5ml of solution A (0.1mM $CaCl_2$, 1mM $MgCl_2$ and 0.32M sucrose) supplemented with protease and phosphatase inhibitor cocktails (Sigma). This homogenate was adjusted to 1.25M Sucrose and 0.1mM $CaCl_2$ to a total volume of 5ml. 5ml of 1M sucrose was overlaid on this and ultracentrifuged at 28000 rpm (100,000×g) for 3 hrs in a SW 40 Ti rotor using a Beckmann L7 Ultracentrifuge. The band at the interface of 1.25 and 1 was collected with a needle as SPM. The SPM was diluted with 5X 0.1mM $CaCl_2$ and centrifuged at 12000rpm (15000×g) for 20 minutes.

For PSD preparation, a 500μl aliquot of SPM was diluted with ice cold 0.1mM $CaCl_2$ to 2.5ml, followed by the addition of 2.5ml of 40 mM Tris-HCl pH 6 supplemented with 2% Triton-X 100 and protease and phosphatase inhibitors, bringing the final volume to 5ml with 20mM Tris and 1% Triton-X 100. The samples were left in

cold room rocker for 30 minutes and centrifuged at 18000 rpm (35,000×g) for 20 minutes. The supernatant, designated as the vesicular fraction (SV), was then diluted with 5X chilled acetone and left in -20°C overnight. The pellet was air dried and dissolved in 1 ml CaCl2, then 1 ml 40mM Tris pH 8 with 2% Triton-X 100 , was added for the final concentration of 20mM Tris and 1% Triton-X. The sample was left on a rocker for 60 minutes and centrifuged at 36000 rpm (140,000×g) for 30 minutes. The supernatant, designated as the parasynaptic membrane fraction was acetone precipitated at -20°C overnight. The pelleted PSD was air dried and dissolved in 20mM Tris pH 7.4. Acetone precipitated SV and PPF fractions were centrifuged at 15000 rpm (24,000×g) for 30 minutes and pellets were dissolved in 500μl of 20mM Tris pH 7.4 with triple detergent.

3.3   Western Blotting:

The samples were transferred on PVDF membrane (Millipore) and probed with the following antibodies: mouse monoclonal PSD-95, 1:1000 (Upstate or NeuroMab, UC Davis, CA), rabbit polyclonal pS295-PSD-95 1:250 (Abcam), mouse monoclonal synaptophysin 1:5000 (Chemicon), mouse monoclonal β-actin 1:5000 (Sigma), rabbit polyclonal ErbB4, goat polyclonal NR1, goat polyclonal NR2A (Santa Cruz) , NR2B 1:1000 (a gift from Dr. Barry Wolfe, Georgetown University Medical Center, Washington, DC 20057, USA), rabbit polyclonal vGlut1 (Synaptic System), mouse monoclonal Munc18 and RAB3 (BD Biosciences). The blots were developed using chemiluminescent reagents ECL or ECL-Plus, or a combination of both (GE Healthcare). 400 μgs of SF or 10 μg of PSD from the same subject were immunoprecipitated after 2 hours preclearing with Protein A agarose with 6 μg of goat polyclonal NR1 antibody (Santa Cruz) in immunoprecipitation buffer (25 mM Tris-HCl, pH 7.4, 200 mM NaCl, 2 mM EDTA, 0.5 mM EGTA supplemented with protease and phosphatase inhibitors from Sigma) at 4°C overnight. The samples were incubated with 25 μl of Protein A agarose Plus (Pierce) for 2 hrs at RT. The immunoprecipitated samples were separated on a 7.5% SDS precast gel (Biorad) and probed with mouse monoclonal PSD-95, 1:1000 (NeuroMab), Goat Polyclonal NR1 and NR2A 1:500 and mouse monoclonal PLCγ1 1:250 (Santa Cruz).

3.4 Electron Microscopy:

Pellets were fixed in 2.5% glutaraldehyde/2% paraformaldehyde, embedded in epon, and post-stained with urayl acetate and bismuth subnitrite. Ultrastructural examination was performed with a JEOL JEM -1010 electron microscope. Images were captured with a Hamamatsu CCD ORCA digital camera, using AMT Advantage software version 5.4.2.308 (Advanced Microscopy Techniques).

3.5 Multidimensional fractionation-tandem mass spectrometry:

PSD fractions were prepared and purity confirmed by western blot analysis of PDZ domain and synaptophysin (Figure 2-1). Each pellet was washed 3 times with 20mM Tris pH 7.4 at

Figure 2-1. Subcellular fractions were analyzed by WB. Abbreviations: T: total tissue extracts, C: cytosolic extracts, S: SPM, synaptosomal membrane, V: SV, vesicular fraction, P: PPF: presynaptic fraction, D′: PSD isolated by the method 1, ': D:PSD isolated by the method 3. NR: NMDA receptor, Synph: synaptophysin, vGlut1: vesicular glutamate reuptake site.

4°C and suspended in 25mM ammonium bicarbonate with 6M guanidine hydrochloride. Protein concentration was determined by Coomassie Plus reagent (Promega, Madison, WI) with a BSA standard curve read at 595nm on an EL808 Microplate Absorbance Reader (BioTek, Winooski, VT. Two enrichments per biological sample were pooled to give 600 µg PSD protein. 2D LC-MS/MS was performed using a variation of the method described by Trinidad et al. [109]. Cysteine side chains were reduced and alkylated by incubation with 5mM dithiothreitol (DTT) for 45 min at 60°C and 15mM iodoacetamide

for 45 min at room temperature in the dark. The mixture was diluted to a final concentration of 1M guanidine with 25mM ammonium bicarbonate and 75µg modified trypsin (Promega, Madison, WI). The mixture was adjusted to a pH of 8.0 and incubated for 12 hrs at 37°C. Digests were desalted with a Peptide Macrotrap Cartridge (MICHROM Bioresources, Inc, Auburn, CA) and lyophilized to ~5 µl. Peptides were re-suspended in 100µl strong cation exchange (SCX) buffer A (30% acetonitrile, 5mM KH_2PO_4, pH 2.7). SCX was performed on the entire sample using an Agilent 1100 series HPLC with Chem Station for LC (Agilent Technologies, Santa Clara, CA) using a PolySULFOETHYL column, 2.1mmID x 100mm, 5µ, 300Å (The Nest Group, Southborough, MA). SCX buffer B consisted of buffer A with 350mM KCL. The gradient was held at 0% B for 9 min and then went from 0% B to 29% B over 54 min, 29% B to 75% B over 45 min, and 75% B to 100% B over 9 min, with a flow rate of 100 µl/min. Fractions were collected every three minutes. The first 5 fractions were pooled, giving a total of ~ 50 fractions per sample. Fractions were lyophilized and re-suspended in reverse phase (RP) buffer A (0.5% acetonitrile 0.1% formic acid in $H_2$0). One tenth of each individual SCX fractions was injected on a 5µl loop from a CTC pal auto-sampler (Leap technologies, Carrboro, NC) and peptides loaded onto Vydac Everest C18 column, 300Å, 5µm, 100mm, 500µm ID (The Nest Group) at 20 µl/min in 100% RP buffer A with an Express C100 system (Eksigent Technologies, Dublin, CA). The mobile phase was diverted to waste for the first 10 min to remove KCl and other salts. The flow rate was then reduced to 12µl/min and peptides were eluted over a 50 min gradient from 0% to 40% RP buffer B (5% $H_2$0, .1% formic acid in acetonitrile). After elution the column was washed for 10 min with 100% RP buffer B and equilibrated for 10 min with 100% RP buffer A. The LTQ mass spectrometer (ThermoFisher Scientific, San Jose, CA) was operated in the positive ion mode using electrospray ionization with a capillary temperature of 200°C. Nitrogen was used as a sheath gas at 41 and an auxiliary gas at 12 (arbitrary units). MS spectra were acquired for a mass range of 400 – 1200 *m/z* over 30 milliseconds. The top 5 most intense ions per spectra were selected and sequenced with a collision induced dissociation energy (CID) of 35.0 and activation energy of 25 (arbitrary

units). A dynamic exclusion window was applied to prevent the selected ions from being sequenced for 200 ms after the initial acquisition.

3.6 Peptide and protein identification and scoring

The data sets were searched against the International Protein Index (IPI) human protein sequence database (version 3.43, number of protein sequences: 72,346, total length of database entries: 30,410,250 amino acid residues) for peptide sequences using SEQUEST 3.1 (ThermoFisher, San Jose, CA). Raw mass spectra were converted to DTA peak lists using BioWorks Browser 3.2 (ThermoFinnigan) with the following parameter settings: peptide mass range 300-5000 Da, threshold 10, precursor mass ±1.4 Da, group scan 1, minimum group count 1, minimum ion count 15. SEQUEST searches specified that peptides should have a maximum of two internal tryptic cleavage sites and possess two tryptic termini, with methionine oxidation and cysteine carbamidomethylation as possible modifications and used a peptide mass tolerance of ±1.4 Da and a fragment ion tolerance of 0. The search results were converted into pepXML format. Peptide identification probabilities were calculated by executing PeptideProphet as implemented in the Trans-Proteomics Pipeline version 2.8 (Institute for Systems Biology, Seattle, WA)[144]. SEQUEST results were processed using the "-Ol" tag, which uses ΔCn* values unchanged.

Results from both biological replicates were combined in a single statistical analysis of protein expression using the EBP 1.0 as described previously[145]. Briefly, EBP estimates both sensitivity and false identification rate and has been validated empirically for LTQ ion trap data using a reversed/forward sequence database search approach[145]. EBP combines the probabilities of correct peptide identification across multiple peptide searches using a function that returns the maximum probability from consensus identifications, and penalizes non-consensual identifications. Replicates are integrated by simultaneously estimating multiple sets of model parameters. Peptides whose sequence matches multiple proteins are integrated in the analysis using "Occam's Razor", a principle by which the smallest set of probable proteins that is sufficient to explain the peptide sequence identifications is chosen. When proteins cannot be reliably distinguished by unique peptides, they are reported as a protein group. Only proteins with

expression probabilities corresponding to a false identification rate of less than 0.01 (1%) were reported (1863 proteins). This was equivalent to expression probabilities of $p > 0.90$ in this data set. One hundred thirty two additional proteins with $p > 0.90$ were members of groups of similar proteins, which could not be distinguished based on the peptide evidence. A separate analysis utilizing a forward/reversed database yielded near identical protein identifications at a 1% false positive cut off (data not shown).

MS/MS spectra of at least two peptides each from 63 PSD proteins (Sup. Table 2-1) were validated by comparison with product ions estimated from ProteinProspector (v4.27.2, http://169.230.19.26:8080/). Peptides from select proteins (Sup. Table 2-1) were subjected to targeted MS/MS analysis to further confirm peptide and protein identifications. These addition spectra were not included in LC-MS/MS data analysis statistics.

3.7   Comparison of PSD proteins with previous datasets:

Orthologous sequences for proteins identified in rat and mouse PSD enrichments from Dosemeci et al. and Trinidad et al., respectively, and our human data set were derived from the Mouse and Rat Genome Database (MGD, http://www.informatics.jax.org/). In our data set we saw evidence for 5338 unique IPI protein accessions collected into 2728 protein groups, where each member of a group was indistinguishable from the other, usually different isoforms of a single protein, based on observed peptides. IPI identifiers were assigned to these using the cross-reference information for each entry. These sequences were compared by analyzing the sequence homology between them using BLAST 41. The search was performed using the BLOSUM62 matrix, with gap and extension penalties of 11 and 2, respectively and with a sequence homology cutoff of 90%.

4. Results

4.1   EM and Western Blot analysis of PSD fractions

The integrity of isolated fractions was tested using EM. Figure 2-2A and B show a thin section electron micrograph of SPM and demonstrate strikingly intact synaptsomes that contain synaptic vesicles and filamentous connections to other synaptosomes. Figure 2-2C represents soluble fraction of pH 6 TritonX-100 extraction and shows paired pieces

of electron dense membranes. The more electron dense membrane is thought to be postsynaptic. Figure 2-2D shows that PSD fraction is largely devoid of the fine substructures of synaptic junctions.

The relative purity of these fractions was examined by immunoblotting analysis. Figure 2-1 shows that PSD proteins, NMDAR1, NMDAR2, Homer and PSD-95, were enriched in the PSD fractions, while these proteins are much less represented in the vesicular or parasynaptic fractions. In contrast, presynaptic proteins, Rab3, NRG1, synaptophorin, vGAT, vGlut1, were mostly enriched in fraction vesicular but not in the PSD fraction.

4.2   Protein identification

Two biological samples of PSD fractions, enriched by Method 2, were analyzed by 2D LC-MS/MS. Peptide identifications were assigned by SEQUEST (ThermoFisher) and peptide and protein probabilities determined by Empirical Bayes Protein Identifier (EBP). At a 1% false positive threshold 1863 nonredundant proteins or protein groups were identified.

A separate analysis utilizing a reverse database yielded near identical protein identifications at a 1% false positive cut off (data not shown).

Inspection of the
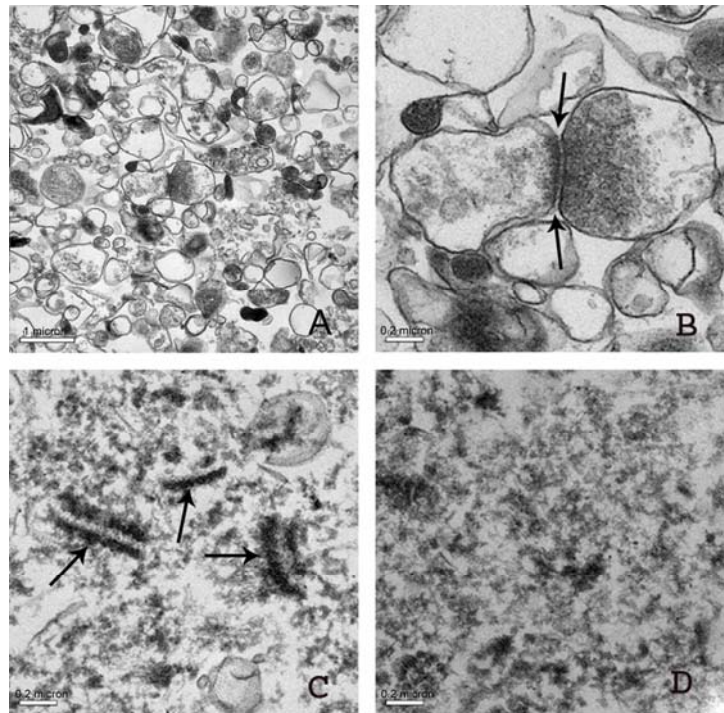
Figure 2-2. (A, B) Thin sections of SPM pellets show surprisingly intact synaptosomes and intact synaptic vesicles (A, B) as well as filamentous crossbridges (see arrows in B). **(C)** Synaptic membrane fractions extracted by Triton-X 100 at pH 6.0 show paired electron dense profiles representing synaptic junctions (see arrows in **C**). **(D)** PSD fraction obtained as an insoluble phase after synaptic membranes were extracted with Triton-X 100 at pH 8.0. Note that presynaptic specialization is removed and that the PSD is thinner than shown in A and B.

identifications revealed proteins with well-theorized functions in the PSD, as identified by review of recent literature[109, 146], such as the Discs Large Homologs (IPI00552511, IPI00647950 & IPI00790650), Homer (IPI00003566), SHANK (IPI00019794), G proteins (e.g. IPI00290928), glutamate receptors (e.g. IPI00297933), and various kinases (e.g. IPI00007128) and phosphatases (e.g. IPI00008380). Peptides from 36 consensus PSD proteins, as identified in Collins et al. [147], were selected and confirmed by spectra inspection and/or targeted MS2 analysis of peptide ions. The complete data set can be viewed at Peptide Atlas, sample IDs 040804_HumanBrain and 052104_HumanBrain. For a complete list of proteins and protein groups see: Supplemental Table 2-2 (Appendix 2) or http://spreadsheets.google.com/pub?key=pDgU17zRNrsAy-GrFicBkLQ

4.3   Grouping of protein identifications

To gain a broader view of these data, protein identifications were grouped by cellular compartment, biological process and molecular function using gene ontology (GO) annotations where available (Supplemental Figure 2-1A, B & C). While many proteins segregated to biological processes and molecular functions associated with the PSD, such as localization, stimuli response, molecular transduction, structural, and regulators of enzymatic activity, a large number of the proteins were found to be involved in processes not associated with the PSD most notably metabolism and gene expression. These types of contaminants have routinely been observed in similar analyses PSDs prepared from rodents. While it is possible that these identifications represent proteins with hitherto unknown function in the microdomain, they are much more likely contaminants from the biochemical fractionation, the result of either close association with the PSD microdomain (presynaptic proteins) or common biopsychical properties (mitochondrial membranes).

4.4   Comparison to similar analyses of rodent PSDs

We sought to further validate our findings by comparing our data set to those from previous LC-MS/MS analyses of mammalian PSD enrichments. To that end we compared our protein identifications to those obtained from mouse brain PSD enrichments[148] and an IP of the PSD-95 protein complex from rat brain PSD enrichments [149]. Close to 800 proteins were shared between the Trinidad dataset and our own when

compared by sequence homology of >90% including PSD proteins and likely contaminants such as mitochondrial, ribosomal and pre-synaptic (Data not shown). Additionally, when compared by sequence homology 28 of the 62 proteins listed in Supplemental Table 2-1 were found in one or both of the rodent sets. To reduce the impact of sequence variation between species, the proteins reported in Supplemental Table 2-1 were compared to the rodent data sets by IPI identifier. In this analysis, all but 10 of the 63 theorized proteins we found were present in one or both of the rodent data sets.

5. Discussion

2D LC-MS/MS was employed to characterize the protein composition of PSD fractions. PSD enrichments from two biological samples were combined in a statistical analysis, which integrates data from consensual and non-consensual peptide identifications in a Bayesian fashion[145]. Our list of identified proteins appears highly inclusive, yet provides an extensive coverage of known PSD proteins, as evidenced by the proteins cataloged in Supplemental Table 2-1. The number of proteins in the PSD is presently unknown [146]. Using immuno-EM, EM tomography, and scanning transmission EM, Chen et al (2005) and Petersen et al (2003) have estimated that an average PSD with a 360 nm diameter and a total molecular mass of 1.10±0.36 gigadaltons, could be composed of 10,000 proteins of 100kD[150, 151].

Proteomic analyses are prone to detecting contaminants that are either highly abundant in target tissues or co-enriched during biochemical fractionation [146]. Indeed, this list high highly comparable to an analysis of mouse PSDs that utilized a similar 2DLC-MS/MS strategy in terms of both confirmed PSD proteins and suspected contaminants. The next step is to determine which of these proteins are specific to the PSD or highly enriched in this microdomain compared to others and total homogenates.

CHAPTER THREE

DEVELOPMENT AND VALIDATION OF A MASS SPECTROMETRY METHOD FOR THE QUANTIFICATION OF TARGETED PROTEINS IN SUBCELLULAR FRACTIONS PREPARED FROM HUMAN POSTMORTEM BRAIN TISSUE

1. Abstract

Synaptic architecture and its adaptive changes require numerous molecular events that are both highly ordered and complex. A majority of neuropsychiatric illnesses are complex trait disorders, in which multiple etiologic factors converge at the synapse via many signaling pathways. Investigating the protein composition of synaptic microdomains from human patient brain tissues will yield valuable insights into the interactions of risk genes in many disorders. These types of studies in postmortem tissues have been limited by the lack of proper study paradigms. Thus, it is necessary not only to develop strategies to quantify protein and posttranslational modifications at the synapse, but also to rigorously validate them for use in postmortem human brain tissues. In this study we describe the development of a liquid chromatography-selected reaction monitoring method, utilizing a stable isotope-labeled neuronal proteome standard prepared from the brain tissue of a stable isotope-labeled mouse, for the multiplexed quantification of target synaptic proteins in mammalian samples. Additionally, we report the use of this method to validate a biochemical approach for the preparation of synaptic microdomain enrichments from human postmortem prefrontal cortex. Our data demonstrate that a targeted mass spectrometry approach with a true neuronal proteome standard facilitates accurate and precise quantification of over 100 synaptic proteins in mammalian samples, with the potential to quantify over 1000 proteins. Utilizing this method, we found that protein enrichments in subcellular fractions prepared from human postmortem brain tissue were strikingly similar to those prepared from fresh mouse brain tissue. These findings demonstrate that biochemical fractionation methods paired with targeted proteomic strategies can be utilized in human brain tissues, with important implications for the study of neuropsychiatric disease.

2. Introduction

Synaptic architecture and its adaptive changes require numerous molecular events that are both highly ordered and complex[60, 152]. Molecular and cellular research into these processes has, until recently, been limited to technologies that can examine one molecule to the next within a cascade. In the last decade, mass spectrometry (MS)-based

proteomic methodologies, paired with biochemical fractionation techniques, have enabled us to begin cataloging the proteomes and signaling of mammalian synaptic microdomains[60, 111, 153-155] and microdomain specific protein complexes[114, 133, 156]. These studies have revealed that synaptic architecture and plasticity involve numerous interactions between multiple signaling mechanisms with robust crosstalk and protein interactions[114 133 86 109]. These findings also dovetail with decades of genetic studies into neuropsychiatric disease, which have identified dozens of risk genes spread across multiple pathways at the synapse[157, 158]. Historically, signaling cascades and molecular disease models have been depicted as a string of molecular events that are connected in tandem. Such views were shaped in part by the methodologies that permitted the measure of a handful of protein events at a time. MS-based proteomic methodologies can monitor numerous proteins and posttranslational modifications simultaneously, permitting us to examine signaling pathways in the context of many other intracellular molecular events. The next challenges in the field of neuroscience will be to establish methodologies for quantitative assessment of proteomes in specific microdomains of neural tissues, to monitor these numerous molecular events simultaneously, and to understand them within the context of nonlinear intracellular trafficking, protein interactions and posttranslational modifications.

Postmortem brain studies are a critical component of neuropsychiatric research as brain tissues of patients may harbor pathophysiologic information of the illnesses. A majority of neuropsychiatric illnesses are complex trait disorders, in which multiple etiologic factors converge at the synapse via many signaling pathways[157, 158]. The application of advanced molecular and cellular technologies to access synaptic microdomains, however, has been limited in postmortem brains by confounds such as therapeutic intervention, agonal state, and postmortem interval. Thus, there is a pressing need to validate and focus these biochemical fractionation and MS proteomic methods for use with human postmortem brain tissue. The vast majority of previous neuroproteomic studies have employed two dimensional separation/tandem MS approaches to perform qualitative analyses of mammalian synaptic preparations[133, 153, 155]. Protein quantification has been accomplished utilizing either synthetic stable isotope-labeled peptide

standards[111] or isobaric peptide labeling methods, such as iTRAQ[109, 123]. Sample workup can complicate the application of isobaric tagging in an efficient and reproducible manner[159], while synthetic peptide standards are costly and have difficulty controlling for confounds in sample preparation, most notably protein digestion[160]. Stable Isotope Labeling by Amino acids in Cell culture (SILAC) can produce only a partially labeled neural proteome[161] and we have found that full expression levels and synaptic architecture of brain tissue are difficult to reproduce in fully labeled cultures. The recent availability of Stable Isotope Labeling in Mammals (SILAM) mouse tissue allows for the generation of a stable isotope labeled neuroproteome within the context of native tissues to serve as an internal standard for the quantification of a vast number of proteins[162]. Walther et al. recently utilized SILAM tissue to quantify over 4000 proteins in mouse hippocampus and cortex[163]. Considering the high level of homology between mammalian neuronal transcripts[75], we investigated the suitability of this stable isotope-labeled proteome to serve as a protein standard for human tissue as well as additional model organisms.

In this study we first describe the development and validation of liquid chromatography-selected reaction monitoring (LC-SRM)/MS-based methodology for studies of mammalian synapses. Quantification of 189 neuronal proteins was conducted utilizing a $[^{13}C_6]$ lysine-labeled brain proteome internal standard ($[^{13}C_6]$ brain ISTD) prepared from $[^{13}C_6]$lysine SILAM mouse brain tissue. We also report the application of this method to further validate biochemical fractionation of human postmortem brain tissue for the study of synaptic biology in human disease. We observed highly reproducible enrichment of proteins into synaptic microdomains in a function- and family-specific manner. These protein enrichments were remarkably comparable between fresh-frozen mouse and human postmortem tissues. Additionally, bioinformatic analyses indicate that this method has the capability to quantify thousands of additional neuronal proteins in many model systems. These experiments demonstrate that the biochemical fractionation coupled with LC-SRM/MS and $[^{13}C_6]$ brain ISTDs provides a powerful tool for investigating the protein composition of synaptic microdomains in

mammalian tissues, with broad application to neuropathology and neurological studies in humans and model systems.

3. Materials and Methods

3.1 Brain tissues:

Prefrontal cortex (Figure 3-1B) tissue slices from three cognitively and neurpathologically normal subjects without were obtained from the University of Pennsylvania (UPenn) Brain Bank. Consent for tissue collection was granted prospectively by patients. Autopsy consent was granted by the next-of-kin at time of death. Postmortem enrollment, brain autopsy, and neuropathological assessment were conducted under UPenn Conte Core A, IRB numbers 703835 and 188200. After death, the cases were stored at 2-4°C until transport to UPenn, where all autopsies were performed. Upon sagittal bisection, a hemispheres from each case was cut into coronal slabs, which were frozen overnight at -80°C and then sealed in plastic bags for long-term storage at -80°C. Tissue samples from the other hemisphere were fixed and prepared for microscopic analysis. The cases were examined by trained neuropathologists for gross and microscopic abnormalities diagnostic of diverse neurodegenerative dementias. We selected fresh frozen tissue from the prefrontal cortex because its large volume allowed repeated sampling without depleting resources available for other studies on precious normal human brain tissue.   Within this restriction, we selected tissues with a wide range in age, sex, and postmortem interval (PMI) (Figure 3-1B). Mouse brain tissues consisted of the forebrain plus midbrain olfactory bulb, were dissected from three male C57/BL6 mice 8-12 months old.

3.2 Biochemical fractionation:

Synaptic fractions were obtained using a biochemical method we previously validated for use in human postmortem brain tissue (Figure 3-1)[153]. 300-350 mg grey matter was homogenized in 1.5 ml solution A (0.32 M sucrose, 1mM MgCl2 and 0.1mM CaCl2) with a Teflon pestle. ~100 μl of the homogenate (H) was saved, solubilized with 1% SDS and clarified by centrifugation. The remaining homogenate was centrifuged at 2,500 RPM for 15 min. The pellet was discarded and 100 μl of the supernatant agitated on a rocker at 4°C with a final concentration of 0.5% digitonin, 0.2% sodium cholate and

0.5% NP-40for 1 h, centrifuged at 14,000 RPM for 20 min, and the supernatant was saved as the Synaptosomal fraction (SF). The remainder of the supernatant prepared from the 2500 RPM spin was adjusted to 1.25 M sucrose with 2M sucrose and 1mM CaCl2to a final volume of 5 ml. 5 ml of 1 M sucrose was overlaid and the gradient ultracentrifuged at 28,000 rpm for 3 h in a SW 40 Ti rotor using a Beckmann L7 Ultracentrifuge. The band at the interface was collected, diluted 1:10 in 0.1 mM CaCl2 and centrifuged at 12,000 RPM for 20 min. The supernatant was discarded and the pellet, the intermediate membrane fraction (IM), was dissolved in 1 ml 20 mM Tris pH 6.0 and sonicated with three 10-second pulses. 1 ml 20 mM Tris pH 6.0 with 2% Triton X-100 (Sigma) was added to the solution and agitated on a rocker at 4°C for 30 min, followed by centrifugation at 18,000 RPM for 30 min. The supernatant, the Vesicular fraction (V), was precipitated in acetone at-20°C overnight. The pellet was air dried, dissolved in 1 ml 20 mMTris pH 8.0, sonicated with three 10-second pulses, mixed with 1 ml of 20 mM Tris pH 8.0 with 2% Triton X-100, agitated on a rocker at 4°C for 45min and centrifuged at 36,000 RPM for 1 h. The resulting supernatant, the Parasynaptic membrane fraction (P), was precipitated in acetone at -20°C overnight. The pellet, the PSD fraction (D), was air dried, washed three times with 20 mM Tris pH 8.0 and dissolved in 300 μl 20 mM Tris pH 7.4 with 1% SDS. Following acetone precipitation, the V and P fractions were centrifuged at 3,000 RPM for 30 min and dissolved in 100 μl 20 mM Tris pH 7.4 with 1% SDS.

To prepare the $[^{13}C_6]$ brain ISTD, 400 mg labeled MouseExpress brain tissue (Cambridge Isotopes, MA) was homogenized in 4 ml buffer A as described above, centrifuged at 1,000 x g for 10 min to clarify, agitated on a rocker at 4°C for 30 min, and centrifuged at 10,000 x g for 20 min. The pellet, a crude membrane fraction, was dissolved in 2 ml 20 mM Tris pH 7.4 with 1% SDS. Total protein in all preparations was quantified with the micro BSA assay (Pierce) and all solutions were supplemented with protease and phosphate inhibitor cocktails (Sigma) as well as 1 mM sodium fluoride and sodium orthovanidate (Sigma).

3.3   Sample preparation for LC-SRM/MS and LC-tandem MS (MS/MS):

Sample preparation for LC-SRM/MS and LC-tandem MS (MS/MS): Synaptic preparations were mixed with the $[^{13}C_6]$ brain ISTD at a ratio of 2:1($\mu g/\mu g$) and processed for MS analysis as described in Cheng et al. 2006. Briefly, preparations were heated with LDS buffer at 95°C for 20 min, separated on a 1.5 mm 4-12% Bis-Tris Gel (Invitrogen), cut into three fractions for LC-SRM/MS and five for LC-MS/MS (Figure 3-1C& D), chopped into ~ 2 mm cubes, washed in 50% acetonitrile (ACN) containing 25 mM NH4HCO3, reduced with 10 mM DTT, alkylated with iodoacetamide (Sigma), and digested with trypsin (Promega) 1:5 by mass, overnight at 37°C. Peptides were recovered from gel cubes into 50/50 H2O/ACN with 3% formic acid by vortex-mixing and sonication for 20 min each. Samples were then desalted with Oasis® HLB cartridges (Waters), filtered with 0.22 μm Ultra free-MC filter cartridges (Millipore), then dried almost to completion and suspended in 45μl H2O with .1% formic acid.

3.4   MS methods:

For LC-SRM/MS analyses, all peptide preparations were run on a TSQ Vantage triple stage quadrupole mass spectrometer (ThermoFisher Scientific) with an Eksigent 2Dnano LC (Eksigent) and a CaptiveSpray source (Michrom). 5 μl (~2.5μg protein) sample was loaded on to a Magic C18 column (Michrom) at 1 μl/min for 12 min, and eluted at 750nl/min over a 25 min gradient from 3-35% mobile phase B (ACN containing .1% formic acid). SRM transitions were timed using 1 – 1.5 min retention windows, depending on the number of SRMs to be assayed. Transitions were monitored, allowing for a cycle time of 1 sec, resulting in a dynamic dwell time, never falling below 10 msec. The MS instrument parameters were as follows: capillary temperature 275 oC, spray voltage 1100 V, and a collision gas of 1.4 mTorr (argon). The resolving power of the instrument was set to 0.7 Da (FWHM) for Q1 and Q3. Data were acquired using a chrom filter peak width of 4.0 sec.

LC-MS/MS analyses were conducted by Dr. Gene Ciccimaro on a Q Exactive (ThermoFisher Scientific) quadrupole orbi-trap hybrid instrument with an Easy nLC-II (ThermoFisher Scientific) nano-pump/autosampler. 3μl peptide sample (~ 1 ug) was loaded and resolved on a 20 cm x 75 μm proteopepII C18 packed tip column over a 90 min gradient at a flow rate of 350 nL/min, 0-35% mobile phase B (ACN, .1 formic acid).

A data-dependent top 10 method was used to acquire a 70,000 resolution full scan to trigger 10 17,500 resolution HCD scans. Ions were isolated for MS/MS analysis with a 2.0 Da window on the quadrupole. Average cycle times were 1 sec. Each sample was analyzed in triplicate.

LC-MS/MS data analysis: Raw files from triplicate injections were searched together within Proteome Discoverer 1.3 (ThermoFisher Scientific) using SEQUEST and the human refseq. database (release 47, ftp://ftp.ncbi.nih.gov/refseq/H_sapiens/mRNA_Prot/). Search parameters allowed trypsin to cleave after Lysine and Arginine and have 2 missed cleavages. Precursor ion mass tolerance was set to 15 ppm and fragment ion mass tolerance was 20 mmu. The dynamic modification of methionine (oxidation = 15.995 Da) and lysine (13C6 = 6.020 Da), in addition to the static modification of cysteine (carbamidomethylation = 57.021 Da) was accepted on up to 4 residues per peptide. Within the Proteome Discoverer Software, SILAC pairs were identified using the "2 plex" workflow node, and all peptides were rescored using the Percolator[164]algorithm node. Finally, peptides were filtered at 1% FDR.

SRM transition design and validation: Method development began with the selection of ~300 synaptic proteins of interest from published multidimensional MS/MS analyses of mouse and human brain tissue biochemical fractions[109, 153] as well as the LC-MS/MS analysis described in this study. RAW data from the two analysis of human tissue were searched in Proteome Discoverer™ 1.1(ThermoFisher Scientific) using SEQUEST. Proteome Discoverer™files were loaded into ProteinCenter™(ThermoFisher Scientific), and sorted by function and subcellular location using Gene Ontology (GO) terms. Targets for inclusion in the LC-SRM/MS assay were selected with a bias towards well-annotated synapse proteins, such as glutamate receptors, kinases, phosphatases, vesicular fusion, amino acid metabolism, energy metabolism, protein trafficking, ion conductance, cytoskeleton, and scaffolding. Peptides for proteins of interest were then filtered based on the following criteria: 1) presence of lysine to incorporate the "heavy" label, 2) non-redundant to a selected protein or protein group (determined by BLAST search) and 3) 100% homology across mouse and human sequences (determined by BLAST search).

Acceptable peptide sequences, along with MS2 spectra, were imported into Pinpoint™ (Thermo-Scientific). Initially, five mass transitions were selected for each target peptide and its "heavy" counter-part. Validation experiments were performed in 1:1 mixtures of human IM fraction and the [$^{13}C_6$] brain ISTD. Pinpoint™ was used to visually and statistically validate SRM transitions.

3.5   Western blot analysis

To confirm biochemical enrichment, all preparations were assayed by Western blot for parasynaptic (P), postsynaptic (D) and vesicular (V) proteins prior to MS analysis (27). Briefly, 10μg of each fraction was separated on 7.5% SDS precast gels (Biorad), transferred to a PVDF membrane (Millipore), blocked with 5% milk, .05% TBST for 30 min, and probed with the following antibodies: mouse monoclonal PSD-95, 1:1000 (Upstate or NeuroMab, UC Davis, CA), Na/K ATPase channel subunit α 1:1000 (Santa Cruz) and Gα 1:500 (Cell Signaling). The blots were developed using chemilluminescent reagents ECL or ECLPlus, or a combination of both (GE Healthcare).

3.6   Modeling of Postmortem Interval in Mice

Modeling of Postmortem Interval in Mice: 10 male 8-12 month old C57/B6 mice were sacrificed by CO2 and cervical dislocation, per protocol, and placed at 4°C. The brains were removed from the crania at 0, 4, 8, 12 and 16 h post sacrifice, separated from the cerebellum and olfactory bulbs, frozen on dry ice, stored at -80°C and subject to biochemical fractionation. The D fractions were analyzed by LC-SRM/MS as described above.

3.7   LC-SRM/MS data and statistical analysis

Peak areas and area ratios were calculated within Pinpoint. Raw files generated by LC-SRM/MS analysis were loaded into Pinpoint files containing target proteins/peptides/transitions. All individual SRM transitions and integration areas were manually inspected. Transitions where the signal-to-noise (S/N) ratio of the "labeled" species below 3 were excluded from analysis. The ratios of the integrated areas for "light" endogenous peptides and "heavy" [$^{13}C_6$]brain ISTD peptides were calculated to obtain peptide measures using multiple transitions per peptide. The average of these peptide ratios determined the relative amount of each protein. Protein enrichment values

in the SF, V, P and D fractions were calculated by normalizing protein measures in each fraction to measures in the H fraction. The coefficient of variations (CV), expressed as a percent, were calculated to assess precision of peptide quantification across injections, accuracy of protein quantification from multiple peptides, and reproducibility of fractionation from different animals or subjects.

Unsupervised hierarchical clustering was used to construct self-organized heat maps of protein and fraction by enrichment values with Cluster 3.0 and Treeview[165, 166]. Enrichment values were log2 transformed, median centered by enrichment and fraction, then normalized by protein and fraction. Un-centered Pearson correlation was used as the similarity metric and the clustering method was centroid linkage. Pearson correlation coefficients were calculated in Cluster 3.0. ANOVA, and Student's t-test were used to calculate significance for the effects of species and fraction on enrichment CVs, species and protein group on enrichment values, and PMI and protein group on protein measure.

3.8   Dilution curve preparation

To confirm that "light"/"heavy" peptide SRM measures were within linear range, a dilution curve was prepared by varying the ratio of a human total homogenate (H) fraction / $[^{13}C_6]$brain ISTD from 0.05 to 19. Five mixtures were prepared, (µg H/ µg $[^{13}C_6]$brain ISTD): 1/19, 3/17. 10/10, 17/3 and 19/1. These preparations were analyzed by LC-SRM/MS in duplicate and the prepared L/H ratio plotted against the observed L/H ratio for each light-heavy peptide pair.

3.9   Comparison of human and mouse protein sequences

Dr. Steve Seeholzer graciously performed this analysis. Human and mouse protein sequence databases were assembled from the orthologous protein accessions listed in the HomoloGene database (http://www.ncbi.nlm.nih.gov/homologene, release 65). The Entrez efetch utility was used to retrieve the mouse and human fasta format sequences from the Entrez protein database. Proteins were digested in silico with trypsin while retaining peptides ending with lysine and $6 \leq$ length ≤ 25. Human peptides were additionally filtered to retain only proteotypic peptides. For each human protein, the number of peptides having an identical amino acid sequence to any mouse peptide was

tabulated. A separate analysis was limited to the 1400 proteins identified in a proteomic study of mouse (Bl6) synaptosomes (Seeholzer and Kalb, unpublished).

4. Results

4.1 LC-MS/MS analysis of postmortem human brain intermediate membrane fraction spiked with [^{13}C$_6$] brain ISTD:

The combined analysis of all five gel bands resulted in the identification of 2,556 protein groups by 2 or more unique peptide sequences. In total, 230,841 peptide spectral matches were attained, allowing for 27,650 unique peptide sequence identifications. 2,802 labeled lysine containing peptides were identified, while 2,211 were bioinformatically unique to a single protein group and 1,798 were observed as a "heavy/light" pair. The median heavy/light ratio was 0.27. Supplemental Figure 3-1A shows the ratio distribution of all observed unique peptide pairs. These unique labeled peptide pairs corresponded to 619 proteins, 325 of which were represented by 2 or more unique pairs. Supplemental Figure 3-1B shows the protein distribution by the number of unique peptide pairs. Dr. Gene Ciccimano performed this analysis.

4.2 Fidelity of Peptide SRMs

To ensure that the desired peptide was assayed, rigorous selection criteria were employed for the inclusion of peptide LC-SRM/MS transitions. After a peptide met the three initial criteria described above: non-redundancy, presence of lysine and 100% sequence homology between mouse and human tissues, multiple validation experiments were conducted to confirm peptide SRM accuracy. Candidate "light"/"heavy" peptide SRMs were evaluated for A) retention time, B) similar y-ion ratios (within 25%), C) presence in the correct gel fraction, and D) a signal to noise greater than 3. Peptide SRM pairs for which more than one identical peak was observed were omitted. Out of the approximately 300 initial proteins selected, 2-4 SRMs for 1-4 peptides from 189 proteins met these criteria (Sup. Table 3-1, Appendix 2). Of these 189, 110 were measured by one peptide, 53 by two, and 25 by three or more.

4.3 Precision of Protein Quantification

To assess LC-SRM/MS technical precision, four 30 μg aliquots of a human intermediate membrane fraction were individually mixed with 15 μg [^{13}C$_6$] brain ISTD,

prepared for LC-SRM/MS analysis and injected in triplicate over several days. A subset of 118 proteins was monitored in this experiment. First, analytical precision of peptide quantification over repeated injections was assessed. The median CV for peptide measures across three repeated injections was 4.3% and CV correlated with the signal intensity of the light peptide SRM (R^2 = .7) (Supplemental Figure 3-2). Variability from sample preparation was also assessed. The median CV% across 4 repeated preparations was 3.8%, with the vast majority under 10% (Figures 3-2A&B). Finally, we assessed precision of protein quantification by calculating variability between the peptides that were quantified for the same protein. The median CV for proteins quantified with two or more peptides was 12%, with the majority of CVs being under 20% (Figure 3-2D). This indicates that LC-SRM/MS with a [$^{13}C_6$]brain ISTD has excellent precision and highly reproducible sample preparation.

4.4   Quantitative Analysis of Subcellular Fractions

We analyzed the relative protein composition of five neuronal biochemical fractions: Homogenate (H), Synaptosomal (SF), Vesicular (V), Pre-synaptic density (P) and Post-Synaptic density (D), prepared from three human postmortem prefrontal cortex sections and three mouse brains (Figure 3-1). Enrichment was confirmed by Western blot for protein markers of fractions D, V and P (Figure 3-3). The enrichment of all fractions except for P from mouse 3 was confirmed. This preparation was analyzed with the other samples and included in hierarchical clustering, but was dropped from average enrichment and enrichment variability calculations. The fractions were mixed, 2:1 by
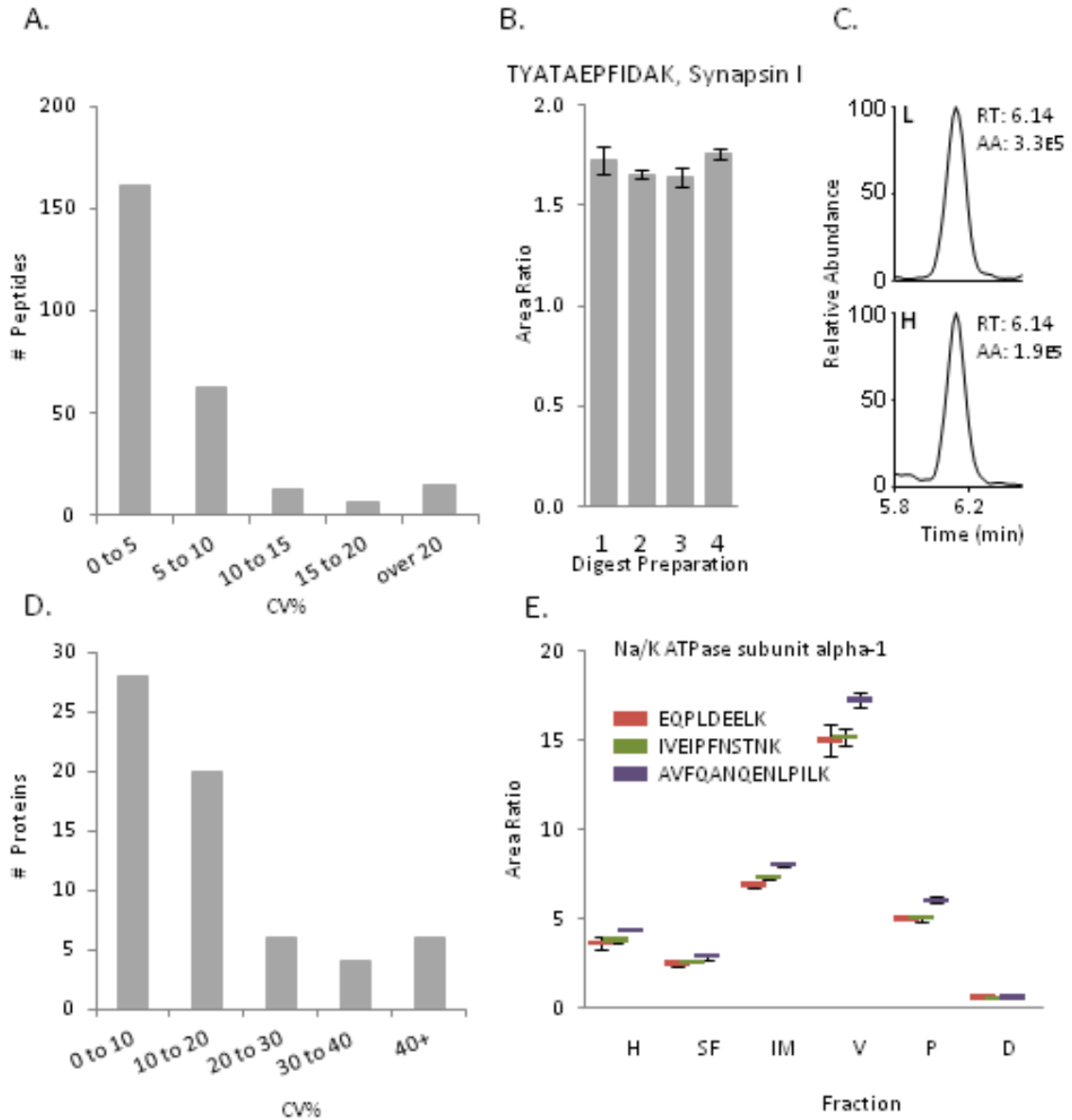
Figure 3-2. **Precision of peptide quantification.** To assess variability in sample preparation, four 30 μg aliquots of a human IM fraction were individually mixed with 15 μg [$^{13}C_6$]brain ISTD, and analyzed by LC-SRM/MS with triplicate injections. The coefficient of variance, expressed as a percentage (CV%), was calculated for each peptide measured in the four fractions. A, depicts the distribution of the peptide CV%s, showing the vast majority under 10%. B, shows light/heavy area ratios for the TYATAEPFIDAK peptide, which is unique to Synapsin I. Error bars are standard deviations (SD) of the triplicate injections. C, chromatographic peaks from LC-SRM/MS analysis of TYATAEPFIDAK. CV% of peptide measures for the same proteins were calculated to assess accuracy of protein measures derived from multiple peptide SRMs. D, shows the distribution of these CV%s. E, shows the consistency of peptide measures for the same protein across 6 fractions prepared from human subject 1.

mass, with $[^{13}C_6]$brain ISTD, separated into three fractions by SDS-PAGE (Figure 3-1C) and analyzed by LC-SRM/MS with duplicate injections (Sup. Table 3-1, Appendix 2). To ensure a continued high level of precision in peptide and protein measurement, peptide SRMs in this data set were re-evaluated for variability, intensity and signal-to-noise ratio using the criteria described above. Additionally, as post-translational modifications can confound protein measurements derived from peptide SRMs, peptide trends across different fractions from the same individual were manually inspected for consistency, as in Figure 3-2E. Proteins lacking consistent peptide measures were removed. It is important to note that even minute differences in peptide measurement for the same protein were consistent across all fractions. For example the AVFQANQENLPILK peptide, from Na/K ATPase subunit alpha-1, was slightly elevated in all fractions compared to the other two peptides (Figure 3-2E). The 150 proteins that met these criteria in both human and mouse preparations were used as the basis for comparing fractionation between the two species (Sup. Table 3-2, Appendix 2).

4.5   Protein and peptide quantification accuracy

Accuracy of protein measures was assessed by comparison with Western blot for three synaptic proteins: guanine nucleotide binding protein subunit α, sodium/potassium ATPase channel subunit α 1 and PSD-95. We observed consistent agreement in relative protein measures between the two methods (Figure 3-3).

The light/heavy peptide ratios were found to be linear over the range of the dilution curve for most peptides, with some deviating from linearity at the first and/or last point. The average R^2 for 195 peptides assayed was .96. Figure 3-4 shows representative dilution curves for CaMKIIα, CDK5, NR1 and PSD95.

4.6   Protein enrichment

Protein enrichment values were calculated by normalizing protein measures in the SF, V, P and D fractions to protein measures in the H fraction. Averages and CVs of protein enrichment values and protein measures in H were calculated for each species. Median CVs for enrichment values were under 30% for all preparations from both species (Figure 3-4A). In four of the five preparations (H, SF, P and D) the average CV was significantly lower in mice, but a two-way ANOVA did not reveal a significant

interaction between species and fraction p = 0.2. A substantial number of proteins had CVs above 30% (Supplemental Figure 3-3). At first, we suspected that proteins with high CVs in a fraction would have low average enrichment values, while more abundant "bona fide" proteins would have more consistent values. Regression analysis, however, found no correlation between average enrichment value and CV in any of the fractions (data not shown), necessitating the sorting of proteins by both enrichment value and variability.

To gain this more comprehensive view of the data, unsupervised hierarchical clustering was used to group proteins and fraction by protein enrichment value (Appendix 3, Sup. Figures 3-6, 3-7 & 3-8). In both species we observed segregation of preparations into discreet groups by fraction identity (Figure 3-5B & C).
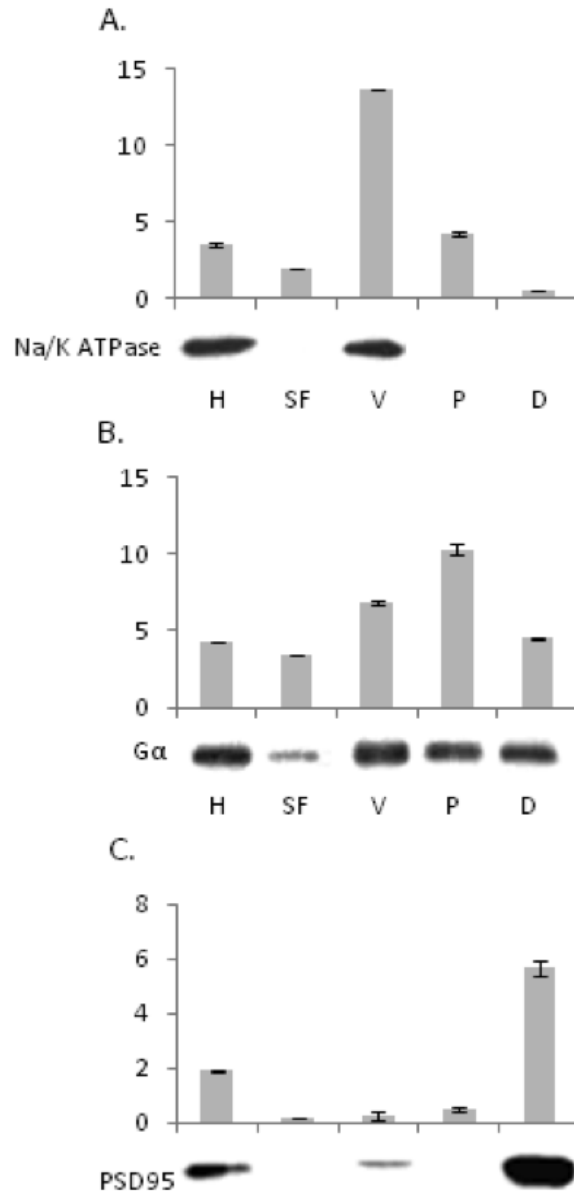
Figure 3-3. **Confirmation of protein enrichment in biochemical fractionation and accuracy of protein quantification.** Prior to LC-SRM/MS analysis, Western blot was used to confirm success of biochemical fractionation. Levels of Na/K ATPase channel subunit 1 α, guanine nucleotide binding protein subunit α, and PSD-95 were used to confirm enrichment of vesicular (V), parasynaptic (P) and postsynaptic density (D) fractions, respectively. LC-SRM/MS quantification of these proteins was then compared to Western blot. A, B and C, show representative blots and LC-SRM/MS area ratios from human subject 2. Error bars are standard deviations of duplicate injections.

Clustering analysis of human and mouse preparations together revealed that biochemical fractions within species had the tightest grouping, followed by fraction identity, regardless of species (Figure 3-5D). Many protein groups clustered by high enrichment values were both similar across species and in agreement with previously published analyses of these preparations. Kinases, scaffolding proteins and glutamate receptors were enriched in postsynaptic density (D) fractions (Figure 3-6A, Supplemental Figure 8A), SNARE complex proteins and vesicular amino acid transporters were enriched in vesicular (V) fractions (Sup. Figure. 3-8B), and guanine nucleotide binding protein subunits and voltage-dependent ion channels were enriched in parasynaptic (P) fractions (Sup. Figure 3-8C). Synaptosomal (SF) fractions were rich in cytosolic enzymes (Sup. Figure 3-8D). Clustering analysis of human and mouse fractions together also highlighted two striking differences between mouse and human preparations. First, it identified a subset of "contaminant" proteins that were enriched in human D fractions, but not in mouse fractions (Sup. Figure 3-8E). Second, all septin proteins measured were enriched in mouse D and P fractions, but not in human fractions (Sup. Figure 3-8F)

Figure 3-4. **Representative dilution curves.** A human total homogenate fraction (H) **was** mixed with the $[^{13}C_6]$brain ISTD in the following ratios (μg): 1/19, 3/17. 10/10, 17/3 and 19/1. These preparations were analyzed by LC-SRM/MS in duplicate and the prepared L/H ratio plotted against the observed average L/H peptide ratio (peptide measure) for each protein. This figure show's representative curves for CaMKIIα, CDK5, NR1 and PSD95. The 19/1 point is not shown to highlight the midrange of the curve, but does not deviate from the slope reported here.

The enrichment values were heavily processed prior to hierarchical clustering. To more closely investigate the similarities and differences between human and mouse preparations, we compared the average enrichment values for the protein groups identified by the clustering analysis in V and D. In the V fraction, enrichment values for vesicular proteins were more similar to each other in mice, as compared to humans (Figure 3-6B &

D). In D, enrichment values for kinases, scaffolding proteins and glutamate receptors were roughly twice as high in mouse (Figure 3-6C & E). A two-way ANOVA confirmed a significant interaction between species and the protein group for average enrichment value ($p < 0.0001$). Enrichment values for the "contaminant" proteins were, on average, 12-fold higher in the human D compared to mouse ($p = 0.022$), the most extreme of which was creatine kinase brain isoform with a 72-fold higher enrichment value (Sup. Figure 3-4A). The septins had, on average, 3-fold higher enrichment values in the mouse D compared to human D ($p = 0.017$) (Sup. Figure 3-5). Interestingly, we observed some reciprocal enrichment between the D and SF fractions for both of these protein families (Sup. Figures 3-4 and 3-5).

To test if postmortem interval (PMI) contributed to these differences, we analyzed D fractions prepared from mouse tissues with PMIs ranging from 0 to 16 h. Measures of "contaminant" proteins in D increased with PMI, while measures for glutamate receptors and scaffolding proteins decreased (Sup. Figure 3-4C & D). A two-way ANOVA confirmed a significant interaction between the two protein groups, PSD proteins vs. contaminants, over PMI ($p = .007$). The protein measures for the septins in fraction D, however, increased steadily to a PMI of 12 h, before decreasing after 16 h (Sup. Figure 3-5C).

5. Discussion

Deregulated synaptic activity is implicated in a host of neurological and psychiatric diseases, but strategies to address synaptic protein function in human postmortem brain tissues are limited. Many neuropsychiatric diseases, such as autism, depression and SCZ, are believed to arise from complex interactions between many synaptic signaling cascades in specific subcellular microdomains[74, 75, 88, 156-158], the remnants of which are present in the postmortem brain tissues of patients. Therefore, the ability to assess protein expression and trafficking events in postmortem brain tissue, with high precision and accuracy, is essential. Various MS-based proteomics strategies have been applied in rodent and non-human primate tissue, with limited application in postmortem human tissue[109, 111, 116, 155]. Here we report, for the first time, the targeted and precise relative quantification of over 150 synaptic proteins in 5 distinct sub-cellular preparations from

human postmortem brain tissues. This study demonstrates that the core protein components of synaptic microdomains are consistently enriched in biochemical fractions prepared from human tissue. Additionally, we identified proteins whose partitioning through fractionation is affected by PMI and other postmortem confounds. This validated fractionation – stable isotope dilution LC-SRM/MS methodology will further the investigation of synaptic function in a variety of neuropsychiatric diseases.

5.1   LC-SRM/MS

LC-SRM/MS with a $^{13}C_6$-brain ISTD allowed the simultaneous quantification of over 150 proteins with precision and reproducibility. We observed low variability in peptide measures over repeated injections (Sup. Figure 3-2) and preparations (Figure 3-2), as well as a high level of accuracy in protein quantification as assessed by multiple peptide SRMs (Figure 3-2), Western blot (Figure 3-3) and dilution curve (Figure 3-4). Although the analytic precision correlated with intensity of the analyte signal (R2 = 0.7), the median CV for peptide quantification was 4.3% with the majority of peptides < 10% across three orders of magnitude of signal intensity (Figure 3-2 and Sup. Figure 3-2). This compares favorably with other multiplexed protein quantification strategies. For example, antibody based protein arrays, when applied to similar protein preparations from human postmortem brain tissue, have an average CV of 14% (personal communication, Dr. Steve Arnold, unpublished data). The [$^{13}C_6$]-brain ISTD was critical for this high precision over such a large dynamic range. This standard is prepared from [$^{13}C_6$]lysine SILAM mouse brain tissue, and thus contains labeled peptides at ratios close to those found in human brain tissues. To better approximate the protein levels we expected to observe in synaptic fractions, as well as to obtain a "simpler" standard proteome, we prepared a crude membrane fraction from the labeled mouse brain tissue to serve as the [$^{13}C_6$]-brain ISTD. This mouse [$^{13}C_6$]-brain ISTD was mixed with the intermediate membrane fraction from human brain 1:2 (μg/μg), and a bottom up analysis was conducted on the mixed proteome following a simple gel fractionation, in order to verify protein levels between the proteomes, as well as to identify additional candidate peptide pairs for targeted SRM analysis. The results showed peptide pairs with

Figure 3-5. Overview of protein enrichment. Protein enrichment values were calculated for each protein in the SF, V, P and D fractions by normalizing measures in each fraction to protein measures in H. The averages of these values for each fraction were then taken for the three human and three mouse samples and CV%s calculated. A, reports the median CV% of protein enrichment values for each fraction. To sort out protein groups and fraction by enrichment value, unsupervised hierarchical clustering, with Pearson's Correlation as the similarity metric, was utilized. B, shows clustering analysis of the mouse fractions as a heat map, C, the human and D, the mouse and human together. E, is the legend for B, C and D, numbers are arbitrary normalized enrichment values. For full heat maps with protein rows labeled, see Appendix 3.
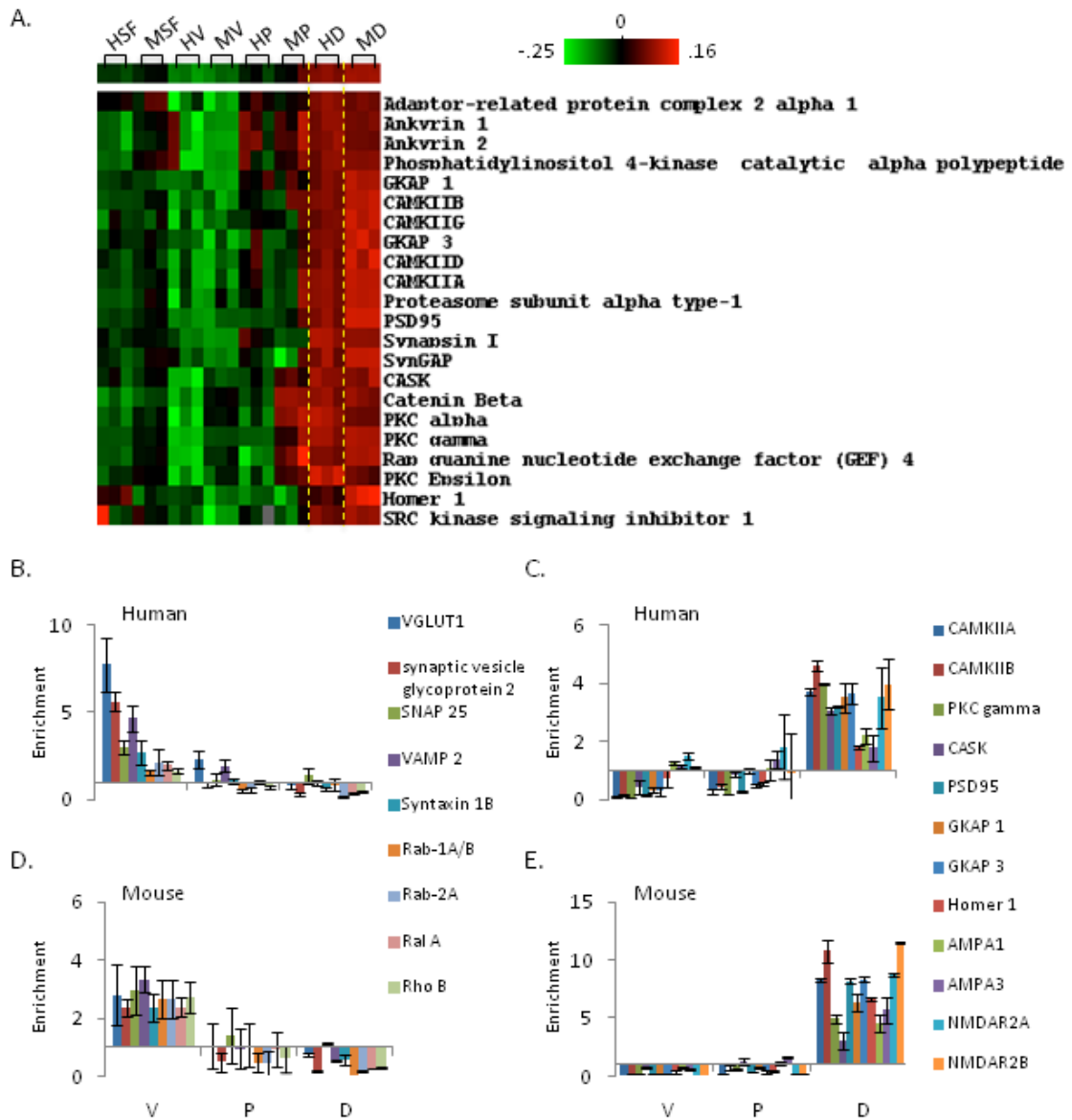
Figure 3-6. Comparison of human and mouse vesicular and postsynaptic density fractions. A, a zoomed-in image from Figure 4D, depicts enrichment of postsynaptic density proteins in D fractions prepared from human and mouse tissues. The Pearson's Correlation Coefficient for this grouping was .72. To more closely contrast human and mouse fractions, we compared enrichment values for a subset of the proteins grouped in the clustering analysis. B, shows enrichment of vesicular proteins in the human (V) fraction and D, those proteins in the mouse V fraction, while C and E show enrichment of kinases, scaffolding proteins and glutamate receptors in the human and mouse D fractions. Error bars are standard deviations of three individuals/animals. Note that in C and E, protein enrichment is higher in the fractions prepared from mouse tissue.

methodology will further the investigation of synaptic function in a variety of neuropsychiatric diseases.

5.1   LC-SRM/MS

LC-SRM/MS with a $^{13}C_6$-brain ISTD allowed the simultaneous quantification of over 150 proteins with precision and reproducibility. We observed low variability in peptide measures over repeated injections (Sup. Figure 3-2) and preparations (Figure 3-2), as well as a high level of accuracy in protein quantification as assessed by multiple peptide SRMs (Figure 3-2), Western blot (Figure 3-3) and dilution curve (Figure 3-4). Although the analytic precision correlated with intensity of the analyte signal (R2 = 0.7), the median CV for peptide quantification was 4.3% with the majority of peptides < 10% across three orders of magnitude of signal intensity (Figure 3-2 and Sup. Figure 3-2). This compares favorably with other multiplexed protein quantification strategies. For example, antibody based protein arrays, when applied to similar protein preparations from human postmortem brain tissue, have an average CV of 14% (personal communication, Dr. Steve Arnold, unpublished data). The $[^{13}C_6]$-brain ISTD was critical for this high precision over such a large dynamic range. This standard is prepared from $[^{13}C_6]$lysine SILAM mouse brain tissue, and thus contains labeled peptides at ratios close to those found in human brain tissues. To better approximate the protein levels we expected to observe in synaptic fractions, as well as to obtain a "simpler" standard proteome, we prepared a crude membrane fraction from the labeled mouse brain tissue to serve as the $[^{13}C_6]$-brain ISTD. This mouse $[^{13}C_6]$-brain ISTD was mixed with the intermediate membrane fraction from human brain 1:2 (μg/μg), and a bottom up analysis was conducted on the mixed proteome following a simple gel fractionation, in order to verify protein levels between the proteomes, as well as to identify additional candidate peptide pairs for targeted SRM analysis. The results showed peptide pairs with heavy/light ratios 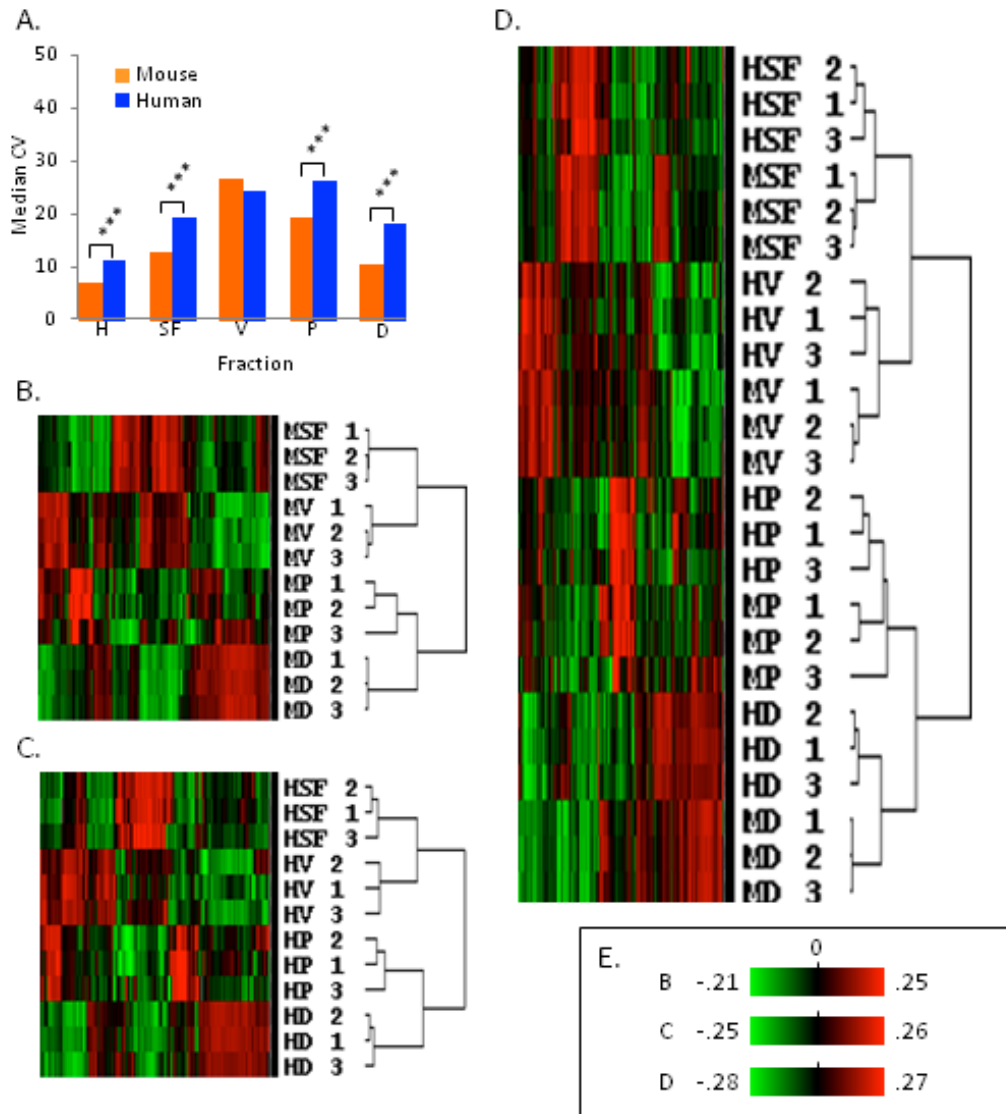ranging from .01 to 100 with a median of 0.27, below the prepared ratio of 0.5 (Supplemental Figure 3-1A). These discrepancies are unsurprising considering that different protocols were used to fractionate the tissues; the priority for human tissue

enrichment was purity, while the labeled mouse tissue was prepared with yield as the primary objective.

LC-SRM/MS analysis using a $[^{13}C_6]$ brain ISTD has several advantages over multi-dimensional separation tandem MS strategies for protein quantification by several of the criteria laid out in Chapter 1. First, time requirements for both experiment and data analysis are greatly reduced. Sample preparation time is reduced, as compared to strong cation exchange, since gel fractionation yield a minimal number of fractions and allows for multiplexed sample preparations within a single gel. Indeed, it is likely that for relatively "simple" proteomes, the first dimension of separation could be omitted. Gradients for SRM/MS are much shorter than tandem MS approaches in which full MS/MS data for peptide identification must be collected. Software, such as Pinpoint and Skyline, has streamlined peptide SRM design, validation and analysis. We validated 189 proteins for LC-SRM/MS quantification with the $[^{13}C_6]$ brain ISTD. This number is dwarfed by multi-dimensional separation tandem MS strategies that utilize labeled ISTDs or isobaric labeling. However, our bioinformatics analysis indicates that this strategy could theoretically be applied to 1152/1189 synaptic proteins (Figure 3-7), 1024 of which have peptides (proteotypic, ending in lysine, $6 \leq$ length ≤ 25) that have been identified in the NIST peptide database. As these libraries grow from incorporation of our own and others' discovery data, so will the number of proteins that can be assayed. Additionally, this methodology will allow researchers to target specific protein families and/or pathways. Posttranslational modifications are often present in low amounts and can only be assayed by the observation of a specific peptide, while proteins can be quantified by numerous peptides. Thus, multi-dimensional separation tandem MS strategies can be ill suited for the reproducible quantification of protein posttranslational modification compared to the targeted peptide SRM strategies.

5.2   Comparison of preparations from mouse and human tissues

Chapter 2 reported that postsynaptic densities could be fractionated from the majority of human postmortem brain tissues[153]. Here, I utilized the accuracy and precision of LC-SRM/MS with a $[^{13}C_6]$-brain ISTD to further examine the reproducibility

of subcellular fractionation in human postmortem brain tissue. I compared the relative enrichment of over 150 proteins in 4 fractions (SF, V, P & D) prepared from the prefrontal cortexes of three human subjects and the brain tissues of three mice (Figure 3-1).

Mouse brains, flash frozen on dry ice immediately after dissection, are mostly free of the postmortem confounds, as well as individual variability, inherent to human brains. In these tissues the median variability of protein enrichment was under 30% for all fractions (Supplemental Figure 3-3). Unsupervised hierarchical clustering of proteins and fractions by enrichment values revealed tight grouping of fraction types (Figure 3-5B). The clustering analysis also returned enriched protein groups in line with current views of synaptic architecture (see Results). Despite the fact that the P fraction from mouse #3 was identified as an outlier, it still clustered with the other two P fractions (Sup. Figure 3-6A), demonstrating the power gained from comparing multiple protein measures.

Human and mouse preparations were compared by enrichment value variability, hierarchical clustering and relative enrichment levels. Variance in protein expression and enrichment values tended to be smaller in preparations from mouse tissue (Figure 3-5A, Sup. Figure 3-3). Considering the individual variability in the humans from which tissue was derived, most notably age (70, 72 & 98), sex (2F, 1M) and PMI (4, 10 and 15 hours), protein enrichment in human fractions should be considered rather consistent. Hierarchal clustering also revealed a striking similarity in enrichment patterns between the same fractions prepared from different species, while highlighting some key differences (Figure 3-5D). The enrichments that drove this clustering were composed of well-documented synaptic molecules (Sup. Figure 3-8). Subcellular fractions prepared from human tissue are consistently enriched for key synaptic proteins in a manner similar to mouse tissue, suggesting that the core protein complexes that make up these microdomains are relatively intact in human postmortem brain despite biochemical procedures for fractionation. Indeed, our group has previously shown that protein-protein

interactions at PSD95, a central protein in postsynaptic protein complexes, are preserved in human brain tissue and survive biochemical fractionation[153].

I observed distinct differences between flash frozen mouse and postmortem human brain tissues. First, although PSD proteins were enriched in D fractions from both species, the enrichment values were 2x higher in fractions prepared from mice (Figure 3-6). I also identified a subset of "contaminant" proteins enriched in D fractions prepared from humans, but not from mice (Sup. Figures 3-4 and 3-8). Interestingly, some of these proteins were enriched in SF fractions from mice, but none were enriched in human SF (Sup. Figures 3-4B and 3-8). These proteins are diverse in both function and cellular localization, suggesting tissue degradation over PMI could cause co-enrichment in the D fraction, diluting the relative amount of postsynaptic density proteins. Experiments with D fractions prepared from mouse brain tissues with simulated PMIs support this assertion. I observed increased amounts of these "contaminant" proteins with decreased amounts of postsynaptic density proteins as PMI increased (Supplemental Figure 3-4C & D). Finally, septin proteins were enriched in the D and P fractions from mice, but not from humans (Supplemental Figures 3-5 and 3-8). Septins are conserved eukaryotic proteins that form cytoskeleton components that provide membrane rigidity and create barriers between subcellular domains in many cell types, including neurons[167]. Additionally, more specialized roles for individual septin family members have been identified on both sides of the synapse. For example, Septin 5 has been shown to inhibit vesicle exocytosis by interacting directly with the SNARE complex[168, 169], while Septin 11 plays a functional role in dendritic arborization of GABAergic synapses[170]. PMI could not explain the differences in enrichment as septin proteins increased with PMI, in contrast to the observations in human tissue (Supplemental Figure 3-5C). While individual septins have known roles at the synapse, the septin cytoskeletons have not been observed to associate tightly with postsynaptic protein complexes[114, 133, 156]. In addition to PMI, another difference between mouse and human tissue is the ratio of white to grey matter. Human cortex samples are cut to maximize the amount of grey matter in the tissue sample, while it is not possible to separate the two in mouse brain. I suspect

this composition of human tissue yields a more pure D fraction in terms of septin contamination. Further experiments, ideally in grey matter dissected from fresh-frozen non-human primate tissue, are required to confirm this hypothesis.

Neuropsychiatric illnesses are associated with alterations in synaptic biology, which involve a multitude of proteins and signaling mechanisms in a microdomain-specific manner. The ability to assay the proteomes of synaptic microdomains, in which disease factors may converge, is essential to advancing our understanding of these illnesses. Here, I have validated a fractionation – stable isotope dilution LC-MS methodology for the precise and targeted quantitation of over 150 synaptic proteins in subcellular fractions prepared from human postmortem brain tissue. Additionally, we have demonstrated that this method has the potential to be expanded to >1000 synaptic proteins. Thus, this study represents the essential first step in bringing targeted proteomic strategies to bear on the study of neuropsychiatric disease in human brain tissue.
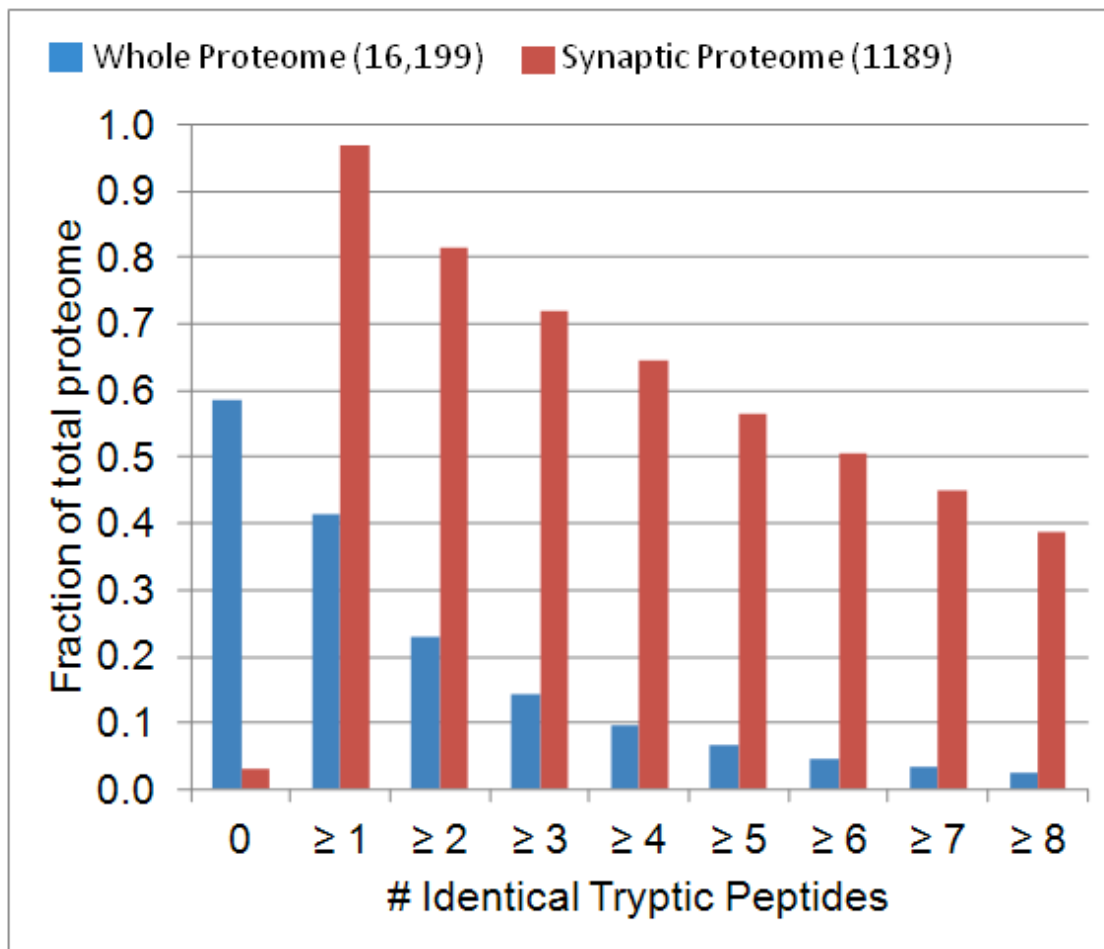
Figure 3-7. Comparison of human and mouse protein sequences. Protein sequences were retrieved for human and mouse homologenes from the total proteome and a representative synaptic proteome. Lysine-containing peptides, between 6 and 25 amino acids in length, were compared between the two species. This analysis shows that the $[^{13}C_6]$brain ISTD can theoretically be used to quantify 80% of the human synaptic proteins identified by more than two peptides. Additionally, the vast majority of these synaptic proteins have peptides in the NIST Libraries of Peptide Tandem Mass Spectra.

CHAPTER FOUR
ALTERED PARTITIONING OF POSTSYNAPTIC DENSITY COMPLEXES IN SCHIZOPHRENIA

1. Abstract

Several lines of evidence point to the PSD as point of convergence for SCZ genetic risk factors. PSD signaling is crucial for regulating NMDA rector function, which is perturbed in SCZ and believed to underlie aberrant plasticity. Additionally, decreased dendritic spine density has been consistently observed in layers 2 and 3 of the DLPFC in SCZ patients. Decreased PSD protein expression seems a likely correlate for decreased spine density, while alter PSD complex protein composition could contribute to NMDA receptor hypofunction in the DLPFC of SCZ. Interesting, investigations by traditional methods, qPCR, Western blot and *in-situ* hybridization, have not consistently observed decreased PSD protein expression and few studies have investigated the protein composition of synaptic microdomains in postmortem tissues.

To investigate PSD protein expression and partitioning, the biochemical fractionation - $[^{13}C_6]$-brain ISTD - LC-SRM/MS method, developed and validated in Chapter 3, was utilized. 185 proteins were quantified in whole tissue homogenates prepared from 15 pairs of SCZ subjects and matched controls. 107 proteins were quantified in PSD enrichments from 9 pairs. Protein expression was largely unaltered between SCZ and control tissues, while enrichment of PSD proteins was elevated in preparations from SCZ subjects. Despite this enrichment, the relative amounts of postsynaptic proteins, normalized to PSD95, was unaltered between the two groups. These changes could not be attributed to neuroleptics effects, assayed in the PFC tissue of rhesus monkeys and did not correlate with PMI or subject age. These data suggest that partitioning, not expression, of PSD complex proteins is the major molecular correlate of decreased spine density in the LPFC of SCZ.

2. Introduction

Several lines of evidence point to the PSD as a microdomain that will be critical for the pathophysiology of SCZ: **1)** NR hypofunction is widely believed to be a key component for the pathophysiology of SCZ, hypothesized to be present both throughout development and in the tissue of elderly patients[6, 72, 78, 88]. Given that NR complexes are highly concentrated in the PSD[129, 146] and NR activity is critically modulated by PSD protein composition[44, 59], it is highly likely that such functional dysregulation of NRs is

associated with altered PSD protein compositions and/or interactions. **2)** Several SCZ risk genes, e.g. ErbB4, NRG1, RGS4 and DISC1 directly impact NR signaling at the PSD[72, 74, 77, 88], implicating the PSD as a point of convergence for genetic factors. **3)** NR and PSD complexes are localized to the spines of excitatory synapses. Decreased spine density has been observed in layers 2 and 3 of the DLPFC without neuronal loss[35, 36, 43]. Decreased spine density is likely the result of perturbed neuroplasticity caused by NR hypofunction[94, 171]. Thus, dysregulated PSD protein expression and partitioning could be both cause and consequence of SCZ disease processes. NR hypofunction and the genetics of disease risk implicate altered PSD protein dynamics, as a *cause* of dysfunctional neuroplasticity, while decreased spine density, believed to be the *consequence* of dysfunctional neuroplasticity, suggests that PSD protein expression should be decreased in the DLPFC.

A myriad of strategies have been employed to investigate postsynaptic protein and transcript levels in the PFC tissues of SCZ subjects in an effort to observe the predicted molecular dysregulations. However, the results of these studies have been contradictory (See Table 1-1 for a review of recent findings). While many groups observe no difference in protein expression between control and disease tissues, other groups report small differences in one or two mRNA transcripts[97-105], but often with low statistical significance, and without controlling for multiple hypothesis testing. Presently, there are no consistently observed changes in mRNA or protein expression of PSD proteins in SCZ.

This lack of consistent observations is perhaps not surprising considering the complexity of predicted synaptic protein expression and partitioning changes, as well as the technical hurdles protein and mRNA strategies must overcome to measure them. Histological studies have the advantage of being able to visualize the object of study (the spine) allowing for unit quantification and a spatial resolution not achievable in other molecular assays such as Western blot, real-time PCR and microarray. As for mRNA quantification, great progress has been made in resolving cortical layers and neuronal sub-populations[106-108]. However, while the results of these studies are extremely informative, they may not be reflective of protein levels in whole cells or spines of

human postmortem tissue. Likewise immunohistochemistry has special resolution for protein amounts, but is limited in the number of proteins that can be assayed.

Inconsistencies between mRNA and protein findings in the DLPFC of SCZ patients could be explained by the following: **1)** Current approaches lack the sensitivity, spatial resolution and, in the case of protein assays, multiplexed capability to observe the altered protein expression expected to parallel decreased spine density and NR function. **2)** The predicted molecular correlates of decreased spine density and NR activity are not manifested in mRNA and/or protein expression levels, but in altered partitioning, interactions and posttranslational modifications. **3)** Both **1** and **2**. That is, protein expression is unaltered and current approaches lack the precision and resolution to confirm the null hypothesis with high confidence.

Clearly, approaches with enhanced sensitivity, spatial resolution and multiplexed capability, among other methodological improvements are required to overcome these technical issues and elucidate the molecular correlates of decreased dendritic spine and NR hypofunction. This study represents an attempt to address some of these technical issues and perform a more thorough search for molecular perturbations in the PFC of SCZ. Here, biochemical fractionation and $[^{13}C_6]$-brain ISTD-LC-SRM/MS were utilized for the multiplexed quantification of over 200 synaptic proteins in whole tissue homogenates and over 100 proteins in biochemical PSD enrichments. This approach allowed for the precise, accurate and multiplexed quantification of synaptic protein expression and partitioning to the PSD. While this method has spatial resolution for a synaptic microdomain, the PSD, it cannot resolve between cortical layers or neuronal subtypes. Thus the experiments described below represent a first step in deciphering the molecular complexity of the synapse in SCZ.

Figure 4-1. Subject age and postmortem interval. A, shows subject postmortem interval (PMI) in hours (h). **B**, shows subject age in years (y).

3. Materials and Methods

65

3.1   Human lateral frontal cortex tissue

Psychiatric subjects met Diagnostic and Statistical Manual of Mental Disorders Fourth Edition (DSM-IV) diagnostic criteria for SCZ. Diagnosis was determined by consensus of at least two board-certified research psychiatrists after comprehensive review of medical records, direct clinical assessments and interviews with caregivers. Autopsy consent was obtained from the next of kin or a legal guardian in all cases, based on a protocol approved by the Institutional Review Board at the University of Pennsylvania. Control and psychiatric subjects were matched for sex, age, smoking history and postmortem interval (Sup. Table 4-1 and Figure 4-1).

3.2   Rhesus monkey PFC tissue

Dr. Scott Hemby (Wake Forrest University) generously supplied DLPFC tissue from rhesus monkeys treated with treated with different neuroleptics for six months: clozapine (5.2 mg/kg daily dose), low does haloperidol (0.14 mg/kg daily dose), high dose haloperidol (2.0 mg/kg twice daily) and vehicle. Each group consisted of five males and five females with the exception of the high haloperidol group, which had four of each. These animals are extensively described elsewhere [172]. Only tissue from the male animals was utilized for the experiments described here, while the females will be analyzed at a later date.

3.3   Biochemical fractionation

Whole tissue homogenates and PSD enrichments from the lateral PFC (LPFC) of 30 subjects were prepared in three batches (Sup. Table 4-1). Batch 1 was prepared using a variation of the protocol described in Chapter 3, section 3.2, that omitted the 2500 RPM spin after the homogenization step. Batch 2 was prepared using the protocol described in Chapter 3, section 3.2. Due tissue amount limitations, the remaining human tissue and all rhesus monkey tissues were processed using an abridged protocol:

50 mg grey matter was homogenized in .5 ml solution A (0.32 M sucrose, 1mM $MgCl_2$ and 0.1mM $CaCl_2$) with a Teflon pestle. ~ 45 µl of the homogenate (H) was saved, solubilized with 1% SDS and clarified by centrifugation. The remaining homogenate was centrifuged at 1,000 x g for 10 min to remove nuclei and incompletely homogenize material. The pellet was discarded and the supernatant (S1) centrifuged at

10,000 x g for 15 min. The Pellet (P2) was suspended in 120 μl solution A, to which 960 μl .5% Triton X-100 solution (10 mM Tris pH 7.4, 1 mM EDTA, 1mM EGTA) was added. This mixture was agitated at 4°C for 20 min and then centrifuged at 36,000 RPM for 20 min. The supernatant (S3) was saved and the pellet (P3) suspended in .5 ml 1 % Triton X-100 buffer (10 mM Tris pH 7.4, 1 mM EDTA, 1mM EGTA) by pipetting and probe sonication (three times for 5 seconds on low setting). The mixture was then agitated at 4°C for 30 min and centrifuged at 36,000 RPM for 30 min. The supernatant (S4) was saved and the pellet (P4), enriched for the PSD, was dissolved in 200 μl 20 mM Tris pH 7.4 with 1% SDS. All solutions were supplemented with 1 x protease and phosphate inhibitor cocktails (Sigma) as well as 1 mM sodium fluoride and sodium orthovanidate (Sigma). See Supplemental Figure 4-1 for a comparison of representative PSD and presynaptic protein enrichments from these preparations and those from Chapter 3.

Total protein amounts in all preparations were quantified with the micro BCA assay in duplicate (Pierce). Success of PSD enrichment was assessed post hoc by LC-SRM/MS.

3.3   Sample preparation and LC-SRM/MS:

10 μg PSD enrichments and 20 μg whole tissue homogenate preparations were mixed with the $[^{13}C_6]$ brain ISTD at a ratio of 1:1 (μg/μg) and processed for LC-SRM/MS analysis as described in Chapter 3, section 3.3, but with one difference. After separation on a 1.5 mm 4-12% Bis-Tris Gel (Invitrogen), the lane was divided into two fractions at the 64 kDa marker.

LC-SRM/MS was conducted as described in Chapter 3, section 3.4, with an expanded set of transitions. Subsequent to the experiments described in Chapter 3, additional data sets became available and additional proteins of interest were identified by parallel projects in the Hahn Lab. As of writing, peptide-SRMs for over 200 proteins have been validated. The development of these additional SRMs drew upon the NIST and PeptideAtlas databases (Ref), along with a recent 2DLC-MS/MS analysis of mouse synaptic membrane enrichments performed in Dr. Steve Seeholzers laboratory (Seeholzer and Kalb unpublished). Human PSD enrichments and homogenates were first assayed for

a subset of these proteins. This subset included 127 synaptic proteins (Sup. Table 4-3, Appendix 2) that were either found to be enriched in the PSD (see Chapter 3) or are known to have postsynaptic roles. For example, a majority of G protein subunits was neither enriched nor un-enriched in PSD fractions, but are known to be active in postsynaptic processes (Ref). A handful of presynaptic molecules were also included to assess purity of PSD enrichments. The homogenate peptide preparations were also assayed in a separate LC-SRM/MS run for an additional set of 96 non-PSD neuronal proteins (Sup. Table 4-4, Appendix 2).

3.5   Data processing, informatics and statistics

LC-SRM/MS data was processed as described in Chapter 3, section 3.7, as was calculation of protein amount and protein enrichment values.

Success of biochemical fractionation was assessed by investigation of enrichment values for the PSD proteins NR1, PSD95 and CaMKIIα, as well as the SNARE complex proteins synapsin 2, syntaxin 1B, syntaxin binding protein and synaptobrevin (VAMP). Subjects for which the two of three PSD protein enrichment values were below 2 and/or two of the four SNARE complex enrichment values were at or above 1 were dropped from analysis (calculations not shown).

Three types of data sets were generated from LC-SRM/MS analyses of human and rhesus monkey PFC preparations: 1) Protein measures in total homogenate preparations, 2) Protein measures in PSD fractions, and 3) Protein enrichment values. Total homogenate protein measures were normalized to beta tubulin. The rationale for this choice and the associated caveats are considered in section 5.2 of the discussion. PSD protein measures were normalized over PSD95 to assess the relative ratios of core PSD proteins. As in Chapter 3, section 3.7, protein enrichment values were the [PSD protein measures] / [total homogenate protein measures] without the introduction of an additional normalization factor.

Outlier subjects or animals were identified by manual inspection for the number of individual protein or enrichment value outliers and principle component analysis of the entire dataset, run as a plug-in in Excel. Normalized protein or enrichment value outliers were defined as > [(Group Mean) + (2 * standard deviation)]. Principle component

outliers were defined as a subject or animal having two (or more) vector values greater than two standard deviations away from the vector mean. In the event that a subject or animal was identified as an outlier by either of these methods, it was only dropped from analysis provided that its absence did not affect the assignment of significance in all data analyses (calculations not shown).

The enrichment and expression datasets were processed in a similar fashion: To begin, the average of protein measures (or protein enrichment values) for each group (SCZ and CTL) were calculated in Excel, and the distribution of these averages plotted in GraphPad Prism 5. The ratio of the SCZ average over the control average (SCZ/CTL) was calculated for each protein, and the distribution of these ratios plotted.   The distribution shape range, mean and median was considered in evaluation of the dataset and evaluation of normalizing factors. As a preliminary evaluation, two-tailed Students t-test was used to assign P-values to individual proteins for between-group differences (SCZ vs CTL). Proteins were then ranked by P-value. Proteins with a P-value < .2 were identified and divided into two groups based by SCZ/CTL ratio: > 1 and < 1. The ranked protein lists were then submitted, as a list of official gene symbols, to the DAVID Functional Annotation Tool, and searched for Kegg pathway and gene ontology (GO) term enrichment. The full list of quantified proteins, submitted as non-redundant International Protein Index (IPI) identification numbers, served as the background. The results of this analysis were used to inform the grouping of proteins by direction of regulation and functional annotation for further analysis. Two-way ANOVA in GraphPad Prism 5 was used to assign significance of diagnosis (human) or drug (rhesus monkey) effect on protein measures or enrichment values for identified protein groups. Considering the relatively loose criteria used to group the proteins and the propensity for Type I errors in postmortem experiments, a Bonferroni correction was employed in assigning diagnosis or drug effect significance to grouped protein values. 17 two-way ANOVAs were run on data from experiments in humans and 17 on data from experiments in rhesus monkeys, so P-values for assigning significance were set at .0029 (.05/17). P-values determined by T-test for individual protein regulation are reported, but are not discussed in terms of significance.

Correlations between subject PMI, age and significantly regulated protein values were assessed in GraphPad Prism 5. Only the subset of data generated from rhesus monkey tissue experiments, required to control for neuroleptic drug effects, are reported here.

Unsupervised hierarchical clustering was performed on a manually selected subset of non-normalized protein values from human total homogenates, human PSD enrichments and rhesus monkey PSD enrichments as described in Chapter 3, section 3.7.

4. Results

4.1 Protein levels in whole tissue homogenates

223 proteins were quantified in whole tissue homogenates derived from the LPFC of 15 SCZ subjects and matched controls. Of these, 185 met the criteria described in Chapter 3 for inclusion in analysis (Sup. Table 4-5, Appendix 2). Sample #2 (batch 1) showed inconstancies in HPLC; irregular peptide retention times were observed despite retiming of the method and multiple LC-SRM/MS runs, requiring the exclusion of sample #2 from analysis.

Initial analysis began with plotting distributions of average beta tubulin-normalized protein values for each group (SCZ and CTL). Distribution of average normalized protein values was highly similar between SCZ and control (Sup. Figure 4-2 A&D). Next the ratio of these averages (SCZ/CTL) was taken and the distribution of these values plotted. The ratios (SCZ/CTL) of average normalized expression values fell over a normal distribution, ranging from .5 to 1.3 with a median and mean of 1.03 (Figure 4-2A). Of these, twelve were up-regulated in SCZ with a $P < .2$ (Figure 4-2D). Proteins with the GO terms *macromolecule catabolic process* (GO:0009057 $P = .004$) and *protein amino acid autophosphorylation* (GO:0046777, $P = .0015$), were significantly enriched against a background of 185 IPI entries. Based on this analysis and a manual inspection of these data the regulation of all assayed members of the CaMKII family (α, β, δ and γ) were assessed as a group by two-way ANOVA as were ubiquitin enzymes and proteasome subunits. CaMKIIs were significantly increased as a group ($P = .0002$, Figure 4-2B), as were the proteolysis pathway enzymes proteasome subunit alpha-1

70

D.

P	SCZ/CTL	OGS
0.0096	1.33	PSMA1
0.0202	1.31	CAMK2A
0.0217	1.25	CAMK2B
0.0365	1.33	GRIN2B
0.0786	1.20	UCHL1
0.0894	1.18	UBR4
0.1419	1.19	CAMK2G
0.1465	1.10	CDK5
0.1486	1.19	KCTD12
0.1593	0.79	VIM
0.1789	1.14	PRKACA
0.1914	1.14	VAMP2
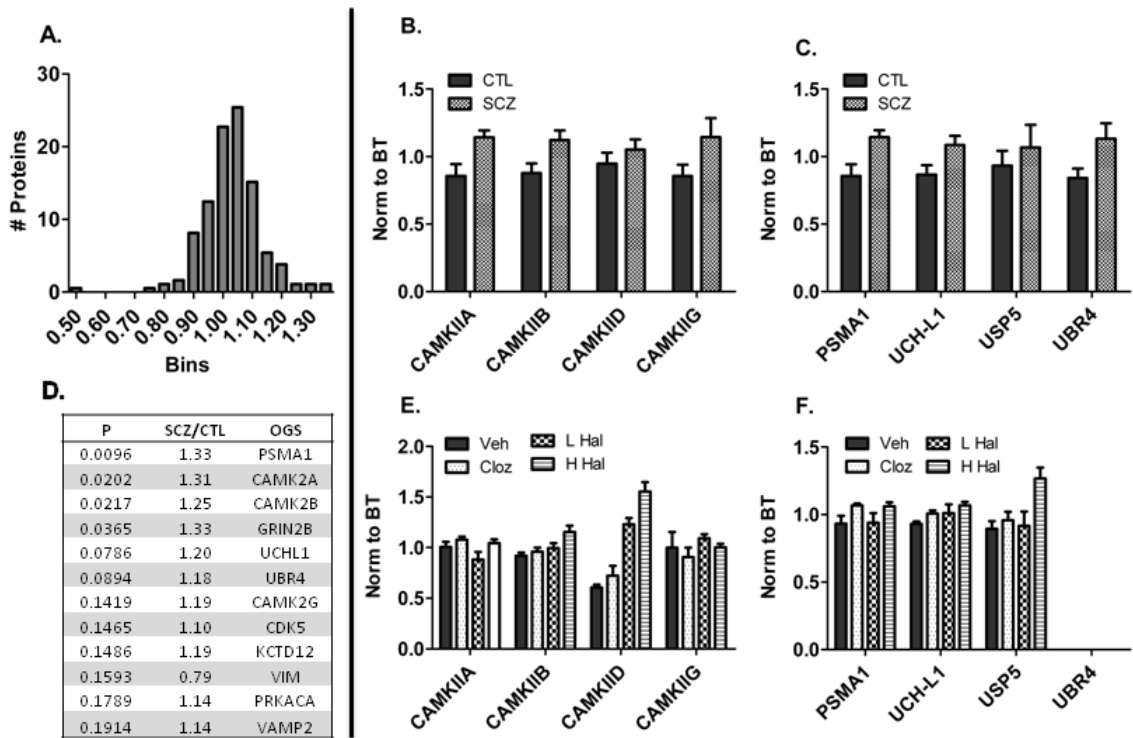
Figure 4-2. Differentially expressed proteins in the schizophrenic LPFC. Quantitative measures of 222 proteins, normalized to beta tubulin, were assessed in whole tissue homogenates prepared from the LPFC of 15 schizophrenic subjects and matched controls and rhesus monkeys treated with neuroleptics. The average protein measure was taken for each group and the schizophrenia average divided by the control average (SCZ/CTL) to obtain a ratio of dysregulation for each protein. **A**, shows the distribution of these dysregulation ratios. The tight normal distribution about the mean/median (1.03) is reflective of the low number of different protein levels between the two groups. **D**, lists the proteins whose between group difference has a P-value < .2. *P = P-value, two-tails T-test, SCZ/CTL = average schizophrenia protein value / average control protein value, OGS = Official Gene Symbol*. **B** and **C**, show average normalized values for CaMKII (B) and proteolytic (C) proteins in human samples, while **E** and **F**, show the same values in tissues from rhesus monkeys. *CTL = control subjects, SCZ = schizophrenia, Veh = vehicle, Cloz = , L Hal = low dose haloperidol and H Hal = high dose haloperidol.* Error bars are standard error of the mean.

(PSMA1), E3 ubiquitin-protein ligase (UBR4), ubiquitin isopeptidase T (USP5) and ubiquitin carboxyl-terminal esterase L1 (UCH-L1) (P = .0012, Figure 4-2C).

To control for antipsychotic drug effects, the expression of these proteins was assessed in total homogenate fractions from rhesus monkeys treated with clozapine, low haloperidol, high haloperidol or vehicle for six months. While CaMKIIδ was significantly up-regulated by both doses of haloperidol, none of the antipsychotics induced the broad

increase of CaMKII proteins observed in SCZ tissue (Figure 4-2E). Antipsychotic drug treatment had a significant effect on proteasome pathway protein levels (P = .0002). Both clozapine and high haloperidol induced a small increase in PSMA1 and USP5 levels. High haloperidol induced a greater up-regulation of USP5, as compared to other regulations observed in this group. Neither PMI nor age correlated with amounts of these proteins in human tissue (Sup. Figure 4-5).

4.2   PSD protein enrichment

Enrichments from 9 control and 8 SCZ subjects, representing 8 pairs and one orphan control subject from batches 2 and 3, and all enrichments from rhesus monkey tissue met the criteria for inclusion described above. 107 synaptic proteins were quantified in these PSD preparations (Sup. Table 4-3, Appendix 2). Enrichment values for 104 of the synaptic proteins were calculated (Sup. Table 4-6, Appendix 2). In light of potential confounds due to the different protocols used to enrich PSD fractions in batches 2 and 3, data analysis was performed on the six pairs from batch 3 as a stand-alone data set (referred to henceforth as "6 pairs") and on batches 2 and 3 together (referred to henceforth as "9 pairs"). Batch 2 consisted of only three pairs, lacking the statistical power to be considered alone.

Principle component analysis did not identify any subject or animal as an outlier (data not shown), but enrichment values for the majority of PSD proteins in sample #22 were outliers when considered in the context of 9 pairs, but not of 6 pairs. The removal of this sample (#22) from the 9 pairs dataset did not alter the statistical outcome of any of the analyses detailed below. For these reasons, sample #22 was dropped from the 9 pairs analysis.

The ratio (SCZ/CTL) of average enrichment values for 6 pairs ranged from .23 to 1.64 in a graphical shape suggesting an asymmetrical bimodal distribution (Sup Figure 4-3A). The median and mean were 1.05. Of the 6 pairs enrichment values, 22 were elevated and 10 were decreased in SCZ as compared to controls with a P < .2 (Sup. Tables 4-2A & B). The ratio (SCZ/CTL) of average enrichment values for 9 pairs fell over a more symmetrical distribution than that of 6 pairs, ranging from .44 to 2.07 with a median and mean of 1.3 (Sup. Figure 4-3C). Of the 9 pairs enrichment values, 29 had
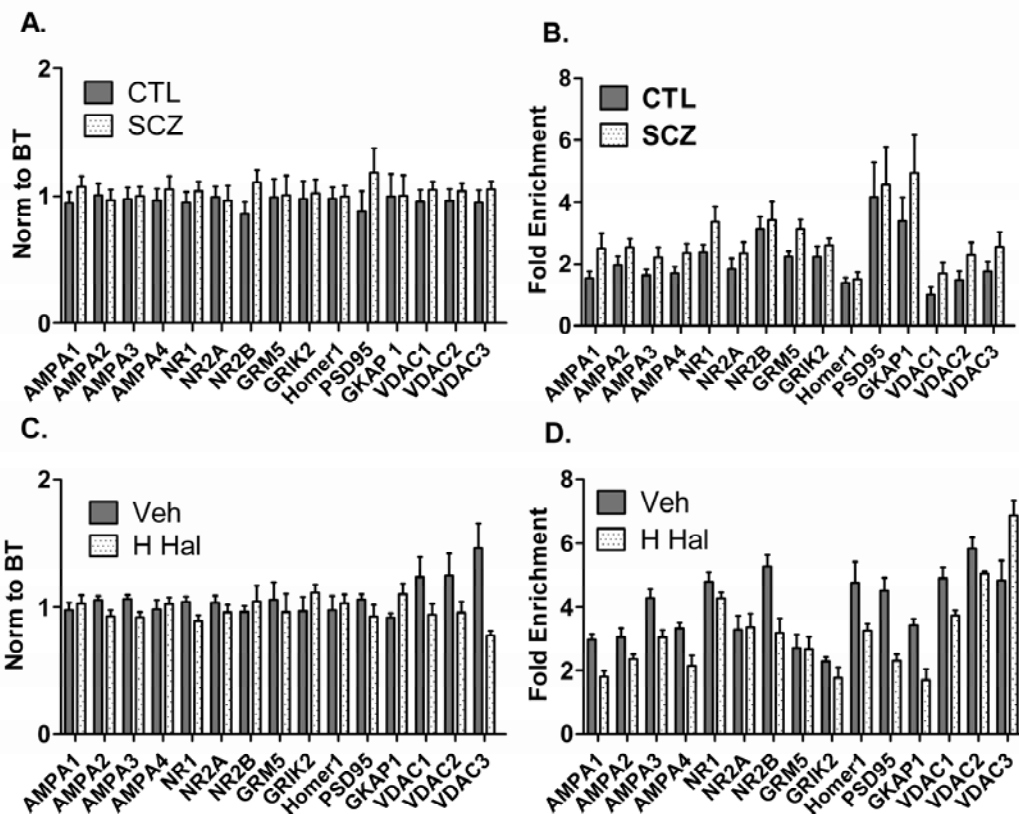
Figure 4-3. Enrichment, but not amount, of postsynaptic glutamate receptors and scaffolding proteins is altered in the LPFC of schizophrenia subjects. Biochemical fractions enriched for PSDs were prepared from the LPFC of 9 schizophrenic subjects and matched control and rhesus monkeys treated with different neuroleptics. Quantitative measures of 107 proteins were aszsayed therein by LC-SRM/MS. Enrichment values for 104 of these proteins were calculated by divideing un-normalized protein measures in PSD enrichments by un-normalized protein measures in whole cell homogenates. A, shows average beta tubulin-normalized protein measures from 15 pairs of human tissue. PSD protein levels, as a group, were not significantly impacted by diagnosis (P = .16), but NR2B did show a trend upward (P = .07). B, shows average protein enrichment values from 9 pairs of human tissue, which were significantly increased in PSD preparations from disease tissue, with average increase of 35% above control (P < .0001). C, shows average beta tubulin-normalized protein measures from rhesus monkey tissues. PSD protein levels, as a group, were not significantly impacted by neuroleptic treatment (P = .65), but NR1 was significantly decreased in H Hal (P = .03). D, shows average protein enrichment values from rhesus monkey tissues, which were significantly decreased by H Hal (P = .0076). Error bars are standard error of the mean. *CTL = control, SCZ = schizophrenia, Veh = vehicle, and H Hal = high dose haloperidol*

elevated enrichment values and 2 had depressed enrichment values with a P < .2 (Sup.

Figure 4-2C & D). Lists of elevated proteins from both data sets include glutamate

receptors, kinases and voltage-dependent anion channels, along with the occasional

scaffolding protein. Notably, both lists include all AMPA and NR subunits assayed (Sup. Tables 4-2 A & C). Proteins that were decreased in the 6 pairs included G-protein subunits (GNB1, GNAs and GNAi1), protein phosphatases (PPP1R7 and PPP2R1A) and SNARE complex proteins (SYN2, STX1B and STXBP1) (Sup Table 4-2 B). Pathway analysis in DAVID indicated that the group of proteins with enhanced PSD enrichment in SCZ patients (in the 9 pair cohort) was enriched for the functional annotation

Figure 4-4. Relative amounts of PSD proteins are similar in PSD enrichments from LPFCs of control and SCZ subjects. Biochemical fractions enriched for PSDs were prepared from the LPFC of 9 schizophrenic subjects and matched controls and rhesus monkeys treated with different neuroleptics and assayed by LC-SRM/MS. Quantitative measures of core PSD proteins were normalized to PSD95. **A**, shows average PSD95-normalized protein measures from human PSD enrichments. PSD protein levels, as a group, were not significantly impacted by diagnosis, but SAP97 did show a trend downward (P = .08). **B**, shows average PSD95-normalized protein measures from rhesus monkey PSD enrichments. The high dose of haloperidol (H Hal) induced significant changes to PSD protein levels (P < .0001). Error bars are standard error of the mean. *CTL = control, SCZ = schizophrenia, Veh = vehicle, and H Hal = high dose haloperidol*
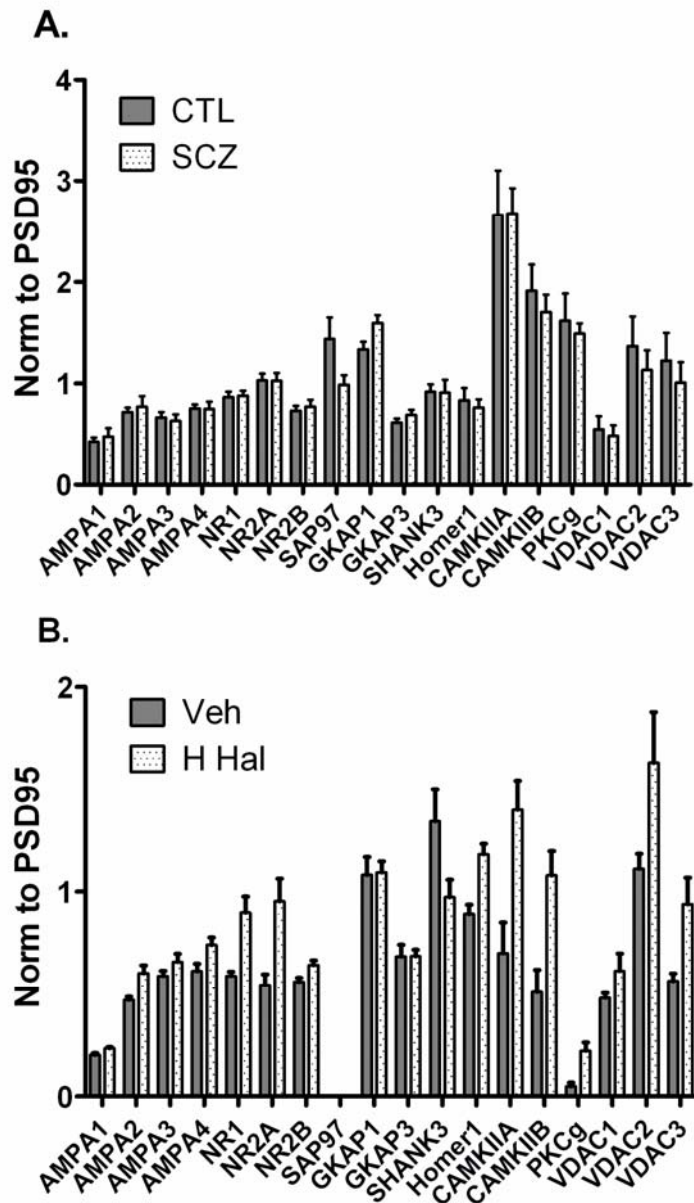
postsynaptic cell membrane (P = .0007).

Based on the preliminary analysis described above, biochemical enrichment values for postsynaptic glutamate receptors, scaffolding proteins and voltage-dependent cation channels were considered as a group. In analyses of both cohorts, diagnosis significantly impacted protein enrichment values (6 Pairs: P < .0001, 9 Pairs: P = .0003), all of which were elevated in PSD preparations from SCZ subjects, as compared to control subjects (Sup. Figure 4-3 D, Figure 4-3 B). Beta tubulin-normalized levels of these proteins in total homogenates were not significantly increased in SCZ patients in any of the three batches alone in combinations of batches (Figure 4-3A, 15 pairs), although NR2B did show a slight increase with and individual P-value of .07.

To determine if neuroleptic treatment could contribute to the observed increase in PSD protein enrichment, the impact of antipsychotic drug treatment on amount and enrichment of these PSD proteins in rhesus monkeys was assessed. Glutamate receptor and scaffolding protein amounts were unaffected by neuroleptics in whole tissue extracts (clozapine and low haloperidol data not shown; for high haloperidol see Figure 4-3C). Voltage-dependent cation channel expression was decreased in all three antipsychotic treatment groups (P = .0005; independent group analysis not shown). In stark contrast to alterations seen in postmortem tissue of SCZ patients, high dose haloperidol decreased the enrichment values of 12 out of 15 postsynaptic proteins in PSD preparations (P = < .0001, Figure 4-3D). Enrichment of VDAC3 was increased while NR2A and GRIM5 were unchanged. Clozapine and low haloperidol treatment did not result in altered enrichment of these proteins (data not shown).

Enrichment values for five additional manually configured protein groups were also investigated in PSD preparations from both human and rhesus monkey tissue. No significant differences were observed between disease and control preparations, while neuroleptics induced diverse and complicated changes. Enrichment of protein phosphatases, presynaptic proteins and septins were unchanged, ankyrins and spectrins were decreased (P = .0004) and neuronal adhesion molecules were increased by low dose haloperidol, while the high dose haloperidol animals showed either no change or a possible decrease (Sup. Figure 4-4).

75

Finally, PMI and age did not correlate with enrichment values for PSD or SNARE complex proteins (see supplementary figure 4-6 for representative histograms).

4.3   Relative amounts of core PSD proteins

To compare relative amounts of core PSD proteins in PSD enrichments, protein measures were normalized to PSD95 measures. No outlying subjects or animals were identified in this dataset. PSD95-normalized values for postsynaptic glutamate receptors, scaffolding proteins, kinases and voltage-dependent anion channels were compared in 9 pairs. The relative amounts of these proteins were nearly identical (Figure 4-4A), with the exception of SAP97, which trended down in the disease group ($P = .083$). No changes were seen in the clozapine and low haloperidol groups (data not shown), while high haloperidol significantly regulated PSD95-normalized values, inducing changes in both directions between the two groups ($P < .0001$, Figure 4-4B). PMI and age did not correlate with PSD95 normalized values of these proteins (Data not shown).

4.4   Unsupervised hierarchical clustering

Unsupervised hierarchical clustering was used to investigate whether relative protein composition could distinguish between disease and control PSD enrichments. Clustering analysis was performed using non-normalized values of selected proteins from 6 pairs. The full 9 pairs could not be used, as the clustering analysis was sensitive to the different enrichment protocols. The analysis returned a striking separation of disease and control subjects (Figure 4-5A), with only one individual "incorrectly" placed out of each group. An identical analysis of non-normalized values for the same proteins from whole cell homogenates was unable to distinguish between disease and control (Figure 4-5B). Interestingly, the segregation of PSD enrichments into two "correct" groupings appears to be driven not by core PSD proteins, but by a diverse group of protein phosphates, presynaptic proteins, GAD65, ankyrins and brain creatine kinase (Sup. Figure 7A). This constellation of relative changes in SCZ contrasts with clustering of vehicle and high dose haloperidol samples, in which parsing of animals is driven by relative differences between the core PSD proteins (Figure 4-5C, Sup Figure 4-7C). Thus, although PSD enrichments from disease subjects and haloperidol treated animals differ significantly

from their respective controls, the nature of this dysregulation is fundamentally dissimilar.

5. Discussion

In this study biochemical fractionation was combined with a quantitative and targeted proteomics approach to evaluate synaptic protein expression and partitioning in the LPFC of SCZ. 185 proteins were quantified in whole tissue homogenates prepared from 15 pairs of SCZ subjects and matched controls. 107 proteins were quantified in PSD enrichments from 9 pairs. This approach yielded a data set with the statistical power to make several highly significant observations. The power of this approach also allows for increased confidence in null results (the finding of few differences in protein expression between SCZ and controls). Four observations were made in these experiments: **1)** The vast majority of normalized protein levels was unaltered in disease tissue, with the exception of small (20%) but significant increases in

Figure 4-5. Hierarchical clustering separates subjects by diagnosis based on protein levels in PSD enrichments but not total homogenates. A. Unsupervised hierarchical clustering, with Pearson's Correlation as the similarity metric, was utilized to group subjects and selected PSD proteins by non-normalized protein values measured in PSD enrichments. SCZ and control were segregated into two groups with one exception. *C = control, S = schizophrenia*. **B,** shows an identical analysis of the same subjects and proteins using non-normalized protein values measured in whole tissue homogenates. *C = control, S = schizophrenia*. **C,** shows an identical analysis of the same subjects and proteins using non-normalized protein values measured in PSD enrichments from rhesus monkeys. *V = vehicle, HH = high does haloperidol.* The open and closed circles were added to enhance visual contrast between the two groups in each analysis. For an expanded version of these heat maps, with protein annotations, see supplemental Figure 4-7.

77
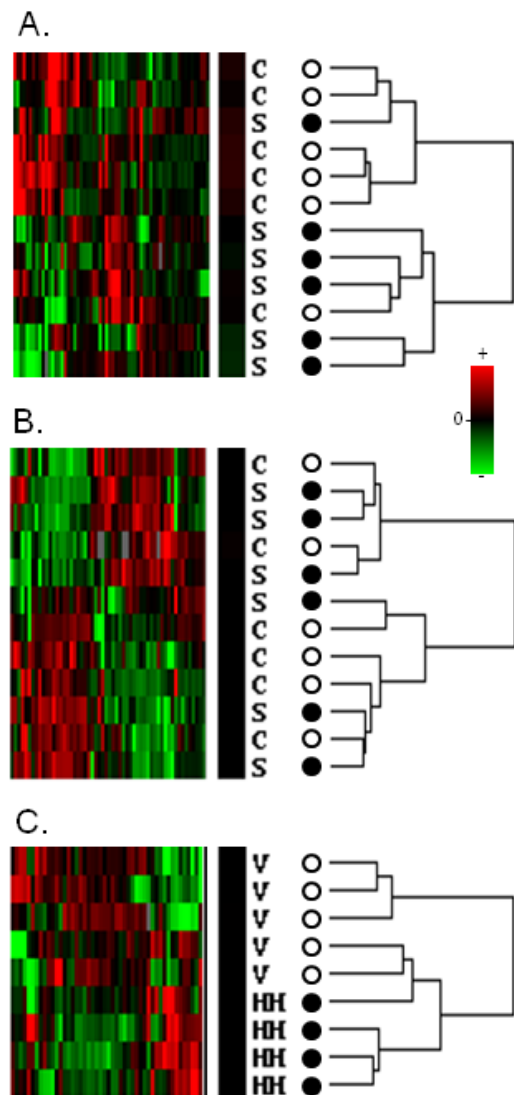
CAMKII and proteolytic pathway proteins (Figure 4-2). **2)** PSD glutamate receptors, scaffolding proteins and voltage-dependent cation channels were, on average, 40% more enriched in PSD preparations from the tissue of SCZ subjects as compared to control subjects (Figure 4-3), while the enrichment of ten other proteins group was unaltered. **3)** Despite the enrichment differences, amounts of postsynaptic glutamate receptors, scaffolding proteins, voltage-dependent cation channels and kinases, normalized to PSD95, were nearly identical in PSD enrichments from the two groups (Figure 4-4). **4)** The protein composition of PSD enrichments from SCZ samples was sufficiently different to allow for unsupervised hierarchal clustering to parse disease and control subjects with striking accuracy, using non-normalized protein values. These four observations strongly support the conclusion that partitioning, not expression, of PSD complex proteins is the major molecular correlate of decreased spine density in the LPFC of SCZ. However, several caveats need to be addressed to increase confidence in these findings. These caveats are addressed in the next section, before further discussion of the findings.

5.1   Planned experiments to address experimental caveats

1. Expanding human and rhesus monkey cohorts: Replicating these findings in an expanded cohort is essential. First, a minimum of 12 additional pairs, prepared in two batches of 6 using the abridged protocol, will be assayed and the samples from batch 2 removed from future analysis. This will result in a final N of at least 18 per group, with all samples prepared by an identical protocol. Additionally, the rhesus monkey cohort generously provided by Dr. Scott Hemby contains 19 more female animals, doubling the N for all groups. These animals will be prepared and analyzed as well.

2. Increasing options for normalization of protein expression: A constant concern with any expression study, in regards determining total protein levels in a given biological sample, is the choice of a loading control. Beta tubulin 3 is often the protein of choice for normalization in brain tissue. It is often used in protein and mRNA expression studies in human and animal brain tissue[173]. Indeed, a recent study of SCZ tissues with similar cytoarchitectural deficits utilized beta tubulin, concluding that it is unaltered in disease[174]. Additionally, multiple proteins and combinations of proteins were evaluated as

potential normalizing factors post hoc, all of them returning similar results. Indeed, relative sample-to-sample difference in protein value for the majority of the 185 proteins quantified mirrored beta tubulin, as is evidenced by the tight distribution of normalized protein values centered at a median/mean of 1.03 (Figure 4-2A). Finally, within our data set, there was no protein in the distribution's higher ranges whose use as a normalizing factor could be biologically justified. These arguments must be balanced against two points: **1)** Beta tubulin is a major structural component of axons and dendrites and several groups have reported decreased volume and dendrite length of pyramidal neurons in additional to spine loss in the DLPFC. Although, these decreases are not as large or significant as, and do not consistently correlate with, decreased spine density. Nevertheless, considering decreased neuron volume and dendrite length, decreased amounts of beta tubulin could mirror decreased pre- and post-synaptic proteins levels, if present. **2)** The list of proteins assayed is, by design, rich in synaptic molecules, limiting the choices for a non-synaptic normalizer and potentially masking disease effects on the entire field. To more thoroughly address this potential confound, future analyses will include peptide SRMs for multiple nuclear, glial and astrocyte markers, even though the use of these proteins would carry its own caveats. For example, a [synaptic]/[nuclear] protein normalization would most likely be confounded by projections from other brain regions. Still, the inspection of this dataset from multiple extra-synaptic normalization perspectives will likely provide additional valuable information.

3. Additional controls for postmortem interval: The studies modeling postmortem interval described in Chapter 3 were performed using the full protocol detailed in that chapter. To thoroughly control for PMI confounds, this experiment will be repeated using the abridged enrichment protocol used to prepare batch 3.

4. Enrichment variability: Accuracy and precision of the LC-SRM/MS assay was rigorously validated at several steps in the protocol and validation of the biochemical fractionation protocol by traditional methods (electron microscopy, Western blot) has been peer reviewed. However, assessment of fractionation reproducibility from the same tissue sample by LC-SRM/MS has not been performed. This omission must be addressed, to complete assessment of method variability at every step of the protocol.

5. Bioinformatics: The informatics and statistical methods applied here identified protein groups with expression and enrichment values significantly regulated by diagnosis or drug treatment. A conservative bar for reaching statistical significance was set to guard against type I Errors. Due to the testing of multiple hypotheses and dataset complexity, this analysis should be considered a first step analysis until a more in-depth and rigorous model can be applied with proper consultation. Ongoing informatics analysis will include assessment of interactions between proteins across tissue preparations and in the context of protein interaction and cellular compartment annotations. Indeed there are several interesting patterns, discussed in final Chapter, that hint at deeper findings buried within this dataset.

5.2 Interpretation of current dataset: A novel hypothesis for the relationship between PSD proteins and spine density in schizophrenia

Decreases in dendritic spine density have been observed in layers 2 and 3 of the DLPFC in SCZ[35, 43]. It logically follows that the levels of proteins that compose spine PSDs would be decreased as well. The results of this study, however, are not consistent with that prediction. Instead, these data suggest that neurons with decreased spine density, compared to controls, have the same amounts of PSD proteins, compared to controls. In this scenario, dendritic spines could contain more PSD protein, an assertion supported by my data. PSD enrichments prepared from SCZ subjects were more enriched for PSD proteins, while the enrichment of other protein groups was unaltered. Additionally, I observed that the relative amounts of PSD complex
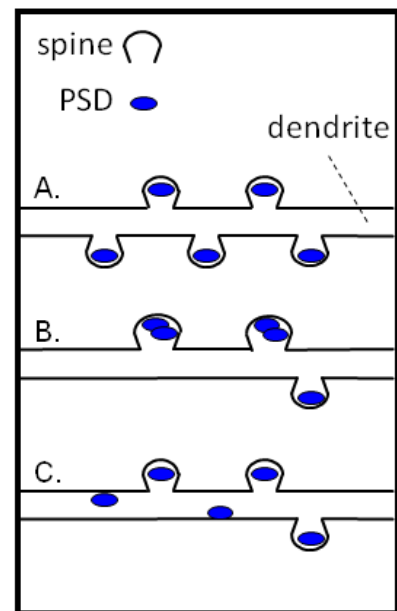
Figure 4-6. Possible configurations of spines and PSDs in schizophrenia. A, depicts the "normal" distribution of PSD complexes in dendritic spines. **B.** and **C.** show two alternate PSD complex distributions in which PSD protein expression is unaltered and spine density is decreased in SCZ. **B.** PSD protein levels, per spine, are increased. **C. "**extra" PSD complexes are present in dendritic shafts and are enriched along with spine localized PSD complexes in biochemical preparations.

members are highly similar between SCZ and control subjects. This suggests that while the amount of PSD complexes at remaining dendrites maybe increased in SCZ, the relative protein composition of these PSD complexes is unperturbed. Interestingly, decreased spine density, but increased spine size, has been observed the cortex of pyramidal neuron NR1 -/- mice [93], suggesting that inhibition of NR function could increase the amount of PSD proteins at dendritic spines. In an alternate scenario, the amount of PSD proteins in remaining spines would be unaltered. Instead the "extra" PSD complexes could exist as lipid rafts[175, 176], in the dendritic shaft. These scenarios are depicted in Figure 4-6. There is however one potential caveat to both of these interpretations.

While this study has excellent precision and some spatial resolution at the PSD microdomain, it was still conducted in a whole LPFC section. Thus differences in synaptic protein expression confined to discreet cortical layers or neuronal subtypes could still be lost in the complexity of a LPFC homogenate. Given that limitation, the consistent increased enrichment of all core PSD proteins in SCZ in this tissue implies that this perturbation is either widespread in the cortex or a large effect confined to a specific neuronal population.

In addition to the caveats discussed above in section 5.2, three experiments are essential to flesh out the implications of these findings. **1)** Laser capture of discreet DLPFC cortical layers followed by LC-SRM/MS to quantify layer specific protein levels would be ideal to confirm or refute the lack of observed differences in protein expression. The feasibility of this experiment is discussed in Chapter 5. **2)** While these findings suggest that decreased spine density is correlated with increase enrichment of PSD proteins they do not prove it. Spine density and PSD protein enrichment will need to be assessed in the same DLPFC tissues of SCZ subjects to determine if such correlation exists. Encouragingly, a similar experiment, in which decreased spine density was significantly correlated with decreased septin7 mRNA levels, has been successfully conducted[177]. **3)** Tissue tomography or electron microscopy, with immuno-gold against PSD-95, in postmortem tissue will be essential for both confirming that the ratio of PSD

complexes to spines is increased in SCZ and for determining the location of these complexes.

CHAPTER FIVE
CONCLUDING THOUGHTS AND FUTURE DIRECTIONS

The goal of this thesis work was to develop a fractionation - mass spectrometry approach for the quantification of synaptic proteins in human postmortem brain tissue and apply this approach to the study of synaptic protein expression and PSD partitioning in the LPFC of SCZ patients. To that end I performed a 2DLC-MS/MS analysis of PSD enrichments prepared from human postmortem LPFC. The resulting peptide spectral library, and ones like it, were used to develop an LC-SRM/MS assay for the multiplexed quantification of peptide SRMs from over 200 synaptic proteins. These peptide SRMs were rigorously validated for fidelity, accuracy and precision in peptide/protein quantification. The LC-SRM/MS assay was then used to further validate biochemical fractionation protocols for the enrichment of synaptic microdomains in human postmortem brain tissue, demonstrating that subcellular fractions prepared from human postmortem brain tissue were strikingly similar to those prepared from fresh mouse brain tissue. Finally, this fractionation – LC-SRM/MS approach was used to quantify close to 200 proteins in whole tissue homogenates prepared from the LPFC of 15 pairs of SCZ and matched controls subjects and 107 proteins in PSD enrichments prepared from the LPFC of 9 SCZ and matched control subjects. A preliminary interpretation of the data from this final experiment strongly suggests that partitioning, not expression, of PSD proteins is altered in the LPFC of SCZ patients. Based on these results, I have proposed two possible models to explain how PSD protein expression in the SCZ DLPFC could be unaltered while dendritic spine density is decreased (Figure 4-6). Additionally, a list of future experiments is included here, which could be utilized to confirm this finding and investigate the accuracy of the two proposed models. This work demonstrates the feasibility and power of combining biochemical methods with a targeted MS proteomics approach to address a specific question in biology.

As noted previously, comparisons of core PSD proteins, normalized by PSD95, found PSD complex composition to be highly similar between SCZ and control. Interestingly, however, when one compares the difference between the average PSD95-normalized values for SCZ over control, the size of that difference appears to be related to the distance between that protein and the PSD in the synapse. That is, the "farther away" a protein is from the PSD in the synapse, the greater the disparity in that proteins

PSD95-normalized value between SCZ and control (Figure 5-1). It is possible that this pattern reflects alterations in the distribution of PSDs throughout the dendrite in SCZ. Alternatively, these differences could reflect a dysregulation in the interaction between the PSD and adjacent microdomains.

The findings reported in Chapter 4 dealt almost exclusively with the increased enrichment of PSD proteins as a group in SCZ. While these findings provide some insight into the distribution of PSD complexes in the dendrites of SCZ subjects, they do not address alterations to PSD complex protein composition that could correlate with NR hypofunction. While
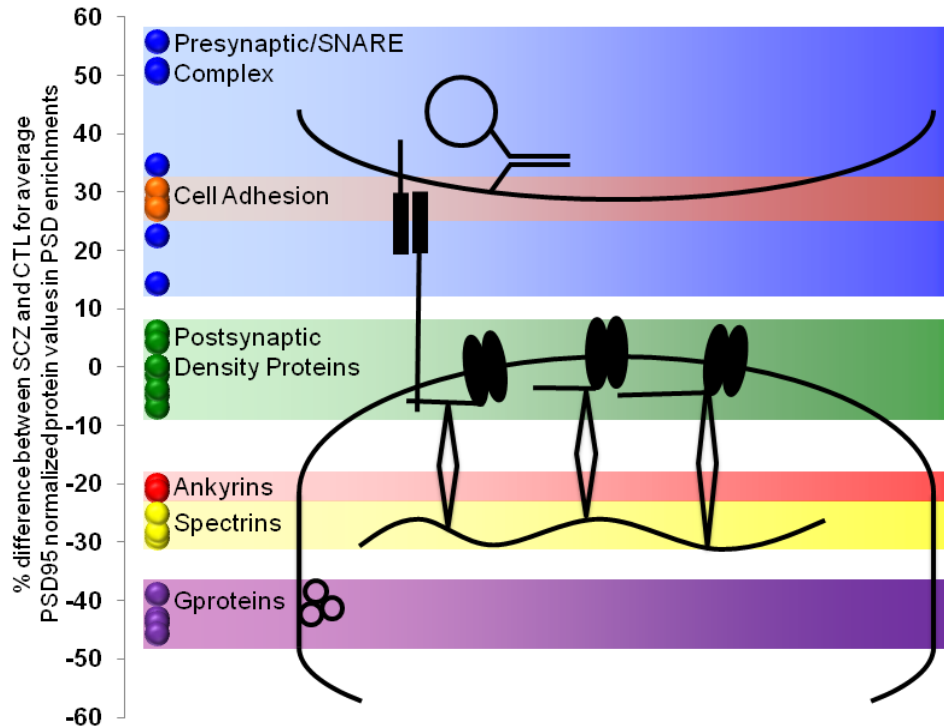
Figure 5-1. PSD95 normalized protein values may be related to postsynaptic density proximity. PSD95 normalized values were calculated for proteins measured in PSD enrichments from 9 pairs. The average value for each protein in the SCZ and control groups was taken and the percent difference ([Control/SCZ] * 100) between the two groups calculated for each protein. The percent differences were then given a sign depending on assumed location in the synapse (- for postsynaptic, + for presynaptic), plotted in one dimension and color coded by functional.

significant differences between disease and control enrichments were observed in the PSD95 normalized dataset, the differences in enrichment, discussed in the last paragraph, must be taken into consideration to interpret these data. The sections below discuss the next challenges in quantitative proteomics in study of human postmortem brain tissue as

well as in the interpretation of protein data from synaptic microdomain enrichments. Selected findings in PSD protein composition and activity will also be presented to illustrate complications in data interpretation.

1. Proteomics in neuroscience

This study represents a first step towards bringing a targeted proteomic approach to bear on the study of neuropsychiatric illness in human postmortem brain tissue. Proteomics investigations can be configured in a variety of ways to achieve numerous goals. Already, a number of different strategies have been employed to assay phosphorylation, ubiquitination, nitrosylation and glycosylation events[60, 109, 178, 179]. In that vein it is my sincere hope that the neuroscience community here at the University of Pennsylvania and beyond will utilize and expand upon the method developed as part of this work to address a variety of questions in the field of neuroscience.

1.1   Layer- or cell type - specific protein quantification in postmortem studies.

The strategy developed in this thesis has spatial resolution for synaptic microdomains but not neuronal subtypes or cortical layers. Thus the data generated here allow for the possibility that PSD protein expression is altered in a specific neuronal population (e.g. interneurons) or cortical layer; the signal for this alteration lost in the noise of a tissue homogenate. Furthermore, these data provide little insight into the cell population driving increased PSD protein enrichment or if these "extra" PSD proteins are localized to dendrites or elsewhere in the neuron. As previously noted, immunohistochemistry, tissue tomography and electron microscopy studies will be essential for addressing these questions. However, these approaches are unable to assay changes to synaptic protein expression and partitioning in a multiplexed fashion. Thus, adapting the targeted method developed here to the quantification of protein extracts from specific neuronal populations or cortical layers is highly desirable. MS proteomics methodologies have been used to profile proteins in single-cell type populations isolated by flow cytometry[180] and laser capture[181]. Indeed laser capture – proteomics has been used to profile cortical lewy bodies[182] and hippocampal neurofibrillary tangles[183] from human postmortem brain tissue. Laser-capture – qPCR has been utilized to quantify mRNA expression in a
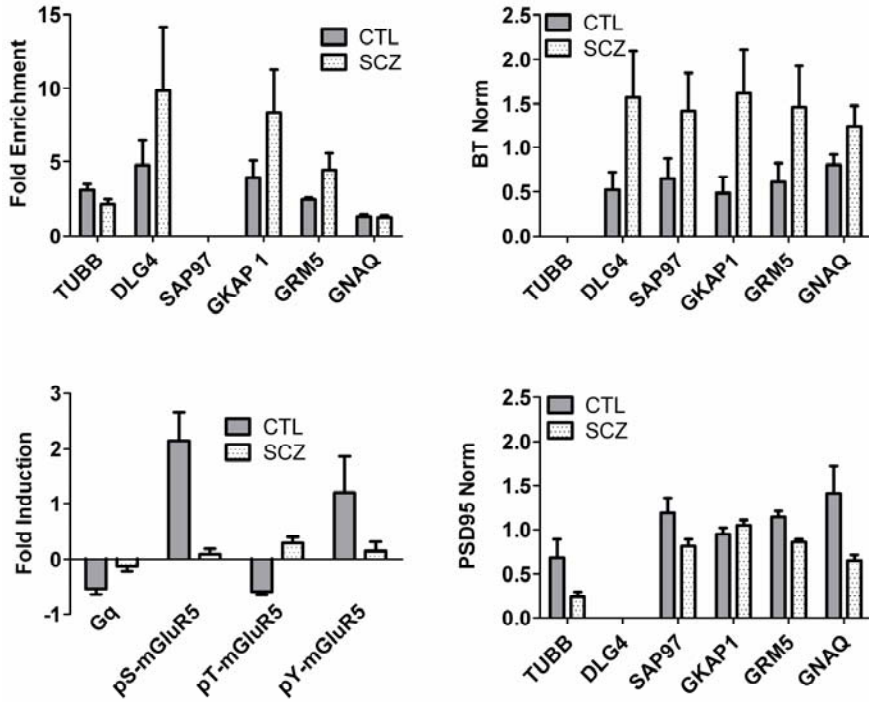
Figure 5-2. Three different perspectives of PSD protein composition in schizophrenia. Three different normalizations for select proteins measured in PSD enrichments from 6 pairs of SCZ and matched controls. **A.** shows fold enrichment values, **B.** protein values normalized to beta tubulin values and **D.** protein values normalized to PSD95. **C.** LPFC slices from 8 pairs of SCZ and control subjects were stimulated with 1μM (RS)-2-chloro-5-hydroxyphenylglycine (CHPG). mGluR5- Gprotein subunit alpha q interaction and mGluR5-phosphorylation was quantified by Co-IP and Western blot after stimulation and at baseline. **C,** shows the fold induction (stimulated /baseline) measure for mGluR5 phosphorylation and G-protein interaction. Note that CHPG induction of phosphorylation, de-phosphorylation and G-protein release is attenuated in SCZ tissues, suggesting that mGluR5 activity is perturbed.

number of cell types in human postmortem tissues from SCZ and bipolar patients[107 184 106]. Thus, a laser-capture – proteomics approach could be able to quantify protein amounts in discrete cortical layers.

The use of LC-SRM/MS, with $[^{13}C_6]$-brain ISTD, has several advantages over LC-MS/MS strategies. One advantage is the low protein

requirement necessary for utilization of this method. The experiments described in Chapter 4 utilized only 10-20 μg of total protein for preparation, with 10-25% of this preparation analyzed in one LC-SRM/MS run. In method development experiments conducted at a ThermoScientific demonstration laboratory (Somerset, NJ) with Dr. Gene Ciccimaro, we successfully monitored PSD protein peptides, at quantitative intensities, in as little as 90 ng of peptide injections. An additional benefit of the LC-SRM/MS method is the $[^{13}C_6]$-brain ISTD which serves as a carrier in addition to its capacity as an internal

standard. Thus, in a theoretical laser capture experiment, isolated cortical layers could be collected in a solution containing an excess of the $[^{13}C_6]$-brain ISTD, SDS and reducing agents. While the optimization and validation of such a protocol would likely be a significant endeavor, it should be possible utilize LC-SRM/MS with the $[^{13}C_6]$-brain ISTD for quantification of synaptic proteins in cortical layers isolated by laser capture.

2. Controlling for enrichment confounds in microdomain protein quantification

Our findings of altered PSD enrichment complicate investigation of the PSD microdomain in SCZ. Specifically, investigations into altered PSD protein complex composition must be considered in the context of increased postsynaptic protein enrichment, lest differences in protein enrichment between SCZ and control tissue be falsely interpreted as altered trafficking to, or interactions at the PSD. An example is used to further explain this point:

In Figure 5-2, the levels of six proteins in PSD enrichments from 6 pairs are considered. The amounts of these proteins, measured in PSD enrichments, are viewed from three different perspectives: First, as enrichment values (5-2A), next as beta tubulin-normalized protein values (5-2B) and finally as PSD95 normalized-protein values (5-2D). If these data are viewed from the perspective of beta tubulin (TUBB) normalization, without taking into account the differences in enrichment, one might conclude that the amounts of all proteins are increased in the SCZ group. Considering the variations in enrichment differences between proteins (5-2A), this interpretation would likely be incorrect. Alternatively, PSD95-normalization (5-2D) likely paints a more accurate picture of relative protein differences within the PSD complex, but the results must still be interpreted with caution. PSD95 normalized values for mGluR5 (GRM5) and Gq alpha (GNAQ) are significantly decreased in PSD enrichments from SCZ subjects (P = .004 and .03). However, mGluR5 shows the increased enrichment in SCZ shared by the core PSD proteins PSD95 (DLG4) and GKAP1, while Gq alpha enrichment values between SCZ and control are highly similar. Thus, one might conclude that the mGluR5 decrease represents dysregulated protein composition "within" the PSD microdomain, while decreased PSD95-normalized Gq alpha values reflect a fundamental disconnect,

88

perhaps in space or in microdomain interaction, between the PSD and its surroundings. It should be noted that this an example of only 6 out of over 100 proteins, used to illustrate confounds that should be considered when analyzing quantitative data in a microdomain enrichment. Going forward a more rigorous statistical consideration of these confounds must be made.

As a finally note, it should be mentioned that despite the complexities associated with interpreting this dataset, this example did provide useful information. Both this experiment and another performed previously on PSD enrichments from a similar cohort (not discussed here) observed decreased PSD95-normalized mGluR5 levels in PSD enrichments from SCZ subjects. We hypothesized that this decrease may correlate with perturbed mGluR5 activity. To investigate this, DLPFC tissue from 8 pairs of SCZ and matched control tissues were sent to Dr. Hoau-Yan Wang, where *ex-vivo* stimulation experiments revealed decreased mGluR5 activity, as measured by receptor phosphorylation and G alpha q subunit release (Figure 5-2C). This final experiment demonstrates the promise of the fractionation – LC-SRM/MS approach in assessing altered protein expression and partitioning events that may be reflective of function deficits at the synapse in SCZ.

APPENDIX 1: Supplemental
Tables and Figures

|	Description	% Cov	Protein Probability	IPI Accession
1	Adaptor-related protein complex	40	1.00	IPI00619900
2	ADP-ribosylation factor GTPase-activating protein 1	29	1.00	IPI00175169
3	A-kinase anchor protein 12	22	1.00	IPI00867627
4	A-kinase anchor protein 5	18	1.00	IPI00307794
5	BR serine/threonine protein kinase 1	15	1.00	IPI00148020
6	Brain Creatine Kinase	72	1.00	IPI00022977
7	Calmodulin	47	1.00	IPI00075248
8	Calpain 1	20	1.00	IPI00025084
9	CAMKII Alpha	43	1.00	IPI00877169
10	CAMKII Beta	40	1.00	IPI00334271
11	cAMP-dependent protein kinase/PKA	41	1.00	IPI00554752
12	Cell division protein kinase 5/CDK5	44	1.00	IPI00023530
13	DLG1/SAP97/GKAP	7	1.00	IPI00552511
14	DLG2/PSD-93/Chapsyn-110	13	1.00	IPI00647950
15	DLG4/PSD-95	24	1.00	IPI00790650
16	Dynamin	59	1.00	IPI00887273
17	Glutamate receptor, ionotropic, AMPA 2	11	1.00	IPI00219216
18	Glutamate receptor, ionotropic, AMPA 3	9	1.00	IPI00298700
19	Glutamate receptor, ionotropic, NMDA 2A	3	1.00	IPI00029768
20	Glutamate receptor, ionotropic, NMDA 2B	6	1.00	IPI00297933
21	Glutamate receptor, metabotropic, 5	5	1.00	IPI00296244
22	Gα 13	24	1.00	IPI00290928
23	Gαi 1	20	1.00	IPI00337415
24	Gαi 2	27	0.97	IPI00748145
25	Gαi o	40	1.00	IPI00398700
26	Gαs	12	1.00	IPI00095891
27	Gβ 1	39	1.00	IPI00026268
28	Gβ 2	47	1.00	IPI00003348
29	Gβ 5	19	1.00	IPI00745232
30	Gγ	40	1.00	IPI00328128
31	Heat Shock Protein 70 12A	50	1.00	IPI00011932
32	Homer 1	21	1.00	IPI00003566
33	Inositol 1,4,5 Triphosphate receptor	5	1.00	IPI00333753
34	L-type calcium channel	10	1.00	IPI00219983
35	MAP Kinase	21	1.00	IPI00003479
36	MAP Kinase Kinase	23	1.00	IPI00219604
37	MAP Kinase Kinase Kinase Kinase	5	1.00	IPI00219510
38	nGEF/Neuronal guanine exchange factor	12	1.00	IPI00749021
39	Nitric oxide synthase, brain	8	0.99	IPI00746356
40	Phospholipase A2	8	1.00	IPI00220209
41	PKCα	28	1.00	IPI00385449
42	PKCγ	27	1.00	IPI00007128
43	PKCε	20	1.00	IPI00024539
44	Protein phosphatase 1	23	1.00	IPI00045550
45	Protein phosphatase 2	20	1.00	IPI00000030
46	Protein tyrosine kinase 2B/PYK	14	1.00	IPI00029702
47	Protein tyrosine phosphatase, receptor type D	8	1.00	IPI00375547
48	Protein tyrosine phosphatase, receptor type S	9	1.00	IPI00332271
49	Proto-oncogene tyrosine-protein kinase/Src	10	1.00	IPI00641230
50	Rap guanine nucleotide exchange factor 2/Rap GEF2	12	1.00	IPI00853219
51	Ras GTPase-activating protein/SynGap	17	1.00	IPI00177884
52	Ras-related protein Rab-10	11	1.00	IPI00016513
53	Ras-related protein Rab-3A	12	1.00	IPI00023504
54	Regulator of G-protein singaling 6/RGS 6	12	1.00	IPI00216329
55	Regulator of G-protein singaling 7/RGS 7	14	1.00	IPI00220661
56	Rho GTPase-activating protein/Rho GAP	11	1.00	IPI00020567
57	Rho guanine nucleotide exchange factor/Rho GEF	26	1.00	IPI00641543
58	Rho-Rac guanine nucleotide exchange factor/Rho-Rac GEF	17	1.00	IPI00291316
59	R-type calcium channel	4	1.00	IPI00218338
60	serine threonine kinase DCLK2	14	1.00	IPI00296360
61	SH3 and multiple ankyrin repeat domains protein 3/SHANK3	14	1.00	IPI00847618
62	Voltage-dependent anion-selective channel	21	1.00	IPI00216024
63	Voltage-gated potassium channel	14	1.00	IPI00021088

Table 2-1. Peptide identifications were confirmed by inspection of MS2 spectra and targeted MS2 analysis of peptide parent masses. Description: IPI identifier. % Cov: Percent of protein sequence covered by observed peptides.

A. Cellular Compartment

B. Biological Process

C. Molecular Function

D.

E.
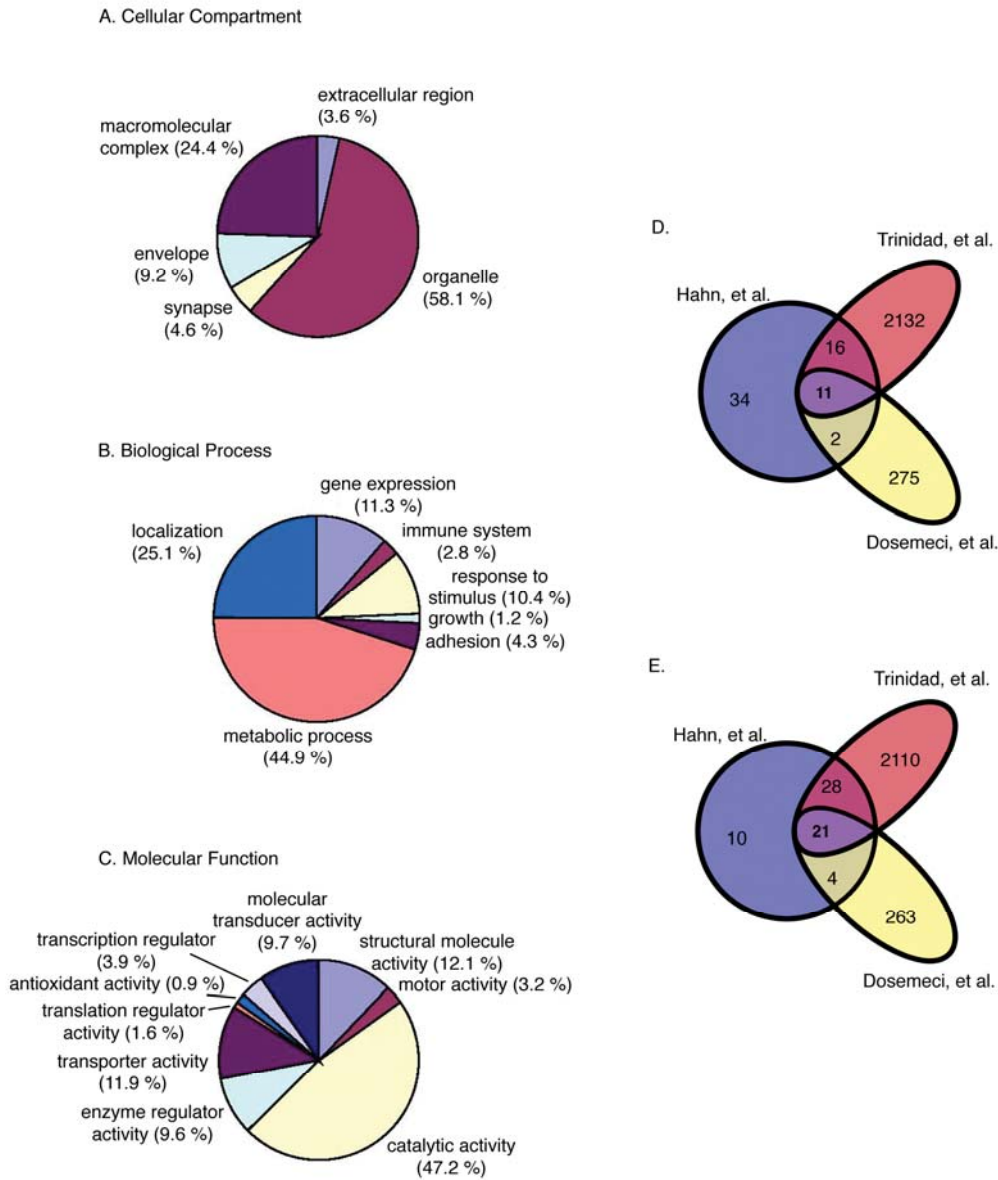
Supplemental Figure 2-1. Proteins identified by 2DLC-MS/MS analysis. (A, B and C) Protein identifications were grouped by GO with respect to Cellular Compartments (A) Biological Processes (B) and Molecular Functions (C). Each categorization shows groups of proteins that may be associated with the PSD and the ones that are likely to be contaminants. (D and E) Protein identifications were compared to the results of previous studies. (D) Sequences from the 63 confirmed proteins were compared to those from Trinidad et al. and Dosemeci et al. data sets with the criteria defined as sequence homology of >90%. (E) Sequences from the 63 confirmed proteins were compared to those from Trinidad et al. and Dosemeci et al. data sets by identification based on IPI description; all but 10 were found in one or both data sets.
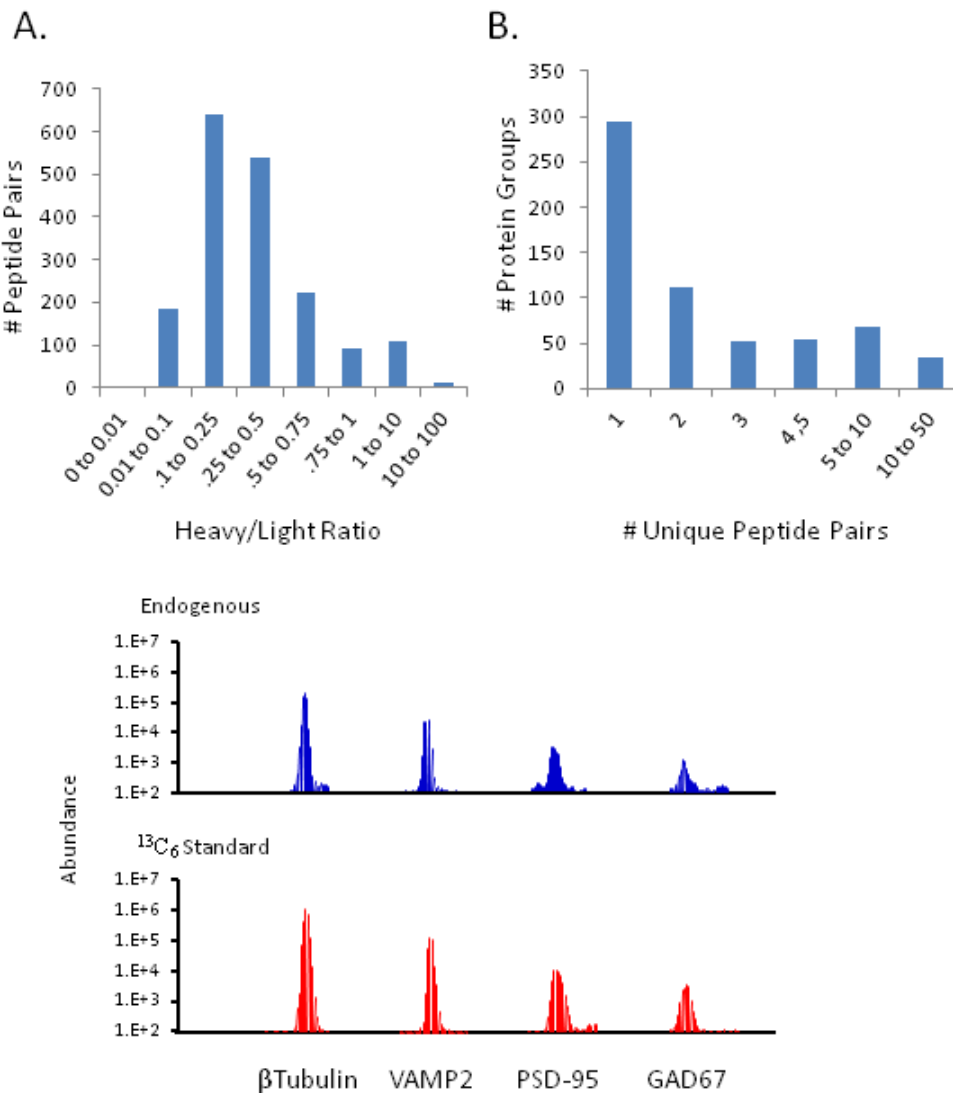
Supplemental Figure 3-1. Distribution of Heavy/Light Ratios and Unique Peptide Pairs. The signal ratio of $[^{13}C_6]$Lysine-Labeled peptides to unlabeled peptides was calculated. A, shows the distribution of ratios for peptides unique to a single protein group. B, shows the distribution of Unique $[^{13}C_6]$Lysine-Labeled peptides observed per protein. C, shows depicts representative chromatographic peaks of light and heavy peptides from four peptides with different expression values. Note that the y axis is log10. This figure highlights the similarity in relative protein expression between the standard and analyte proteomes.

$R^2 = 0.7074$
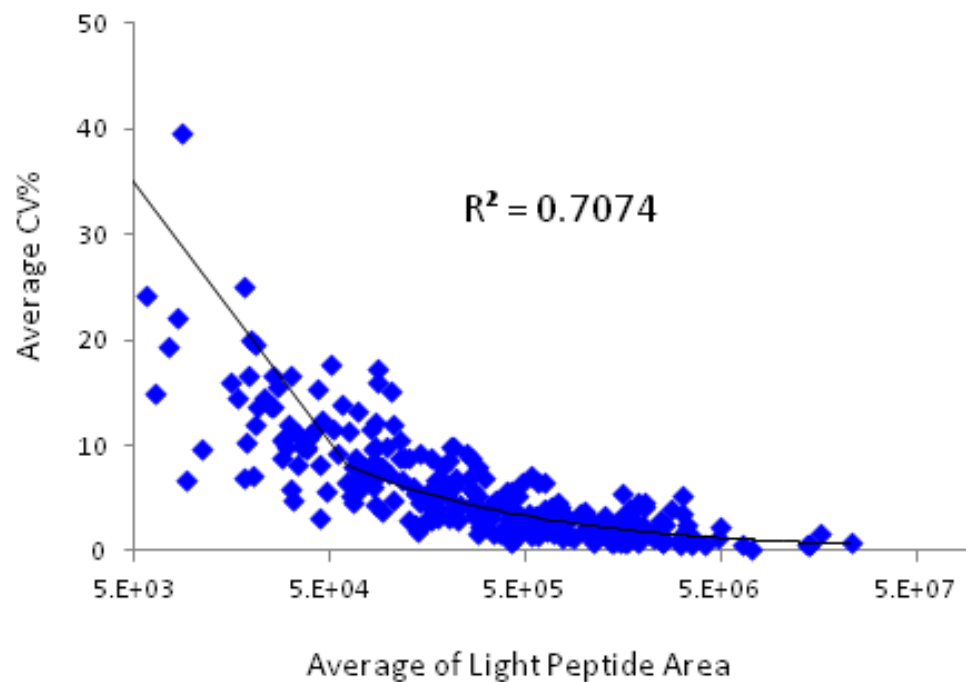
Supplemental Figure 3-2. Technical precision of peptide measures. To assess technical precision in peptide measure, four 30 μg aliquots of a human IM fraction were individually mixed with 15 μg [$^{13}C_6$]brain ISTD and analyzed by LC-SRM/MS with triplicate injections. Peptide measure CV was calculated and the average of these taken for the four repeated preparations. A, shows this average CV number was plotted against the average integrated area of each peptide from all preparations and injections. While CV correlates with peak area (R2 = .71), the CV values but four peptides are under 20%.
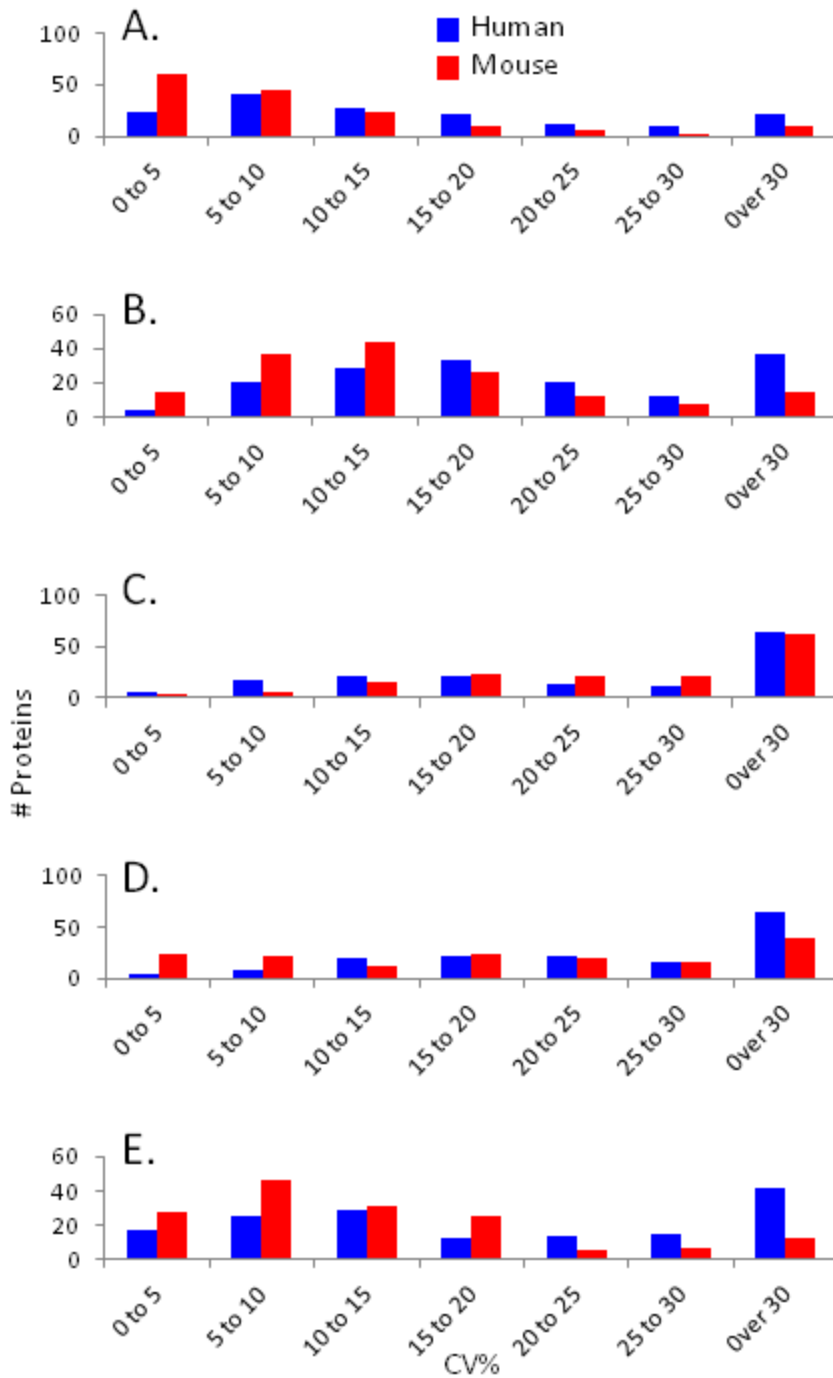
Supplemental Figure 3-3. Distribution of variance in protein quantification by fraction. CVs for protein enrichment values were calculated for each fraction, and the distribution plotted in 5 unit bins up to 30%. A, total homogenate (H). B, synaptosomal fraction (SF).C vesicular (V).D, papasynaptic fraction (P).E, postsynaptic density (D). The distribution shape is often similar between the two species, but the center is often lower in preparations from mouse tissue.
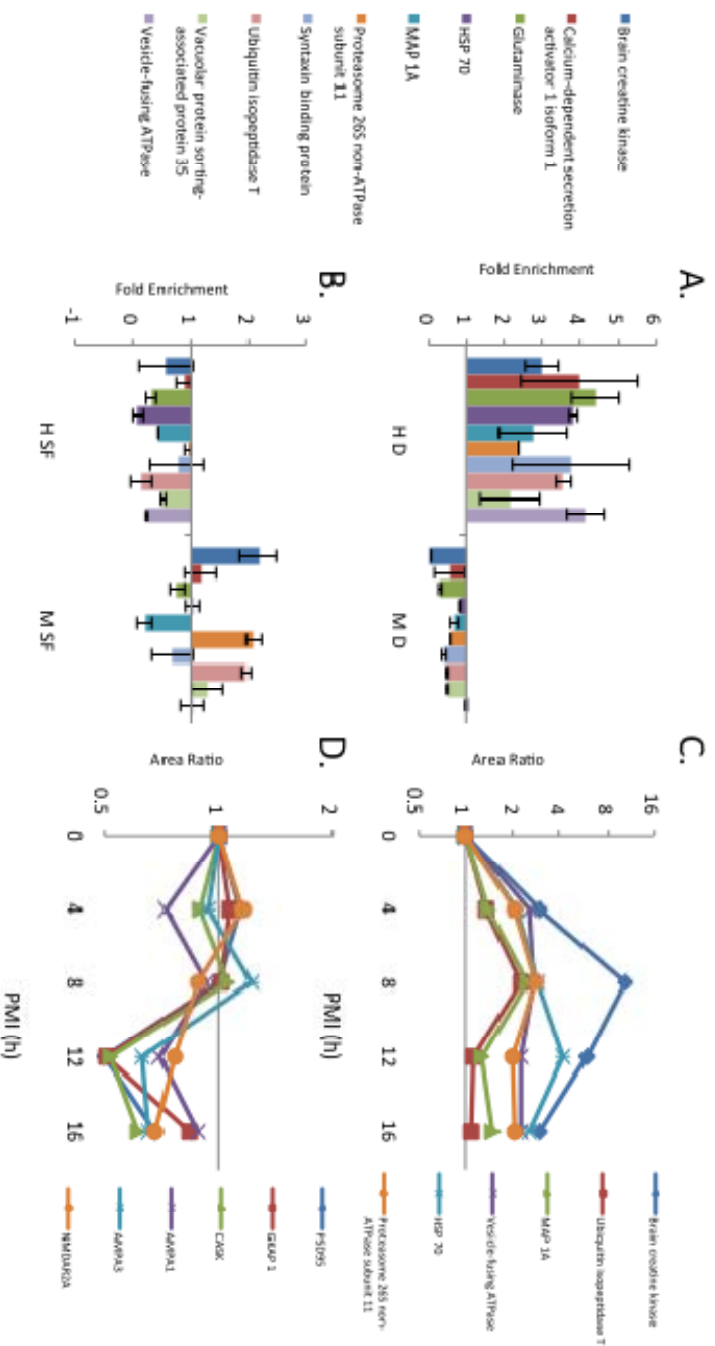
Supplemental Figure 3-4. Postmortem interval and contamination in D fractions. We compared enrichment values for the "contaminant" proteins identified by the clustering analysis found to be differentially enriched in human and mouse D fractions. A, shows enrichments in human (H D) and mouse (M D) postsynaptic density (D) fractions and B, shows enrichments in human (H SF) and mouse (M SF) synaptosomal fractions (SF) and B. Error bars are standard deviation of three samples. To investigate if these differences could be explained by postmortem interval (PMI), D fractions were prepared from mouse brain tissue with simulated PMIs of 0 to 16 hours. C, shows measures of "contaminant" proteins over PMI and D, shows glutamate receptors and postsynaptic scaffolding proteins.
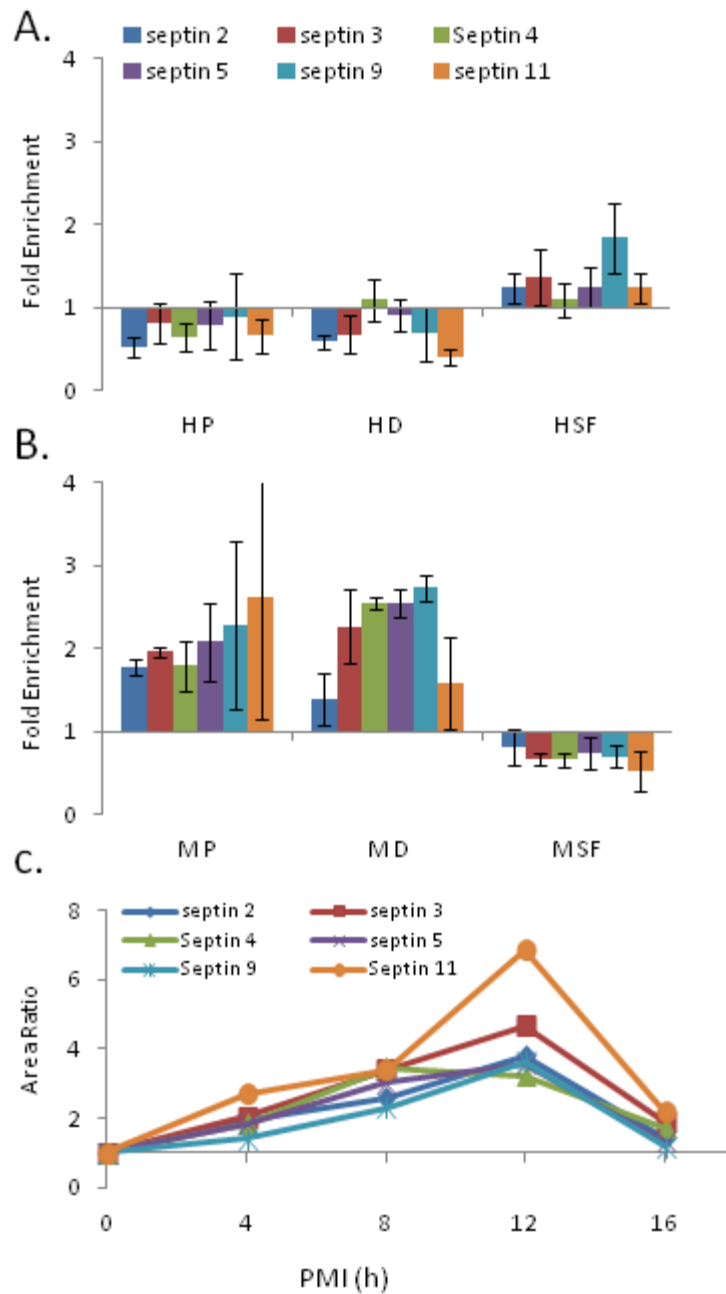
Supplemental Figure 3-5. Differences in septin enrichment are not explained by postmortem interval. We compared enrichment values for septin proteins in three fractions. A show enrichment in human parasynaptic fractions (H P) postsynaptic density (H D) and synaptosomal (H SF). B, shows the same for fractions prepared from mouse, M P, M D and M SF. C, shows measures for septin proteins over increasing postmortem interval (PMI) in D fractions prepared from mouse tissues.

#	Sex	Race	Age	PMI	Rx	Batch
1	F	W	70	10.5	N	1
2	F	W	76	9	S	1
3	M	B	63	5	N	1
4	M	W	71	12	S	1
5	F	W	85	11	N	1
6	F	W	79	17	S	1
7	F	W	72	4	N	1
8	F	W	77	11	S	1
9	M	W	98	15	N	1
10	M	W	89	15	S	1
11	M	W	86	7	N	1
12	M	W	81	9	S	1
13	F	W	91	11.5	N	2
14	F	W	96	12.5	S	2
15	M	W	70	19	N	2
16	M	W	78	19	S	2
17	F	W	92	5	N	2
18	F	W	88	7.5	S	2
19	F	W	74	3.5	N	3
20	F	W	76	9.5	S	3
21	M	W	90	6	N	3
22	M	W	95	8.5	S	3
23	F	W	72	7	N	3
24	F	W	72	11.5	S	3
25	F	W	88	7	N	3
26	F	W	77	5.9	S	3
27	F	W	80	15	N	3
28	F	W	80	16	S	3
29	F	W	81	8	N	3
30	F	W	83	7.5	S	3

Supplemental Table 4-1. Demographics. *# = internal identification number. Sex, F = female, M = Male. Race, W = Caucasian, B = African American. Age (y), PMI = postmortem interval in hours, Rx = diagnosis, N = normal control, S = schizophrenia. Batch = cohort the sample was prepared with, see methods.*
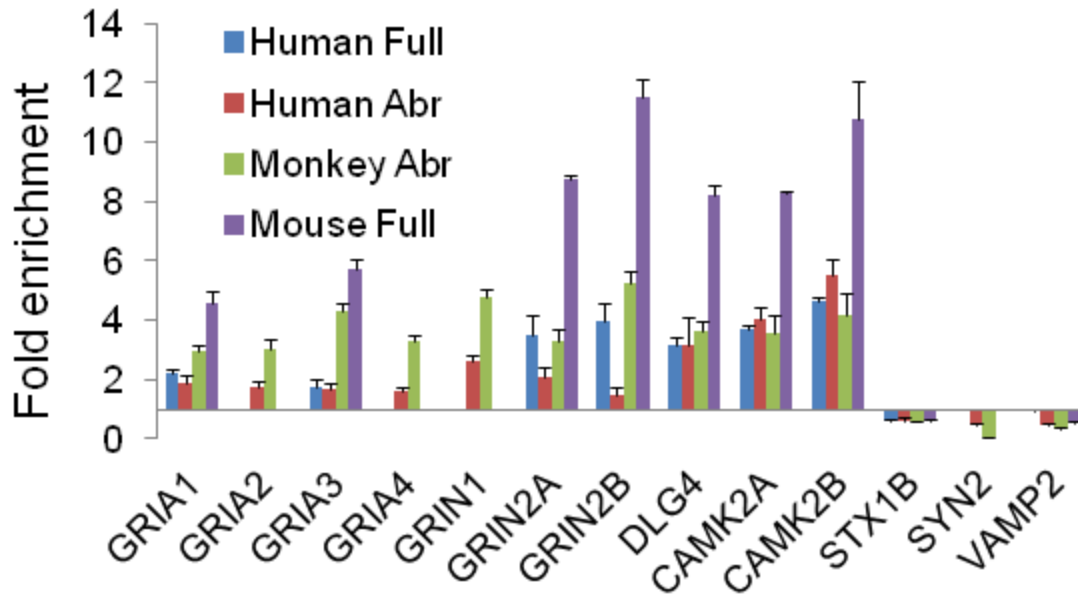
Supplemental Figure 4-1. Comparison of enrichment protocols. This figure contrasts the enrichment values for representative pre- and post- synaptic proteins in PSD enrichments prepared from the three human and three mice using the method described in chapter 3, denoted here as "*Full*" and PSD enrichments prepared from five humans and five rhesus monkeys using the abridge protocol described in Chapter 4, denoted here as "Abr". It is important to know that rhesus monkey brain tissue was dissected from cold saline profused animals, while tissue from mice was vivisected at body temperature. Thus differences in enrichment protocol and dissection protocol likely contribute to differences between these two groups. Fold enrichment values are calculated by dividing the protein value from the PSD enrichment by protein value from total homogenate. The fold enrichment of PSD95 (DLG4), CAMK2A and CAMK2A is similar across human and monkey preparations, while glutamate receptors are more enriched in Abr monkey compared to Abr human. Presynaptic/SNARE complex proteins are un-enriched by all proticoals in all animals. While there are differences in enrichment of PSD proteins, likely owing to PMI confounds in humans, different enrichment protocols and dissection methods, all four of the preparations were enriched, to some extent, for postsynaptic glutamate receptors, PSD95 and kinases, excluding presynaptic/SNARE proteins. *Human Full = three human subjects described in Chapter 3, Human Abr = five control subjects from Chapter 4, batch 3, Monkey Abr = the five vehicle animals described in Chapter 4.*
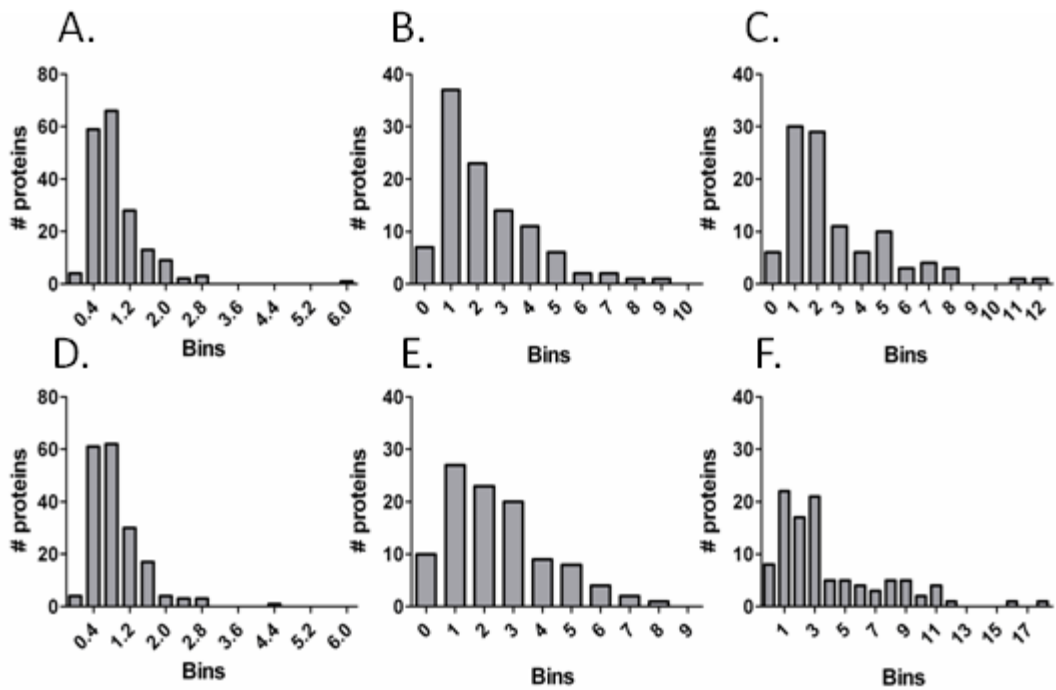
Supplemental Figure 4-2. Distribution of protein levels and protein enrichment values.
A. Beta tubulin-normalized protein levels, total homogenate from 15 control subjects.
B. Protein enrichment values, PSD enrichments from 9 control subjects.
C. Protein enrichment values, PSD enrichments from 6 control subjects.
D. Beta tubulin-normalized protein levels, total homogenate from 14 SCZ subjects.
E. Protein enrichment values, PSD enrichments from 8 SCZ subjects.
F. Protein enrichment values, PSD enrichments from 6 SCZ subjects.
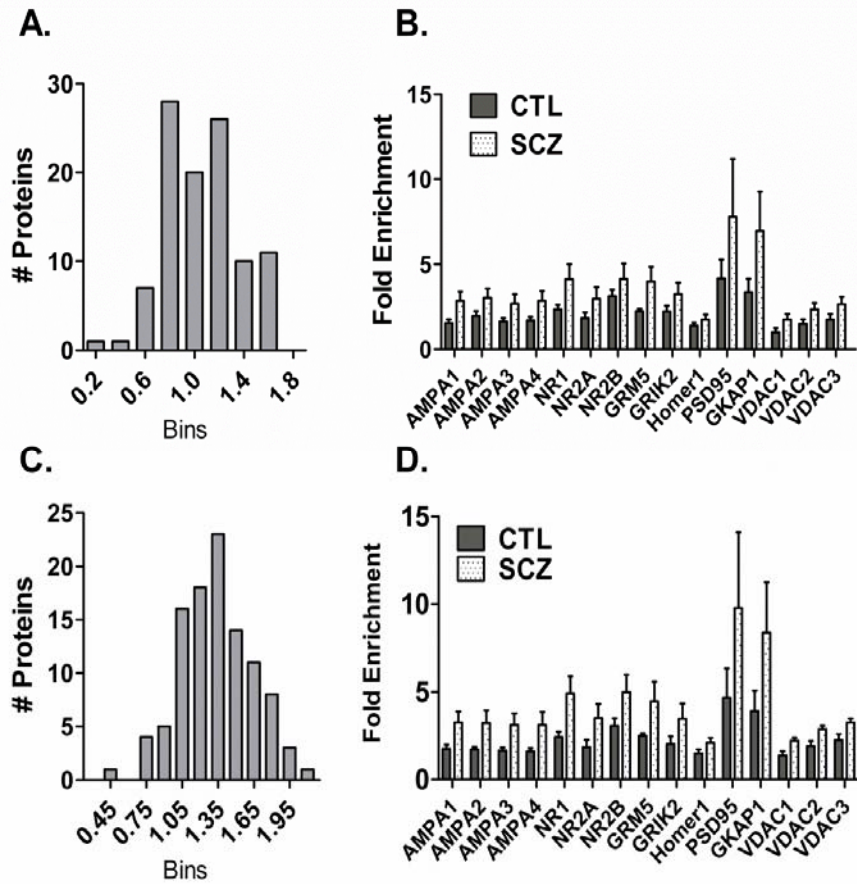
Supplemental Figure 4-3. PSD protein enrichment is elevated in schizophrenia in both the 9 and 6 pair cohorts. Biochemical fractions enriched for PSDs were prepared from the LPFC of 9 SCZ subjects and matched controls. Quantitative measures of 107 proteins were assayed therein by LC-SRM/MS. Enrichment values for 104 of these proteins were calculated by divideing un-normalized protein measures in PSD enrichments by un-normalized protein measures in whole cell homogenates. The average protein enrichment value was taken for each group and the SCZ average divided by the control average (SCZ/CTL) to obtain a ratio of dysregulation for each protein. **A,** shows the distribution of these dysregulation ratios for 6 pairs. **C,** shows the distribution of these dysregulation ratios for 9 pairs. **B,** shows average protein enrichment values from 6 pairs of human tissue, which were significantly increased in PSD preparations from disease tissue, ($P < .0001$). **D,** shows average protein enrichment values from 9 pairs of human tissue, which were significantly increased in PSD preparations from disease tissue, ($P < .0001$). Note, **D.** differs from Figure 4-3B as subject #22, found to be an outlier in the enrichment dataset, is included here (B. &**D.**) but not in Figure 4-3B. *CTL = control, SCZ = schizophrenia.* Error bars are standard error of the mean.

A.

P	S/C	OGS
0.010	1.64	GRIN1
0.012	1.56	GABBR1
0.018	1.57	CAMK2A
0.025	1.35	GRM5
0.035	1.50	VDAC2
0.038	1.59	GRIA2
0.038	1.63	VDAC1
0.049	1.41	CDK5
0.050	1.45	CAMK2G
0.050	1.42	CAMK2B
0.057	1.44	VDAC3
0.058	1.51	GRIA3
0.071	1.35	FLOT1
0.080	1.14	GNAZ
0.087	1.47	GRIA4
0.098	1.42	CAMK2D
0.112	1.62	GRIA1
0.129	1.53	SYNGAP1
0.134	1.27	SLC25A22
0.160	1.26	HOMER1
0.161	1.51	GRIN2A
0.172	1.54	GRIN2B

B.

P	S/C	OGS
0.030	0.54	DNM1
0.055	0.46	SYN2
0.063	0.67	PRKACA
0.086	0.75	GNB1
0.094	0.62	STX1B
0.118	0.61	STXBP1
0.135	0.77	GNA
0.147	0.64	PPP1R7
0.158	0.75	GNAI1
0.208	0.72	PPP2R1A

C.

P	S/C	OGS
0.002	1.29	GNAZ
0.007	1.38	CDK5
0.013	1.54	FLOT1
0.018	1.41	SLC25A22
0.022	1.43	CAMK2D
0.033	1.68	GRIA1
0.045	1.91	GABBR1
0.046	1.40	CAMK2G
0.054	1.33	AP2M1
0.056	1.54	CAMK2A
0.057	1.78	GRM5
0.063	1.75	GRIN1
0.074	1.58	VDAC2
0.085	1.65	GRIA3
0.091	1.39	FLOT2
0.091	1.70	GRIA4
0.092	1.72	VDAC1
0.104	1.24	EEF1A1
0.105	1.29	NDUFA4
0.111	1.52	VDAC3
0.123	1.31	CAMK2B
0.128	1.50	GRIA2
0.140	2.07	GKAP1
0.158	1.63	GRIN2A
0.169	1.48	PDHB
0.184	1.46	GRIA6
0.191	1.60	GRIN2B
0.198	1.85	PI4KA

D.

P	S/C	OGS
0.175	0.77	STX1B
0.165	0.78	PRKACA

Supplemental Tables 4-2. Protein Enrichment differences with a P-value > 2.
A. Proteins with elevated enrichment values in PSD enrichments from 6 pairs.
B. Proteins with decreased enrichment values in PSD enrichments from 6 pairs.
C. Proteins with elevated enrichment values in PSD enrichments from 9 pairs.
D. Proteins with decreased enrichment values in PSD enrichments from 9 pairs.
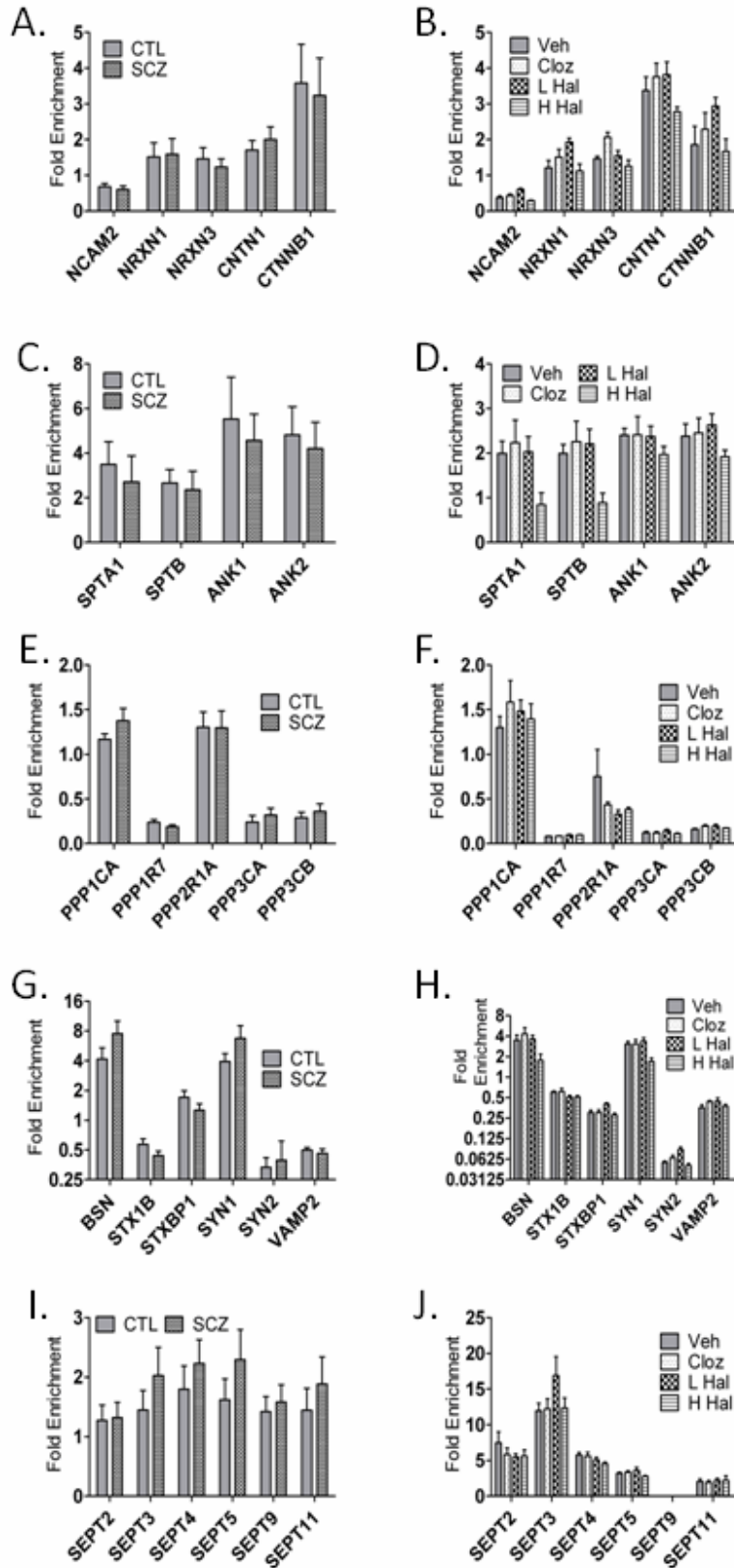
Supplemental Figure 4-4. Enrichment values of five functional protein groups are not regulated by diagnosis. Biochemical fractions enriched for PSDs were prepared from the LPFC of 9 schizophrenic subjects and matched controls and rhesus monkeys treated with different neuroleptics and fold enrichments values calculated. These proteins were manual sorted into five groups by function: **A.** and **B,** neuronal cell adhesion, **C.** and **D,** spectrin and ankrin, **E.** and **F,** protein phosphatases, **G.** and **H,** presynaptic/SNARE complex, **I.** and **J,** septins. The left column (**A, C, E, G & I**) show enrichment values from SCZ and control subjects while the right column (**B, D, F, H & J**) shows values from rhesus monkey treated with neuroleptics. *CTL = control subjects, SCZ = schizophrenia, Veh = vehicle, Cloz = , L Hal = low dose haloperidol and H Hal = high dose haloperidol.* Error bars are standard error of the mean.
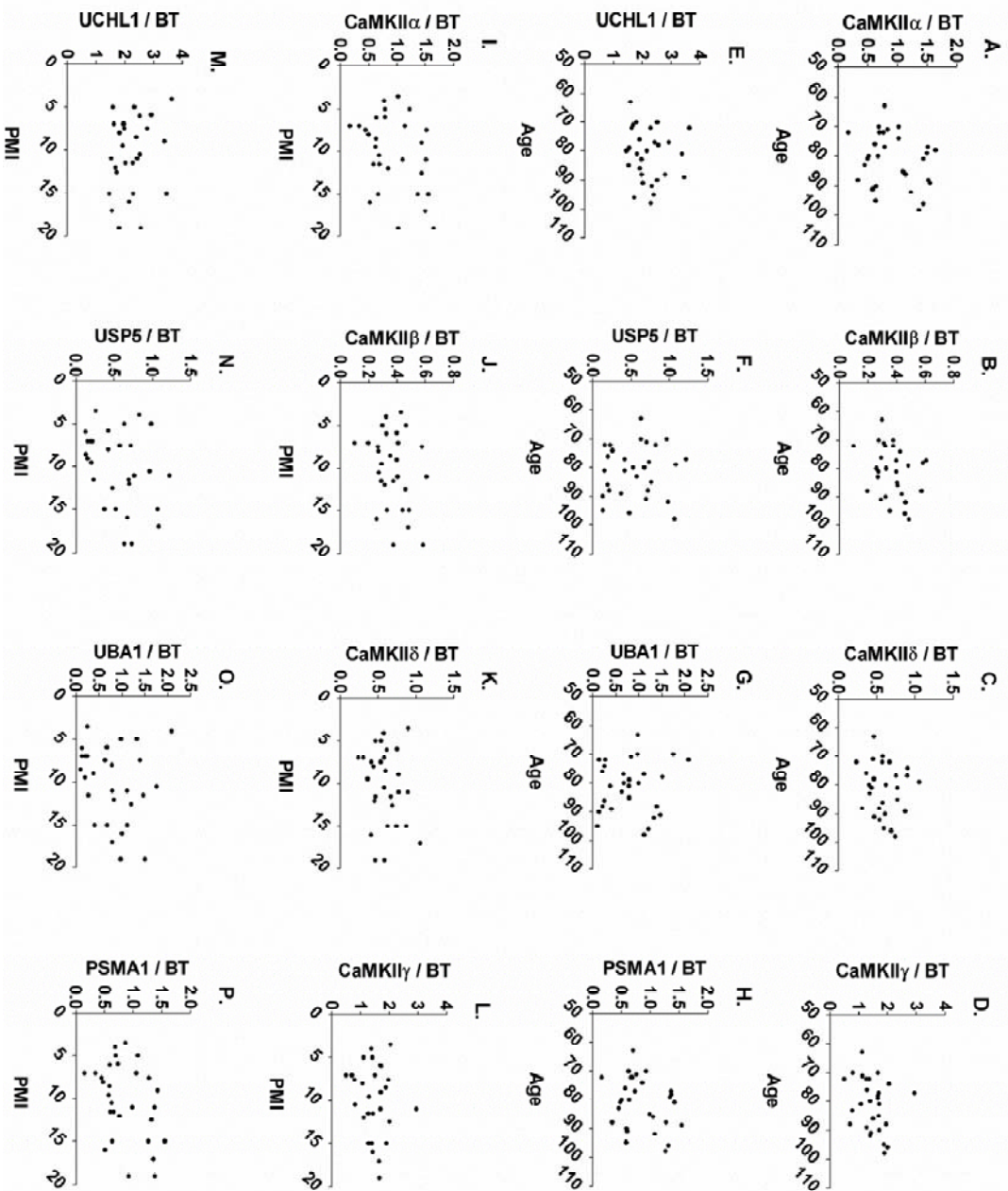
Supplemental Figure 4-5. PMI and age does not correlate with protein expression. Beta tubulin-normalized protein levels for CaMKII and proteolytic proteins were plotted against PMI and age; correlation significance was assessed in GraphPad Prism 5.

104
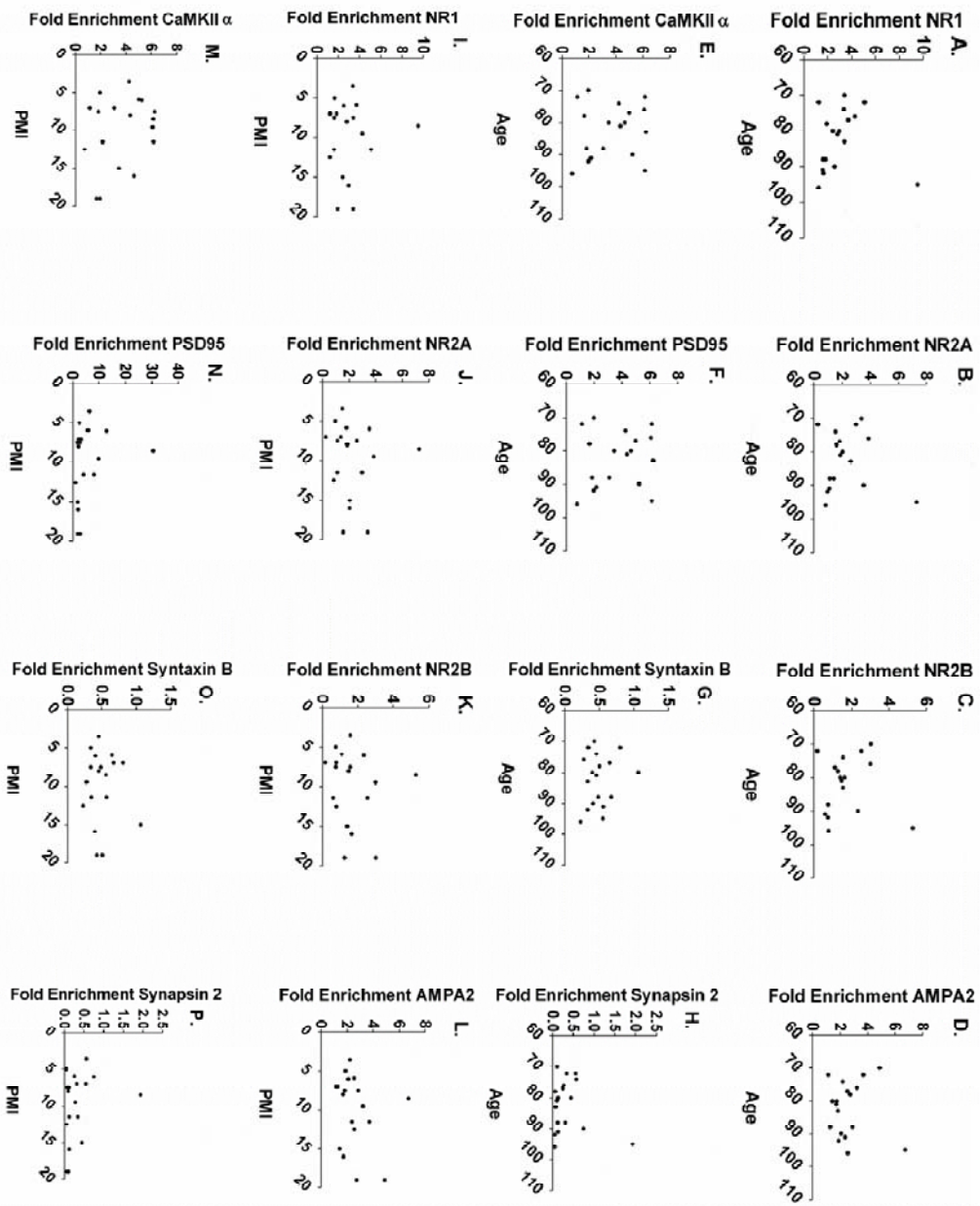
Supplemental Figure 4-6. PMI and age do not correlate with PSD and presynaptic protein enrichment values. Enrichment values for select PSD and presynaptic proteins were plotted against PMI and age; correlation significance was assessed in GraphPad Prism 5.

105
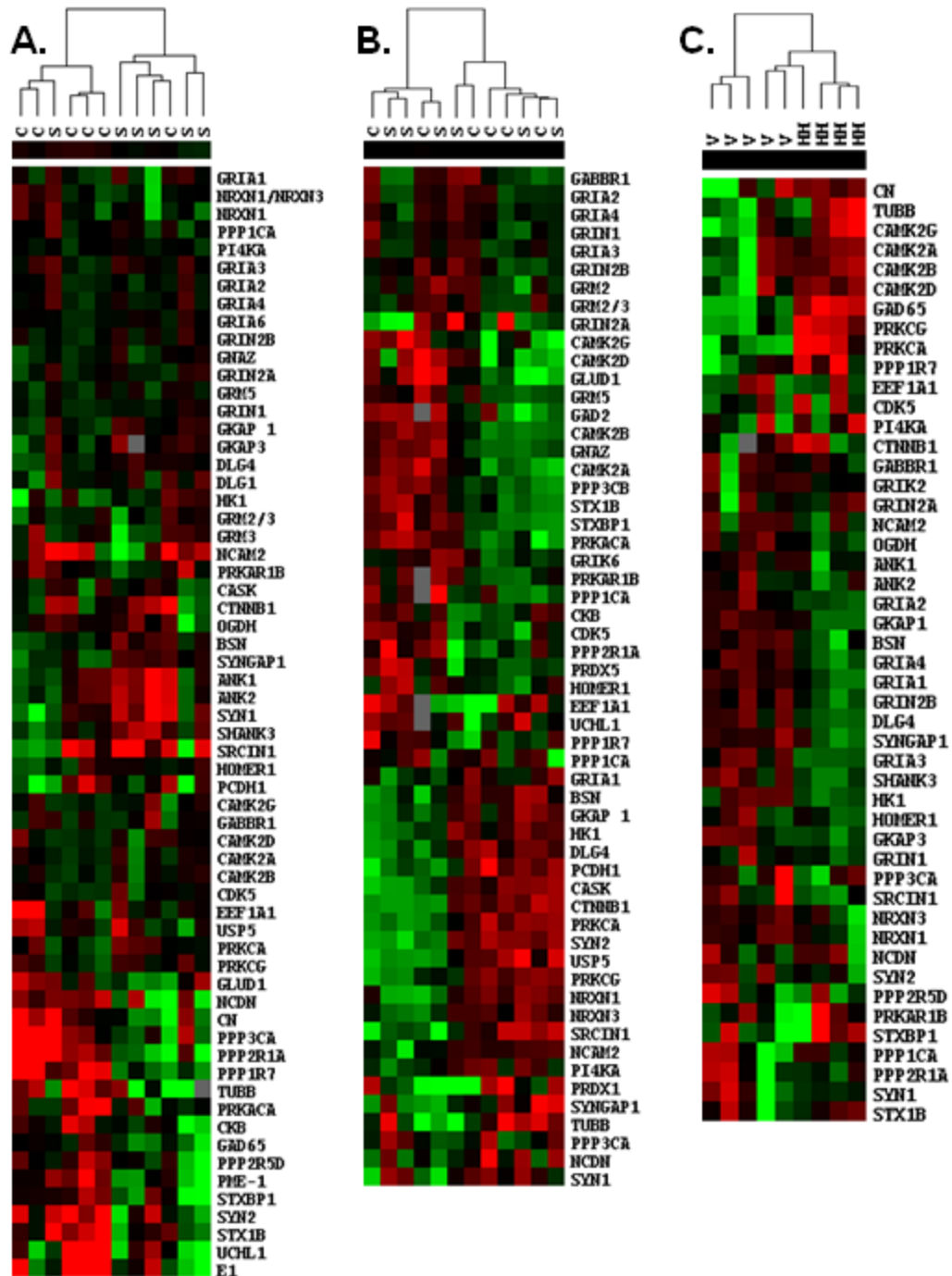
Supplemental Figure 4-7. Unsupervised hierarchical clustering, with Pearson's Correlation as the similarity metric, was utilized to group subjects and selected PSD proteins by non-normalized protein values measured in PSD enrichments. Subjects with different diagnoses were segregated into two groups near perfectly. *C = control, S = schizophrenia*. B, shows an identical analysis of the same subjects and proteins using non-normalized protein values measured in whole tissue homogenates. *C = control, S = schizophrenia*. C, shows an identical analysis of the same subjects and proteins using non-normalized protein values measured in PSD enrichments from rhesus monkeys. *V = vehicle, HH = high does haloperidol*. Proteins are identified by official gene symbol.

REFERENCES

1. Andreasen NC. Symptoms, signs, and diagnosis of schizophrenia. Lancet. 1995; 346(8973):477-481.

2. Carpenter WT,Jr, Buchanan RW. Schizophrenia. N Engl J Med. 1994; 330(10):681-690.

3. Nasar S, Herrmann… E. A Beautiful Mind 2001, .

4. Murphy BP, Chung YC, Park TW, McGorry PD. Pharmacological treatment of primary negative symptoms in schizophrenia: A systematic review Schizophr Res. 2006; 88(1-3):5-25.

5. Fenton WS, McGlashan TH. Natural history of schizophrenia subtypes: II. positive and negative symptoms and long-term course Arch Gen Psychiatry. 1991; 48(11):978 <last_page> 986.

6. Penzes P, Cahill ME, Jones KA, VanLeeuwen JE, Woolfrey KM. Dendritic spine pathology in neuropsychiatric disorders. Nat Neurosci. 2011; 14(3):285-293.

7. Chuma J, Mahadun P. Predicting the development of schizophrenia in high-risk populations: Systematic review of the predictive validity of prodromal criteria. Br J Psychiatry. 2011; 199:361-366.

8. Torrey F, Knable M. **Surviving Manic Depression : A Manual on Bipolar Disorder for Patients, Families, and Providers**. 2nd ed. New York: Basic Books, 2005.

9. Folsom D, Jeste DV. Schizophrenia in homeless persons: A systematic review of the literature. Acta Psychiatr Scand. 2002; 105(6):404-413.

10. Kane JM. Improving treatment adherence in patients with schizophrenia. J Clin Psychiatry. 2011; 72(9):e28.

11. Kane JM, Leucht S, Carpenter D, Docherty JP. Expert consensus guideline series. optimizing pharmacologic treatment of psychotic disorders. introduction: Methods, commentary, and summary. J Clin Psychiatry. 2003; 64 Suppl 12:5-19.

12. Tsuang MT, Stone WS, Faraone SV. Schizophrenia: Vulnerability versus disease. Dialogues Clin Neurosci. 2000; 2(3):257-266.

13. Tsuang MT, Stone WS, Faraone SV. The genetics of schizophrenia. Curr Psychiatry Rep. 1999; 1(1):20-24.

14. McGue M, Gottesman II. The genetic epidemiology of schizophrenia and the design of linkage studies. Eur Arch Psychiatry Clin Neurosci. 1991; 240(3):174-181.

15. Marcelis M, van Os J, Sham P, et al. Obstetric complications and familial morbid risk of psychiatric disorders. Am J Med Genet. 1998; 81(1):29-36.

16. Kandel E. **In Search of Memory: The Emergence of a New Science of Mind** . 1st ed. New York: W. W. Norton, 2006.

17. Gold JM. Cognitive deficits as treatment targets in schizophrenia. Schizophr Res. 2004; 72(1):21-28.

18. Saykin AJ, Shtasel DL, Gur RE, et al. Neuropsychological deficits in neuroleptic naive patients with first-episode schizophrenia. Arch Gen Psychiatry. 1994; 51(2):124-131.

19. Green JF, King DJ. The effects of chlorpromazine and lorazepam on abnormal antisaccade and no-saccade distractibility. Biol Psychiatry. 1998; 44(8):709-715.

20. Davidson M, Reichenberg A, Rabinowitz J, Weiser M, Kaplan Z, Mark M. Behavioral and intellectual markers for schizophrenia in apparently healthy male adolescents. Am J Psychiatry. 1999; 156(9):1328-1335.

21. Cosway R, Byrne M, Clafferty R, et al. Neuropsychological change in young people at high risk for schizophrenia: Results from the first two neuropsychological assessments of the edinburgh high risk study. Psychol Med. 2000; 30(5):1111-1121.

22. Sitskoorn MM, Aleman A, Ebisch SJ, Appels MC, Kahn RS. Cognitive deficits in relatives of patients with schizophrenia: A meta-analysis. Schizophr Res. 2004; 71(2-3):285-295.

23. Green MF. What are the functional consequences of neurocognitive deficits in schizophrenia? Am J Psychiatry. 1996; 153(3):321-330.

24. Fuster JM. The Prefrontal Cortex Amsterdam ; Elsevier/Academic Press, 2008., .

25. Brodmann K (1912) Neue Ergibnisse uber die vergleichende histologische Lokalisation der Grosshirnrinde mit besonderer Berucksichtigung des Stirnhirns. Anat Anzeiger. 41:157-216.

26. Gonzalez-Burgos G, Lewis DA. GABA neurons and the mechanisms of network oscillations: Implications for understanding cortical dysfunction in schizophrenia Schizophr Bull. 2008; 34(5):944-961.

27. Goldman M, DeQuardo JR, Tandon R, Taylor SF, Jibson M. Symptom correlates of global measures of severity in schizophrenia. Compr Psychiatry. 1999; 40(6):458-461.

28. Callicott JH, Mattay VS, Verchinski BA, Marenco S, Egan MF, Weinberger DR. Complexity of prefrontal cortical dysfunction in schizophrenia: More than up or down. Am J Psychiatry. 2003; 160(12):2209-2215.

29.   Barch DM, Sheline YI, Csernansky JG, Snyder AZ. Working memory and prefrontal cortex dysfunction: Specificity to schizophrenia compared with major depression. Biol Psychiatry. 2003; 53(5):376-384.

30.   MacDonald AW,3rd, Carter CS, Kerns JG, et al. Specificity of prefrontal dysfunction and context processing deficits to schizophrenia in never-medicated patients with first-episode psychosis. Am J Psychiatry. 2005; 162(3):475-484.

31.   Fornito A, Yucel M, Wood SJ, et al. Anterior cingulate cortex abnormalities associated with a first psychotic episode in bipolar disorder. Br J Psychiatry. 2009; 194(5):426-433.

32.   Ellison-Wright I, Bullmore E. Anatomy of bipolar disorder and schizophrenia: A meta-analysis. Schizophr Res. 2010; 117(1):1-12.

33.   Akbarian S, Kim JJ, Potkin SG, et al. Gene expression for glutamic acid decarboxylase is reduced without loss of neurons in prefrontal cortex of schizophrenics. Arch Gen Psychiatry. 1995; 52(4):258-266.

34.   Thune JJ, Uylings HB, Pakkenberg B. No deficit in total number of neurons in the prefrontal cortex in schizophrenics. J Psychiatr Res. 2001; 35(1):15-21.

35.   Glantz LA, Lewis DA. Decreased dendritic spine density on prefrontal cortical pyramidal neurons in schizophrenia. Arch Gen Psychiatry. 2000; 57(1):65-73.

36.   Kolluri N, Sun Z, Sampson AR, Lewis DA. Lamina-specific reductions in dendritic spine density in the prefrontal cortex of subjects with schizophrenia. Am J Psychiatry. 2005; 162(6):1200-1202.

37.   Sweet RA, Henteleff RA, Zhang W, Sampson AR, Lewis DA. Reduced dendritic spine density in auditory cortex of subjects with schizophrenia. Neuropsychopharmacology. 2009; 34(2):374-389.

38.   Dorph-Petersen KA, Pierri JN, Wu Q, Sampson AR, Lewis DA. Primary visual cortex volume and total neuron number are reduced in schizophrenia. J Comp Neurol. 2007; 501(2):290-301.

39.   Rosoklija G, Toomayan G, Ellis SP, et al. Structural abnormalities of subicular dendrites in subjects with schizophrenia and mood disorders: Preliminary findings. Arch Gen Psychiatry. 2000; 57(4):349-356.

40.   Pierri JN, Volk CL, Auh S, Sampson A, Lewis DA. Decreased somal size of deep layer 3 pyramidal neurons in the prefrontal cortex of subjects with schizophrenia. Arch Gen Psychiatry. 2001; 58(5):466-473.

41.   Rajkowska G, Selemon LD, Goldman-Rakic PS. Neuronal and glial somal size in the prefrontal cortex: A postmortem morphometric study of schizophrenia and huntington disease. Arch Gen Psychiatry. 1998; 55(3):215-224.

42.   Konradi C, Heckers S. Molecular aspects of glutamate dysregulation: Implications for schizophrenia and its treatment. Pharmacol Ther. 2003; 97(2):153-179.

43.   Lewis DA, Gonz\'alez-Burgos G. Neuroplasticity of neocortical circuits in schizophrenia. Neuropsychopharmacology. 2007; 33(1):141-165.

44.   Sheng M. Postsynaptic signaling and plasticity mechanisms. Science. 2002; 298(5594):776-780.

45.   Hollmann M, Boulter J, Maron C, et al. Zinc potentiates agonist-induced currents at certain splice variants of the NMDA receptor. Neuron. 1993; 10(5):943-954.

46.   Ozawa S. Ca2+ permeation through the ionotropic glutamate receptor. Tanpakushitsu Kakusan Koso. 1998; 43(12 Suppl):1589-1595.

47.   Clements JD, Westbrook GL. Activation kinetics reveal the number of glutamate and glycine binding sites on the N-methyl-D-aspartate receptor. Neuron. 1991; 7(4):605-613.

48.   Rosenmund C, Stern-Bach Y, Stevens CF. The tetrameric structure of a glutamate receptor channel. Science. 1998; 280(5369):1596-1599.

49.   Safferling M, Tichelaar W, Kummerle G, et al. First images of a glutamate receptor ion channel: Oligomeric state and molecular dimensions of GluRB homomers. Biochemistry. 2001; 40(46):13948-13953.

50.   Carroll RC, Zukin RS. NMDA-receptor trafficking and targeting: Implications for synaptic transmission and plasticity. Trends Neurosci. 2002; 25(11):571-577.

51.   Dravid SM, Erreger K, Yuan H, et al. Subunit-specific mechanisms and proton sensitivity of NMDA receptor channel block. J Physiol. 2007; 581(Pt 1):107-128.

52.   Cull-Candy S, Brickley S, Farrant M. NMDA receptor subunits: Diversity, development and disease. Curr Opin Neurobiol. 2001; 11(3):327-335.

53.   Nishi M, Hinds H, Lu HP, Kawata M, Hayashi Y. Motoneuron-specific expression of NR3B, a novel NMDA-type glutamate receptor subunit that works in a dominant-negative manner. J Neurosci. 2001; 21(23):RC185.

54.   Herron CE, Lester RA, Coan EJ, Collingridge GL. Frequency-dependent involvement of NMDA receptors in the hippocampus: A novel synaptic mechanism. Nature. 1986; 322(6076):265-268.

55.   Nakahara K, Okada M, Nakanishi S. The metabotropic glutamate receptor mGluR5 induces calcium oscillations in cultured astrocytes via protein kinase C phosphorylation. J Neurochem. 1997; 69(4):1467-1475.

56. Jia Z, Lu Y, Henderson J, et al. Selective abolition of the NMDA component of long-term potentiation in mice lacking mGluR5. Learn Mem. 1998; 5(4-5):331-343.

57. Pisani A, Gubellini P, Bonsi P, et al. Metabotropic glutamate receptor 5 mediates the potentiation of N-methyl-D-aspartate responses in medium spiny striatal neurons. Neuroscience. 2001; 106(3):579-587.

58. Sheng M. Molecular organization of the postsynaptic specialization. Proc Natl Acad Sci U S A. 2001; 98(13):7058-7061.

59. Hering H, Sheng M. Dendritic spines: Structure, dynamics and regulation Nat Rev Neurosci. 2001; 2(12):880-888.

60. Coba MP, Pocklington AJ, Collins MO, et al. Neurotransmitters drive combinatorial multistate postsynaptic density networks. Science Signaling. 2009; 2(68):ra19-ra19.

61. Jentsch JD, Roth RH. The neuropsychopharmacology of phencyclidine: From NMDA receptor hypofunction to the dopamine hypothesis of schizophrenia. Neuropsychopharmacology. 1999; 20(3):201-225.

62. Krystal JH, Karper LP, Seibyl JP, et al. Subanesthetic effects of the noncompetitive NMDA antagonist, ketamine, in humans. psychotomimetic, perceptual, cognitive, and neuroendocrine responses. Arch Gen Psychiatry. 1994; 51(3):199-214.

63. Lipska BK, Weinberger DR. To model a psychiatric disorder in animals: Schizophrenia as a reality test. Neuropsychopharmacology. 2000; 23(3):223-239.

64. Kilts CD. The changing roles and targets for animal models of schizophrenia. Biol Psychiatry. 2001; 50(11):845-855.

65. Goff DC, Henderson DC, Evins AE, Amico E. A placebo-controlled crossover trial of D-cycloserine added to clozapine in patients with schizophrenia. Biol Psychiatry. 1999; 45(4):512-514.

66. Goff DC, Tsai G, Levitt J, et al. A placebo-controlled trial of D-cycloserine added to conventional neuroleptics in patients with schizophrenia. Arch Gen Psychiatry. 1999; 56(1):21-27.

67. Heresco-Levy U, Javitt DC, Ermilov M, Mordel C, Horowitz A, Kelly D. Double-blind, placebo-controlled, crossover trial of glycine adjuvant therapy for treatment-resistant schizophrenia. Br J Psychiatry. 1996; 169(5):610-617.

68. Heresco-Levy U, Silipo G, Javitt DC. Glycinergic augmentation of NMDA receptor-mediated neurotransmission in the treatment of schizophrenia. Psychopharmacol Bull. 1996; 32(4):731-740.

69.   Singh SP, Singh V. Meta-analysis of the efficacy of adjunctive NMDA receptor modulators in chronic schizophrenia. CNS Drugs. 2011; 25(10):859-885.

70.   Dalmau J, Gleichman AJ, Hughes EG, et al. Anti-NMDA-receptor encephalitis: Case series and analysis of the effects of antibodies. Lancet Neurol. 2008; 7(12):1091-1098.

71.   Hughes EG, Peng X, Gleichman AJ, et al. Cellular and synaptic mechanisms of anti-NMDA receptor encephalitis. Journal of Neuroscience. 2010; 30(17):5866-5875.

72.   Harrison PJ, West VA. Six degrees of separation: On the prior probability that schizophrenia susceptibility genes converge on synapses, glutamate and NMDA receptors. Mol Psychiatry. 2006; 11(11):981-983.

73.   Harrison PJ, Law AJ. Neuregulin 1 and schizophrenia: Genetics, gene expression, and neurobiology. Biol Psychiatry. 2006; 60(2):132-140.

74.   Harrison PJ, Weinberger DR. Schizophrenia genes, gene expression, and neuropathology: On the matter of their convergence. Mol Psychiatry. 2005; 10(1):40-68; image 5.

75.   Bayes A, van de Lagemaat LN, Collins MO, et al. Characterization of the proteome, diseases and evolution of the human postsynaptic density Nat Neurosci. 2011; 14(1):19-21.

76.   Fernandez E, Collins MO, Uren RT, et al. Targeted tandem affinity purification of PSD-95 recovers core postsynaptic complexes and schizophrenia susceptibility proteins. Molecular Systems Biology. 2009; 5:1-17.

77.   Hashimoto R, Hattori S, Chiba S, et al. Susceptibility genes for schizophrenia. Psychiatry Clin Neurosci. 2006; 60 Suppl 1:S4-S10.

78.   Banerjee A, Macdonald ML, Borgmann-Winter KE, Hahn CG. Neuregulin 1-erbB4 pathway in schizophrenia: From genes to an interactome Brain Res Bull. 2010; 83(3-4):132-139.

79.   Huang YZ, Won S, Ali DW, et al. Regulation of neuregulin signaling by PSD-95 interacting with ErbB4 at CNS synapses. Neuron. 2000; 26(2):443-455.

80.   MacLaren EJ, Charlesworth P, Coba MP, Grant SG. Knockdown of mental disorder susceptibility genes disrupts neuronal network physiology in vitro Mol Cell Neurosci. 2011; 47(2):93-99.

81.   Saugstad JA, Marino MJ, Folk JA, Hepler JR, Conn PJ. RGS4 inhibits signaling by group I metabotropic glutamate receptors. J Neurosci. 1998; 18(3):905-913.

82.   Schwendt M, Sigmon SA, McGinty JF. RGS4 overexpression in the rat dorsal striatum modulates mGluR5- and amphetamine-mediated behavior and signaling. Psychopharmacology (Berl). 2011; .

83.   Pitcher GM, Kalia LV, Ng D, et al. Schizophrenia susceptibility pathway neuregulin 1-ErbB4 suppresses src upregulation of NMDA receptors. Nat Med. 2011; 17(4):470-478.

84.   Hahn C, Wang H, Cho D, et al. Altered neuregulin 1--erbB4 signaling contributes to NMDA> receptor hypofunction in schizophrenia. Nat Med. 2006; 12(7):824-828.

85.   Hayashi-Takagi A, Takaki M, Graziane N, et al. Disrupted-in-schizophrenia 1 (DISC1) regulates spines of the glutamate synapse via Rac1. Nat Neurosci. 2010; 13(3):327-332.

86.   Grant SG. Targeted TAP tags, phosphoproteomes and the biology of thought Expert Rev Proteomics. 2010; 7(2):169-171.

87.   Grant SG. A general basis for cognition in the evolution of synapse signaling complexes Cold Spring Harb Symp Quant Biol. 2009; 74:249-257.

88.   Balu DT, Coyle JT. Neuroplasticity signaling pathways linked to the pathophysiology of schizophrenia Neurosci Biobehav Rev. 2011; 35(3):848-870.

89.   McCullumsmith RE, Clinton SM, Meador-Woodruff JH. Schizophrenia as a disorder of neuroplasticity. Int Rev Neurobiol. 2004; 59:19-45.

90.   Hahn CG, Wang HY, Cho DS, et al. Altered neuregulin 1-erbB4 signaling contributes to NMDA receptor hypofunction in schizophrenia. Nat Med. 2006; 12(7):824-828.

91.   Xie F, Padival M, Siegel RE. Association of PSD-95 with ErbB4 facilitates neuregulin signaling in cerebellar granule neurons in culture. J Neurochem. 2007; 100(1):62-72.

92.   Carpenter G. ErbB-4: Mechanism of action and biology. Exp Cell Res. 2003; 284(1):66-77.

93.   Ultanir SK, Kim JE, Hall BJ, Deerinck T, Ellisman M, Ghosh A. Regulation of spine morphology and spine density by NMDA receptor signaling in vivo. Proc Natl Acad Sci U S A. 2007; 104(49):19553-19558.

94.   Balu DT, Coyle JT. Glutamate receptor composition of the post-synaptic density is altered in genetic mouse models of NMDA receptor hypo- and hyperfunction. Brain Res. 2011; 1392(C):1-7.

95.   Mirnics K, Middleton FA, Marquez A, Lewis DA, Levitt P. Molecular characterization of schizophrenia viewed by microarray analysis of gene expression in prefrontal cortex. Neuron. 2000; 28(1):53-67.

96.   Fung SJ, Sivagnanasundaram S, Weickert CS. Lack of change in markers of presynaptic terminal abundance alongside subtle reductions in markers of presynaptic terminal plasticity in prefrontal cortex of schizophrenia patients. BPS. 2011; 69(1):71-79.

97.   Akbarian S, Sucher NJ, Bradley D, et al. Selective alterations in gene expression for NMDA receptor subunits in prefrontal cortex of schizophrenics. J Neurosci. 1996; 16(1):19-30.

98.   Beneyto M, Meador-Woodruff JH. Lamina-specific abnormalities of NMDA receptor-associated postsynaptic protein transcripts in the prefrontal cortex in schizophrenia and bipolar disorder. Neuropsychopharmacology. 2008; 33(9):2175-2186.

99.   Dracheva S, Marras SA, Elhakem SL, Kramer FR, Davis KL, Haroutunian V. N-methyl-D-aspartic acid receptor expression in the dorsolateral prefrontal cortex of elderly patients with schizophrenia. Am J Psychiatry. 2001; 158(9):1400-1410.

100.   Funk AJ, McCullumsmith RE, Haroutunian V, Meador-Woodruff JH. Abnormal activity of the MAPK- and cAMP-associated signaling pathways in frontal cortical areas in postmortem brain in schizophrenia. Neuropsychopharmacology. 2011; .

101.   Funk AJ, Rumbaugh G, Harotunian V, McCullumsmith RE, Meador-Woodruff JH. Decreased expression of NMDA receptor-associated proteins in frontal cortex of elderly patients with schizophrenia. Neuroreport. 2009; 20(11):1019-1022.

102.   Kristiansen LV, Beneyto M, Haroutunian V, Meador-Woodruff JH. Changes in NMDA receptor subunits and interacting PSD proteins in dorsolateral prefrontal and anterior cingulate cortex indicate abnormal regional expression in schizophrenia. Mol Psychiatry. 2006; 11(8):737-47, 705.

103.   Martucci L, Wong AH, De Luca V, et al. N-methyl-D-aspartate receptor NR2B subunit gene GRIN2B in schizophrenia and bipolar disorder: Polymorphisms and mRNA levels. Schizophr Res. 2006; 84(2-3):214-221.

104.   Ohnuma T, Kato H, Arai H, Faull RL, McKenna PJ, Emson PC. Gene expression of PSD95 in prefrontal cortex and hippocampus in schizophrenia. Neuroreport. 2000; 11(14):3133-3137.

105.   Sokolov BP. Expression of NMDAR1, GluR1, GluR7, and KA1 glutamate receptor mRNAs is decreased in frontal cortex of "neuroleptic-free" schizophrenics: Evidence on reversible up-regulation by typical neuroleptics. J Neurochem. 1998; 71(6):2454-2464.

106.   O'Connor JA, Hemby SE. Elevated GRIA1 mRNA expression in layer II/III and V pyramidal cells of the DLPFC in schizophrenia. Schizophr Res. 2007; 97(1-3):277-288.

107.   Pietersen CY, Lim MP, Macey L, Woo TU, Sonntag KC. Neuronal type-specific gene expression profiling and laser-capture microdissection. Methods Mol Biol. 2011; 755:327-343.

108.   Sodhi MS, Simmons M, McCullumsmith R, Haroutunian V, Meador-Woodruff JH. Glutamatergic gene expression is specifically reduced in thalamocortical projecting relay neurons in schizophrenia. Biol Psychiatry. 2011; 70(7):646-654.

109.   Trinidad JC, Thalhammer A, Specht CG, et al. Quantitative analysis of synaptic phosphorylation and protein expression. Mol Cell Proteomics. 2008; 7(4):684-696.

110.   Dosemeci A, Makusky AJ, Jankowska-Stephens E, Yang X, Slotta DJ, Markey SP. Composition of the synaptic PSD-95 complex. Molecular {\&} cellular proteomics : MCP. 2007; 6(10):1749-1760.

111.   Cheng D, Hoogenraad CC, Rush J, et al. Relative and absolute quantification of postsynaptic density proteome isolated from rat forebrain and cerebellum. Mol Cell Proteomics. 2006; 5(6):1158-1170.

112.   Collins MO, Husi H, Yu L, et al. Molecular characterization and comparison of the components and multiprotein complexes in the postsynaptic proteome. J Neurochem. 2006; 97:16-23.

113.   Hahn CG, Banerjee A, MacDonald ML, et al. The Post-Synaptic Density of Human Postmortem Brain Tissues: An Experimental Study Paradigm for Neuropsychiatric Illnesses In Press.

114.   Husi H, Ward MA, Choudhary JS, Blackstock WP, Grant SG. Proteomic analysis of NMDA receptor-adhesion protein signaling complexes. Nat Neurosci. 2000; 3(7):661-669.

115.   Yoshimura Y, Yamauchi Y, Shinkawa T, et al. Molecular constituents of the postsynaptic density fraction revealed by proteomic analysis using multidimensional liquid chromatography-tandem mass spectrometry. J Neurochem. 2004; 88(3):759-768.

116.   English JA, Pennington K, Dunn MJ, Cotter DR. The neuroproteomics of schizophrenia Biol Psychiatry. 2011; 69(2):163-172.

117.   Pennington K, Beasley CL, Dicker P, et al. Prominent synaptic and metabolic abnormalities revealed by proteomic analysis of the dorsolateral prefrontal cortex in schizophrenia and bipolar disorder Mol Psychiatry. 2008; 13(12):1102-1117.

118.   Eberwine J, Belt B, Kacharmina JE, Miyashiro K. Analysis of subcellularly localized mRNAs using in situ hybridization, mRNA amplification, and expression profiling. Neurochem Res. 2002; 27(10):1065-1077.

119.   Phillips J, Eberwine JH. Antisense RNA amplification: A linear amplification method for analyzing the mRNA population from single living cells. Methods. 1996; 10(3):283-288.

120.   Wolters DA, Washburn MP, Yates JR,3rd. An automated multidimensional protein identification technology for shotgun proteomics. Anal Chem. 2001; 73(23):5683-5690.

121.   Mann M. Functional and quantitative proteomics using SILAC. Nat Rev Mol Cell Biol. 2006; 7(12):952-958.

122.   Ong SE, Blagoev B, Kratchmarova I, et al. Stable isotope labeling by amino acids in cell culture, SILAC, as a simple and accurate approach to expression proteomics. Mol Cell Proteomics. 2002; 1(5):376-386.

123.   Li K, Hornshaw MP, van Minnen J, Smalla KH, Gundelfinger ED, Smit AB. Organelle proteomics of rat synaptic proteins: Correlation-profiling by isotope-coded affinity tagging in conjunction with liquid chromatography-tandem mass spectrometry to reveal post-synaptic density specific proteins. J Proteome Res. 2005; 4(3):725-733.

124.   Ross PL, Huang YN, Marchese JN, et al. Multiplexed protein quantitation in saccharomyces cerevisiae using amine-reactive isobaric tagging reagents. Mol Cell Proteomics. 2004; 3(12):1154-1169.

125.   Ting L, Rad R, Gygi SP, Haas W. MS3 eliminates ratio distortion in isobaric multiplexed quantitative proteomics. Nat Methods. 2011; 8(11):937-940.

126.   Xu RN, Fan L, Rieser MJ, El-Shourbagy TA. Recent advances in high-throughput quantitative bioanalysis by LC-MS/MS. J Pharm Biomed Anal. 2007; 44(2):342-355.

127.   Jemal M, Xia YQ. LC-MS development strategies for quantitative bioanalysis. Curr Drug Metab. 2006; 7(5):491-502.

128.   Ciccimaro E, Blair IA. Stable-isotope dilution LC-MS for quantitative biomarker analysis. Bioanalysis. 2010; 2(2):311-341.

129.   Sheng M. Molecular organization of the postsynaptic specialization. Proc Natl Acad Sci U S A. 2001; 98(13):7058-7061.

130.   Okabe S. Molecular anatomy of the postsynaptic density. Mol Cell Neurosci. 2007; 34(4):503-518.

131.   Behan AT, Byrne C, Dunn MJ, Cagney G, Cotter DR. Proteomic analysis of membrane microdomain-associated proteins in the dorsolateral prefrontal cortex in schizophrenia and bipolar disorder reveals alterations in LAMP, STXBP1 and BASP1 protein expression. Mol Psychiatry. 2009; 14(6):601-613.

132.   Talbot K, Cho DS, Ong WY, et al. Dysbindin-1 is a synaptic and microtubular protein that binds brain snapin. Hum Mol Genet. 2006; 15(20):3041-3054.

133.   Dosemeci A, Makusky AJ, Jankowska-Stephens E, Yang X, Slotta DJ, Markey SP. Composition of the synaptic PSD-95 complex. Mol Cell Proteomics. 2007; 6(10):1749-1760.

134.   Degiorgis JA, Galbraith JA, Dosemeci A, Chen X, Reese TS. Distribution of the scaffolding proteins PSD-95, PSD-93, and SAP97 in isolated PSDs. Brain Cell Biol. 2006; 35(4-6):239-250.

135.   Carlin RK, Grab DJ, Cohen RS, Siekevitz P. Isolation and characterization of postsynaptic densities from various brain regions: Enrichment of different types of postsynaptic densities. J Cell Biol. 1980; 86(3):831-845.

136.   Phillips GR, Huang JK, Wang Y, et al. The presynaptic particle web: Ultrastructure, composition, dissolution, and reconstitution. Neuron. 2001; 32(1):63-77.

137.   Phillips GR, Tanaka H, Frank M, et al. Gamma-protocadherins are targeted to subsets of synapses and intracellular organelles in neurons. J Neurosci. 2003; 23(12):5096-5104.

138.   Peng J, Kim MJ, Cheng D, Duong DM, Gygi SP, Sheng M. Semiquantitative proteomic analysis of rat forebrain postsynaptic density fractions by mass spectrometry. J Biol Chem. 2004; 279(20):21003-21011.

139.   Jaffe H, Vinade L, Dosemeci A. Identification of novel phosphorylation sites on postsynaptic density proteins. Biochem Biophys Res Commun. 2004; 321(1):210-218.

140.   Lewis DA. The human brain revisited: Opportunities and challenges in postmortem studies of psychiatric disorders. Neuropsychopharmacology. 2002; 26(2):143-154.

141.   Crecelius A, Gotz A, Arzberger T, et al. Assessing quantitative post-mortem changes in the gray matter of the human frontal cortex proteome by 2-D DIGE. Proteomics. 2008; 8(6):1276-1291.

142.   Hunsucker SW, Solomon B, Gawryluk J, et al. Assessment of post-mortem-induced changes to the mouse brain proteome. J Neurochem. 2008; 105(3):725-737.

143.   Novikova SI, He F, Cutrufello NJ, Lidow MS. Identification of protein biomarkers for schizophrenia and bipolar disorder in the postmortem prefrontal cortex using SELDI-TOF-MS ProteinChip profiling combined with MALDI-TOF-PSD-MS analysis. Neurobiol Dis. 2006; 23(1):61-76.

144.   Keller A, Nesvizhskii AI, Kolker E, Aebersold R. Empirical statistical model to estimate the accuracy of peptide identifications made by MS/MS and database search. Anal Chem. 2002; 74(20):5383-5392.

145.   Lucitt MB, Price TS, Pizarro A, et al. Analysis of the zebrafish proteome during embryonic development. Molecular {\&} Cellular Proteomics. 2008; 7(5):981-994.

146.   Sheng M, Hoogenraad CC. The postsynaptic architecture of excitatory synapses: A more quantitative view. Annu Rev Biochem. 2007; 76:823-847.

147.   Collins MO, Husi H, Yu L, et al. Molecular characterization and comparison of the components and multiprotein complexes in the postsynaptic proteome. J Neurochem. 2006; 97 Suppl 1:16-23.

148.   Price TS, Lucitt MB, Wu W, et al. EBP, a program for protein identification using multiple tandem mass spectrometry datasets. Mol Cell Proteomics. 2007; 6(3):527-536.

149.   Dosemeci A, Makusky AJ, Jankowska-Stephens E, Yang X, Slotta DJ, Markey SP. Composition of the synaptic PSD-95 complex. Mol Cell Proteomics. 2007; 6(10):1749-1760.

150.   Petersen JD, Chen X, Vinade L, Dosemeci A, Lisman JE, Reese TS. Distribution of postsynaptic density (PSD)-95 and Ca2+/calmodulin-dependent protein kinase II at the PSD. J Neurosci. 2003; 23(35):11270-11278.

151.   Chen X, Vinade L, Leapman RD, et al. Mass of the postsynaptic density and enumeration of three key molecules. Proc Natl Acad Sci U S A. 2005; 102(32):11551-11556.

152.   Bard L, Groc L. Glutamate receptor dynamics and protein interaction: Lessons from the NMDA receptor Mol Cell Neurosci. 2011; .

153.   Hahn CG, Banerjee A, Macdonald ML, et al. The post-synaptic density of human postmortem brain tissues: An experimental study paradigm for neuropsychiatric illnesses PLoS One. 2009; 4(4):e5251.

154.   English JA, Dicker P, Focking M, Dunn MJ, Cotter DR. 2-D DIGE analysis implicates cytoskeletal abnormalities in psychiatric disease Proteomics. 2009; 9(12):3368-3382.

155.   Peng J, Kim MJ, Cheng D, Duong DM, Gygi SP, Sheng M. Semiquantitative proteomic analysis of rat forebrain postsynaptic density fractions by mass spectrometry J Biol Chem. 2004; 279(20):21003-21011.

156.   Fernandez E, Collins MO, Uren RT, et al. Targeted tandem affinity purification of PSD-95 recovers core postsynaptic complexes and schizophrenia susceptibility proteins Mol Syst Biol. 2009; 5:269.

157.   Keller MA, Gwinn K, Nash J, et al. Whole genome association studies of neuropsychiatric disease: An emerging era of collaborative genetic discovery Neuropsychiatr Dis Treat. 2007; 3(5):613-618.

158.   Uhl GR, Grow RW. The burden of complex genetics in brain disorders Arch Gen Psychiatry. 2004; 61(3):223-229.

159.   Ishihama Y, Sato T, Tabata T, et al. Quantitative mouse brain proteomics using culture-derived isotope tags as internal standards Nat Biotechnol. 2005; 23(5):617-621.

160.   Brun V, Dupuis A, Adrait A, et al. Isotope-labeled protein standards: Toward absolute quantitative proteomics Mol Cell Proteomics. 2007; 6(12):2139-2149.

161.   Spellman DS, Deinhardt K, Darie CC, Chao MV, Neubert TA. Stable isotopic labeling by amino acids in cultured primary neurons: Application to brain-derived neurotrophic factor-

dependent phosphotyrosine-associated signaling Mol Cell Proteomics. 2008; 7(6):1067-1076.

162.   Zanivan S, Krueger M, Mann M. In vivo quantitative proteomics: The SILAC mouse Methods Mol Biol. 2012; 757:435-450.

163.   Walther DM, Mann M. Accurate quantification of more than 4000 mouse tissue proteins reveals minimal proteome changes during aging Mol Cell Proteomics. 2011; 10(2):M110.004523.

164.   Kall L, Canterbury JD, Weston J, Noble WS, MacCoss MJ. Semi-supervised learning for peptide identification from shotgun proteomics datasets Nat Methods. 2007; 4(11):923-925.

165.   Eisen MB, Spellman PT, Brown PO, Botstein D. Cluster analysis and display of genome-wide expression patterns Proc Natl Acad Sci U S A. 1998; 95(25):14863-14868.

166.   Page RD. TreeView: An application to display phylogenetic trees on personal computers Comput Appl Biosci. 1996; 12(4):357-358.

167.   Estey MP, Kim MS, Trimble WS. Septins Curr Biol. 2011; 21(10):R384-7.

168.   Beites CL, Campbell KA, Trimble WS. The septin Sept5/CDCrel-1 competes with alpha-SNAP for binding to the SNARE complex Biochem J. 2005; 385(Pt 2):347-353.

169.   Amin ND, Zheng YL, Kesavapany S, et al. Cyclin-dependent kinase 5 phosphorylation of human septin SEPT5 (hCDCrel-1) modulates exocytosis J Neurosci. 2008; 28(14):3631-3643.

170.   Li X, Serwanski DR, Miralles CP, Nagata K, De Blas AL. Septin 11 is present in GABAergic synapses and plays a functional role in the cytoarchitecture of neurons and GABAergic synaptic connectivity J Biol Chem. 2009; 284(25):17253-17265.

171.   Balu DT, Basu AC, Corradi JP, Cacace AM, Coyle JT. The NMDA receptor co-agonists, d-serine and glycine, regulate neuronal dendritic architecture in the somatosensory cortex. Neurobiol Dis. 2011; :1-12.

172.   O'Connor JA, Hasenkamp W, Horman BM, Muly EC, Hemby SE. Region specific regulation of NR1 in rhesus monkeys following chronic antipsychotic drug administration. Biol Psychiatry. 2006; 60(6):659-662.

173.   Deo AJ, Cahill ME, Li S, et al. Increased expression of kalirin-9 in the auditory cortex of schizophrenia subjects: Its role in dendritic pathology. Neurobiol Dis. 2011; :1-8.

174.   Deo AJ, Cahill ME, Li S, et al. Increased expression of kalirin-9 in the auditory cortex of schizophrenia subjects: Its role in dendritic pathology. Neurobiol Dis. 2011; .

175.   Allen JA, Halverson-Tamboli RA, Rasenick MM. Lipid raft microdomains and neurotransmitter signalling. Nature Reviews Neuroscience. 2006; 8(2):128-140.

176.   Hering H, Lin CC, Sheng M. Lipid rafts in the maintenance of synapses, dendritic spines, and surface AMPA receptor stability. J Neurosci. 2003; 23(8):3262-3271.

177.   Ide M, Lewis DA. Altered cortical CDC42 signaling pathways in schizophrenia: Implications for dendritic spine deficits. Biol Psychiatry. 2010; 68(1):25-32.

178.   Xu P, Peng J. Dissecting the ubiquitin pathway by mass spectrometry. Biochimica et Biophysica Acta (BBA) - Proteins {\&} Proteomics. 2006; 1764(12):1940-1947.

179.   Peng J, Schwartz D, Elias JE, et al. A proteomics approach to understanding protein ubiquitination. Nat Biotechnol. 2003; 21(8):921-926.

180.   Wiacek C, Muller S, Benndorf D. A cytomic approach reveals population heterogeneity of cupriavidus necator in response to harmful phenol concentrations. Proteomics. 2006; 6(22):5983-5994.

181.   Braakman RB, Luider TM, Martens JW, Foekens JA, Umar A. Laser capture microdissection applications in breast cancer proteomics. Methods Mol Biol. 2011; 755:143-154.

182.   Leverenz JB, Umar I, Wang Q, et al. Proteomic identification of novel proteins in cortical lewy bodies. Brain Pathol. 2007; 17(2):139-145.

183.   Wang Q, Woltjer RL, Cimino PJ, et al. Proteomic analysis of neurofibrillary tangles in alzheimer disease identifies GAPDH as a detergent-insoluble paired helical filament tau binding protein. FASEB J. 2005; 19(7):869-871.

184.   Bitanihirwe BK, Lim MP, Woo TU. N-methyl-D-aspartate receptor expression in parvalbumin-containing inhibitory neurons in the prefrontal cortex in bipolar disorder. Bipolar Disord. 2010; 12(1):95-101.